# Advances in Reverse Osmosis Membrane Engineering and Alginate Recycling: Covalent Surface Modifications for Membrane Performance and Analysis of Molecular Changes and Calcium Crosslinker Removal for Alginate sustainable practices

By

Negar Rahmati

B.Sc., Amir Kabir University of Technology, 2017

M.A., Institute for Color Science and Technologies, 2021

A Thesis Submitted in Partial Fulfillment of the Requirements for the Degree of

Master of Applied Sciences

In the Department of Civil Engineering



University of Victoria

# Advances in Reverse Osmosis Membrane Engineering and Alginate Recycling: Covalent Surface Modifications for Membrane Performance and Analysis of Molecular Changes and Calcium Crosslinker Removal for Alginate sustainable practices

By

Negar Rahmati

B.Sc., Amir Kabir University of Technology, 2017

M.A., Institute for Color Science and Technologies, 2021

## Supervisory committee:

Dr. Heather L. Buckley, Co-Supervisor

Department of Civil Engineering and Department of Chemistry, University of Victoria

Dr. Onita Basu, Co-Supervisor

Department of Civil and Environmental Engineering, Carleton University

# Abstract

The increasing demand for potable water and the environmental impact of conventional plastics present significant global challenges that require innovative solutions. Addressing these issues effectively involves advancements in both water purification technologies and material sustainability. This thesis explores these challenges through two complementary projects: enhancing reverse osmosis (RO) membrane technology and improving the sustainability of alginate-based bioplastics.

Reverse osmosis is a critical water purification technology used to produce fresh water from diverse sources, including seawater and brackish water. Central to this technology are RO membranes, which are predominantly made of polyamide. Despite their effectiveness, these membranes face performance limitations due to biofouling and chemical degradation. Biofouling, caused by microorganisms forming biofilms on the membrane surface, reduces water flux, increases operational pressure, and raises energy consumption. Chemical degradation affects membrane longevity and performance, leading to frequent cleaning and replacement. These issues contribute to significant economic costs and environmental waste.

Chapter 1 explores the attachment of PEI-diazirine onto PET surfaces, with the hypothesis that successful cross-linking in these trials could also be applied to polyamide-based RO due to the reactivity between polyamides and carbenes. The objective was to develop a method for covalent modification of RO membranes using diazirine moieties, which could serve as a foundation for further functionalization. Covalent bonding offers advantages such as improved stability, durability, and compatibility, making it a favorable approach for RO membrane surface modification. In conclusion, the study introduced an innovative approach to enhancing the surface properties of RO polyamide-based membranes by incorporating covalently bonded diazirine-containing molecules. While direct evidence of covalent attachment was not confirmed, indirect observations—such as results from dye and water angle tests, DSC, and FTIR—support the presence of activated diazirine on the surface. These tests disproved the idea that diazirine molecules react exclusively with each other rather than with the surface. This groundwork sets the stage for future functionalization processes to impart foul-release properties to RO membranes.

Chapter 2 focuses on advancing the sustainability of alginate-based bioplastics, particularly those derived from kelp. The study investigates the recycling potential of alginate, aiming to enhance sustainable practices. Recycling alginate helps preserve resources by reintegrating used materials into the production cycle, reducing the need for fresh raw materials. Additionally, recycling alginate-based products reduces waste volume, supports waste reduction goals, and minimizes the environmental impact of landfill disposal.

The research in Chapter 2 builds on optimized sodium alginate extraction methods and evaluates the recycling potential of alginate films produced by these methods. It proposes and assesses a recycling protocol for its effectiveness in terms of yield and purity, focusing on calcium crosslinker removal and structural changes in alginate films. This study provides valuable insights into sustainable alginate recycling, promoting a circular economy by extending the life cycle of materials and reducing waste generation.

Although each chapter addresses different material types and applications, they share a common theme: enhancing material performance while mitigating environmental impact. Improving RO membrane fouling resistance and chemical stability directly contributes to reducing waste and energy consumption in water treatment. For alginate bioplastics, optimizing recycling processes ensures effective material reuse, decreasing plastic waste and the demand for new raw materials.

These projects reflect a broader commitment to sustainability by tackling critical issues in material performance and environmental responsibility. The outcomes from these chapters offer practical solutions that align with global efforts to conserve resources and minimize ecological footprints. Through the development of advanced membrane technologies and sustainable bioplastics, this thesis contributes to a more sustainable future, demonstrating that innovation in material science can drive significant improvements in both industrial applications and environmental stewardship.

In conclusion, this thesis bridges the gap between technological advancement and environmental sustainability. By addressing the challenges of water purification and plastic waste management, it provides valuable insights and practical solutions that enhance material performance and promote a more sustainable approach to resource use.

# Table of Contents

# List of Figures

## Chapter 1

**Chapter 2**

# List of Acronyms, Abbreviations, and Symbols

| | |
|---|---|
| 1H NMR | Hydrogen NMR |
| A | Area |
| AI, AII,AIII | Integration of the under peak area (in NMR) |
| ATR | Attenuated Total Reflectance |
| BSA | Bovine serum albumin |
| Ca | Calcium |
| $Ca^{2+}$ | Calcium ion |
| CaF | Normalized Wt.% of Ca in sodium alginate film |
| CaR | Normalized Wt.% of Ca recycled sodium alginate |
| CAS | Chemical Abstract Service |
| Cl | Chlorine |
| CNR | Surface cleaned membrane, modified with PEI-diazirine, cured, not rinsed |
| CR | Surface cleaned membrane, modified with PEI-diazirine, cured, rinsed |
| DI water | Deionized water with resistivity of 18.2 megohm |
| DSC | Differential Scanning Calorimetry |
| DTAB | A positively charged surfactant |
| EDS | Energy-dispersive X-ray spectroscopy |
| EDX | Energy-dispersive X-ray spectroscopy |
| ε | Tensile strain |
| EX | Kelp-extract sodium alginate (mix of 5 extraction series) |
| EXF | Hydrogel film of kelp-extract sodium alginate |
| F | Force acting |

| | |
|---|---|
| FG | Fraction of individual blocks of G-units |
| FGM/FMG | Fraction of heterogeneous blocks of alternating M and G units |
| FM | Fraction of individual blocks of M-units |
| FR | Flux reduction |
| FRR | Flux Recovery Ratio |
| FTIR | Fourier-transform infrared spectroscopy |
| G-block | Guluronic acid |
| GDL | Gluconic-delta-lactone |
| GPC | Gel Permeation Chromatography |
| Hz | Hertz |
| HV | High voltage |
| I-2 | Commercial sodium alginate from Kimica (Low G content) |
| I-2F | Hydrogel film of I-2 |
| I-2G | Commercial sodium alginate from Kimica (High G content) |
| I-2GF | Hydrogel film of I-2G |
| IP | Interfacial Polymerization |
| KV | Kilovolt |
| $L_0$ | Initial length of the sample |
| LCA | Life Cycle Assessment |
| M-block | Mannuronic acid |
| M/G Ratio | Mannuronic acid to guluronic acid ratio |
| M1 | Molecule1, See Fig 1.5 |
| MF | Material Flow Analysis |
| MG block | Alternating sequences of mannuronic and guluronic acid units (M-G-M-G-...) |

| | |
|---|---|
| mM | Millimolar |
| Mn | Number-average molecular weight (kDa) |
| MT | Mega tone |
| Mw | Weight average molecular weight (kDa) |
| NCNR | Surface cleaned membrane, modified with PEI-diazirine, not cured, not rinsed |
| NCR | Surface cleaned membrane, modified with PEI-diazirine, not cured, rinsed |
| NF membrane | Nanofiltration membrane |
| NG, NM | Average length of homopolymer blocks (MM, GG) |
| NMR | Nuclear Magnetic Resonance |
| PDA | Polydopamine |
| PDI | Poly dispersity index |
| PEG | Polyethylene glycol |
| PEI | Polyethyleneimine |
| PET | Polyethylene terephthalate |
| PHA | Polyhydroxyalkanoates |
| PLA | Polylactic acid |
| PVA | Polyvinyl alcohol |
| RI-2 | Recycled I-2 |
| RI-2F | Hydrogel film of recycled I-2 |
| RI-2G | Recycled I-2G |
| RI-2GF | Hydrogel film of recycled I-2G |
| REX-1 | Recycled EX, trial1 |
| REX-1F | Hydrogel film of REX-1 |
| REX-2 | Recycled EX, trial2 |

| | |
|---|---|
| REX-2F | Hydrogel film of REX-2 |
| RO | Reverse Osmosis |
| SA | Sodium alginate |
| SA | Surfactant |
| σ | Tensile stress (MPa) |
| STEHM | Scanning transmission electron holography microscope |
| TFC | Thin-film composite |
| Tg | Glass transition temperature |
| TPS | Thermoplastic starch |
| UV | Ultra Violet |
| W | Watt |
| W0 | Initial sample weight before drying (after conditioning) |
| Wd | Sample weight after the drying process |
| Wt.% | Weight percentage |
| XEDS | Energy-dispersive X-ray spectroscopy |
| XPS | X-ray photoelectron spectroscopy |
| $\eta$ | Block distribution |

# Acknowledgments

I extend my deepest gratitude to the individuals and institutions who have supported and guided me throughout the journey of completing this thesis:

Professor Heather Buckley: My heartfelt thanks to my supervisor, Dr. Heather Buckley for their exceptional guidance, unwavering support, and expert mentorship during the completion of this thesis. Their dedication to excellence and encouragement have profoundly influenced my academic journey. I am deeply appreciative of their invaluable insights, which have significantly enriched the quality of this research. I am truly fortunate to have had the opportunity to learn from their wisdom and expertise. I offer my sincerest thanks for their patience, belief in my abilities, and commitment to my success

Professor Onita Basu: I am indebted to my thesis Co-supervisor, Dr. Onita Basu, for their invaluable feedback, constructive criticism, and scholarly insights. Their expertise and dedication have significantly enriched the depth and rigor of this study.

Beloved family: I express my deepest appreciation to my beloved family for their unwavering love, support, and encouragement throughout this journey. Their constant belief in me has been a source of strength and motivation. I am grateful for their sacrifices and understanding during challenging times. Their presence in my life fills it with joy and warmth. To my family, I offer my heartfelt thanks for being my pillars of strength.

My heartfelt appreciation goes to my cherished friends from afar who are close to my heart, for their unwavering encouragement, camaraderie, and understanding during challenging times. Their friendship and solidarity have made me feel immensely blessed, knowing that I am surrounded by caring and supportive individuals, regardless of the physical distance that separates us.

I would like to express my deepest gratitude to Green, Safe Water Lab members for their invaluable support and collaboration throughout this journey. A special thanks to Hayley Smith for her insightful contributions and unwavering dedication, Kristen Aasen for her innovative ideas and encouragement during challenging times, and Grace Tieman for her meticulous attention to detail and consistent support. This work would not have been possible without their collective efforts and camaraderie.

I would also like to thank Dr. Stephania Musolino, Dr. Rashid Nazir, Dr. Elaine Humphrey, Christopher Barr, and Dr. Zhaoyang Yuan, whose extensive knowledge was invaluable to my work.

In closing, I extend my sincere thanks to all those who have played a part, however small, in the completion of this thesis. Your support, encouragement, and belief in my capabilities have been invaluable, and I am truly grateful for the opportunity to embark on this scholarly journey.

# Chapter 1: Advancing Reverse Osmosis Membrane Technology: Covalent Surface Engineering with Diazirine Linker for Enhanced Performance

## Abstract

This study examines a novel approach to enhance the surface properties of RO polyamide-based membranes by developing a covalent surface modification procedure. Surface modifications take place via the introduction of covalently bonded diazirine-containing molecules, and modified membranes are compared to not-modified RO surfaces. The primary objective of this study is to establish a foundation by demonstrating that diazirine does covalently attach to polyamide membranes and to establish the groundwork for further functionalization of polyamide membranes, specifically the introduction of foul resistance. The diazirine-containing polyethyleneimine (PEI-diazirine) reagent was employed in the surface modification process and activated using UV radiation. A comparative analysis using differential scanning calorimetry (DSC) was conducted to determine the most effective application method for the diazirine compound, which revealed that the one-side coating procedure outperformed the 24-well plate and soaking methods. Various analytical techniques were employed to assess the surface modifications of the RO membranes, including FTIR-ATR, water contact angle measurements, and dye tests. Furthermore, PET, a surface previously proven to form bonds with diazirine, was utilized as the control surface throughout the study to enable a comparative evaluation of the surface activity of both polyamide and PET towards diazirine. The findings of this study provide valuable insights into the development of surface modification techniques for polyamide membranes, paving the way for future advancements in enhancing their foul-release properties.

Keywords

• Polyamide

• Reverse Osmosis membrane

• Covalent functionalization

• Diazirine

## 1.1 Introduction

The increase in water demand due to population growth, industrialization, and the difficulty in responding to water demand caused by climate change justifies the need for sustainable technologies to address water shortages. [1,2]. According to the Canadian Safe Drinking Water Foundation[3], RO has been successfully used as a filtration technology for desalination to address long-term potable water demands. RO polyamide membranes are crucial in addressing water scarcity because they can produce freshwater from different water sources such as well water, surface water, Brackish water, and seawater [3,4]. Polyamide RO membrane systems are commonly applied in treating drinking water due to their high salt rejection capacity and broader operational pressure and pH compared to cellulose acetatemembranes[5,6]. Due to their capability of removing microorganisms, pollutants, and turbidity from any water source [5], the versatility of RO technology allows its application to smaller scales, such as buildings and villages, or larger scales, such as cities and industries [2,3,5–8]. RO offers the filtration currently available, rejecting most dissolved solids as well as suspended solids[5] (See Fig 1.1).

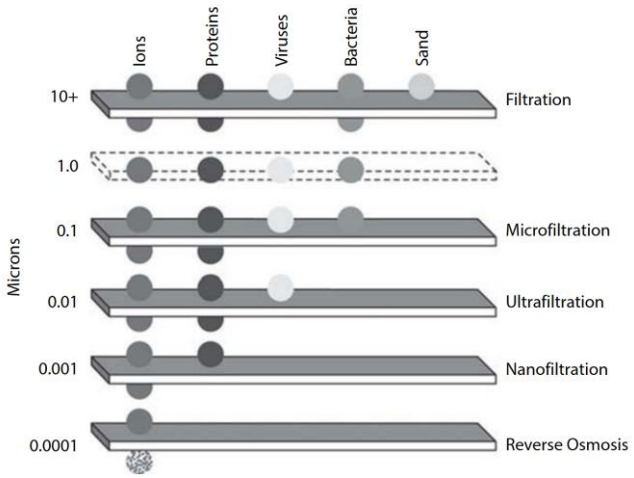


Figure 1.1 "Filtration Spectrum" comparing the rejection capabilities of reverse osmosis with other membrane technologies and with the separation afforded by conventional, multimedia filtration[5].

In addition to drinking water, RO is valuable for industries since it can be applied i) to treat wastewater, decreasing pollutant fluxes into water bodies, ii) to respond to water demand via water reuse, and iii) to recover nutrients from wastewater [8]. Despite the many advantages resulting from

the application of RO to produce fresh water, biofouling, and associated costs are the main barriers that hinder the popularization of this filtration technique [2,4,9].

Biofouling, characterized by forming a layer of microorganisms encased in extracellular polymeric substances (EPS), known as the biofilm matrix on RO membranes, poses a significant challenge[10]. RO membranes, even when fouled with a one-month-old biofilm, maintain performance levels comparable to those of membranes in use for five years[9]. As highlighted by Fazel and Darton [10] , biofouling is a leading cause of more than 60% of RO system failures, either as a primary or secondary contributing factor. The consequences of biofouling include diminished freshwater production, heightened operational pressure, reduced membrane lifespan, and increased demands on energy and operational costs[2,5,10].

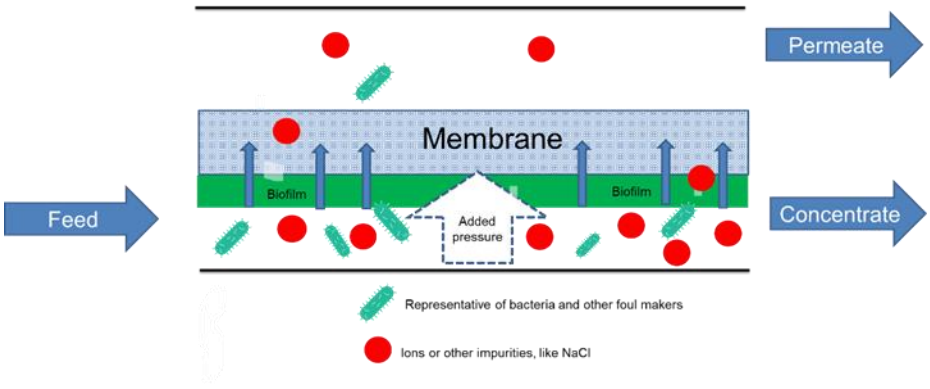


Figure 1.2 Schematic of Reverse Osmosis membrane in operation

Given the challenges outlined, it is imperative to enhance existing membrane technologies by improving membrane performance, durability, and resistance to biofouling. By increasing RO membrane performance robustness increased adoption of RO membranes in meeting escalating demand for potable water in both industrial and domestic applications may be realized.

To achieve enhanced membrane performance, two general methods for tailoring the properties of membranes have been implemented: (1) the additive blending technique and (2) surface modification of pre-formed membranes through surface modifying compounds. In the former technique, the membrane-modifying compounds are blended with membrane-forming polymers to synthesize membranes. This technique requires optimization of the membrane manufacturing process for further implementation in a large-scale production[11], making it an unfavorable approach.

On the other hand, the surface engineering approach employs surface-modifying reagents to alter the surface of a pre-formed membrane. In this technique, various surface modification techniques can apply surface-modifying reagents through grafting or coating onto a pre-formed membrane. This approach is convenient and more accessible to implement on a large scale to modify commercial membranes[11]. Strategies for the modification of membranes through a surface engineering approach include the construction of a super-hydrophilic surface layer[12], reduction of surface roughness[13], the introduction of an antibacterial layer[14], tailoring of electrostatic surface charge[15], and utilization of steric repulsion effect properties[16].

As an illustration, one suggested approach involves applying a layer of hydrophilic and electrically neutral material, such as polyvinyl alcohol (PVA). Commercially available antifouling reverse osmosis (RO) membranes, like BW30FR (FilmTec) and LFC3 (Hydranautics), have been identified to feature coatings comprising neutral PVA layers [17,18]. Compared to the unmodified membrane, the PVA-coated membrane consistently displays a smoother surface, increased hydrophilicity with reduced negative charge density, and improved antifouling and chlorine resistance properties.

Within hydrophilic polymers, PEG (polyethylene glycol) and its derivatives have undergone comprehensive investigation because of their recognized efficacy in resisting fouling [11]. An uncharged, water-soluble polymer, PEG features flexible long chains and a substantial exclusion volume. This composition is particularly effective in hindering the adsorption of hydrophobic or large molecules onto the surface of the membrane.

To enhance resistance to organic fouling, Jeffamine, an amine-terminated PEG derivative, was grafted onto the PA surface in situ using acyl chloride surface groups by Lu et al. [19]. Fouling studies conducted in cross-flow forward osmosis mode, utilizing synthetic wastewater containing surfactant and inorganic salts, reveal a significantly lower flux decline for the in situ modified membranes compared to the pristine PA ($2.8 \pm 1.4\%$ vs. $14.3 \pm 2.7\%$, respectively) and the fouled membranes after cleaning. Notably, the modified membrane completely recovered the initial flux. The modified membrane's antifouling property was attributed to the steric hindrance offered by PEG molecules, increased hydrophilicity (contact angle $< 20C^{o}$), and reduced surface area. A smaller surface area reduces the space available for this initial attachment of microorganisms, lowering the overall risk of biofilm establishment.

Polyethylenimine (PEI) is a cationic polymer with branched structures featuring primary, secondary, and tertiary amine bonds. Bera and Jewrajka undertook modifications on laboratory-made piperazine/trimethyl chloride nanofiltration (NF) membranes using PEI and its derivatives (PEI–PEG and PEI–dextran) to enhance monovalent-to-divalent ion selectivity and antifouling properties [20]. Evaluating the modified membranes' antifouling and anti-scaling properties involved a desalination experiment using seawater with $Na_2SO_4$ and bovine serum albumin (BSA). The Flux reduction (FR) and Flux recovery ratio (FRR) for the modified membrane were 12% and 90%, respectively, whereas for pristine membranes, they were 37% and 72%, respectively. The improved antifouling behavior was attributed to superior steric hindrance by PEI, PEG, and dextrin against organic foulants (BSA), the formation of hydration layers, reduced surface roughness, and the presence of residual carboxylic groups on the membrane surface.

Additionally, bio-inspired materials like polydopamine (PDA) were employed to graft PEI onto the PDA layer. For instance, reverse osmosis (RO) membranes with a polyamide (PA) active layer were modified using PDA-g-PEI, resulting in a membrane with 10–15% higher flux recovery Ratio (FRR) compared to native membranes after cleaning with a brine solution. However, this membrane exhibited a greater affinity for the positively charged dodecyl trimethylammonium bromide (DTAB) than the negatively charged bovine serum albumin (BSA) [21]. Alternatively, PEI was anchored to the PA surface through a secondary interfacial polymerization reaction between residual acyl chloride groups on PA and the primary amine groups of PEI [22]. The hydrophilicity and fractional free volume of the modified thin-film composite (TFC) membranes, which is the portion of a material's volume not occupied by its atoms or molecules, allowing space for molecular movement or diffusion, increased with the rise in PEI molecular weight, consequently enhancing water flux. All modified TFC membranes demonstrated superior anti-fouling behavior compared to the native TFC membrane when subjected to a wastewater filtration test containing surfactant (SA). This improvement can be attributed to enhanced hydrophilicity, fewer active complexation sites of carboxyl groups, and improved steric hindrance with PEI modification in the modified membrane.

RO membranes are typically composed of polyamide structures, inherently possessing limited active sites or functional groups for surface interactions (See Fig 1.3). By introducing additional

active groups, such as through surface modification techniques, the membrane surface can be endowed with enhanced properties beneficial for various applications.

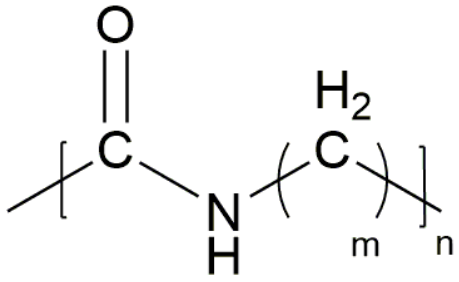


Figure 1.3 General structure of polyamide, For a typical RO membrane, m = 2-20, n = 50-200. ChemDraw 18.0

Diazirine is a chemical compound that generates reactive carbene species when exposed to heat or light. These reactive species have a remarkable ability to insert into specific types of bonds, including C–H (carbon-hydrogen), O–H (oxygen-hydrogen), and N–H (nitrogen-hydrogen), as demonstrated in literature [23].

The efficacy of diazirine cross-linkers capable of integrating into the robust secondary (2°) C–H bonds of PET[1] (See Fig 1.4) suggests that they would exhibit comparable or greater effectiveness than other polymer substrates. Most aliphatic polymers, excluding highly fluorinated materials such as Teflon, possess C–H bonds of similar or lesser strength (e.g., polypropylene, polystyrene). These polymers often contain O–H or N–H bonds that react faster with carbenes, as observed in polyalcohol or polyamides [23].

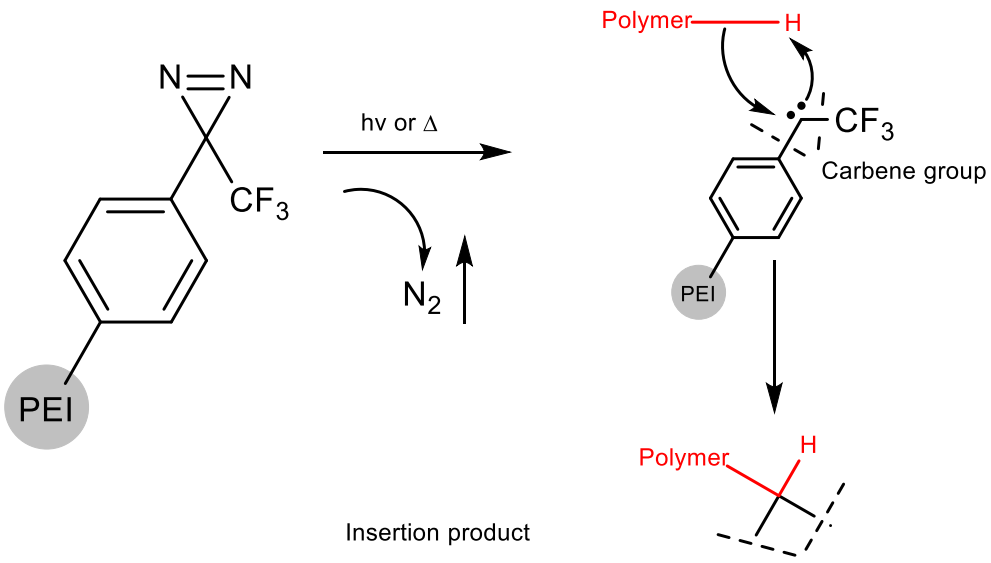


Figure 1.4 Schematic of PEI-diazirine reaction with C-H containing polymer, ChemDraw 18.0

When considering polyamide components commonly found in RO membranes, N–H and aliphatic C–H bonds are dominant chemical bonds relevant to this insertion chemistry. These bonds offer a promising avenue for modification using diazirine chemistry. Notably, the energy barriers associated with inserting N–H bonds are generally lower than those for inserting O–H and C–H bonds. This lower energy barrier suggests that the most probable reaction is the insertion into the N–H bond [1,24] (See Fig 1.5).

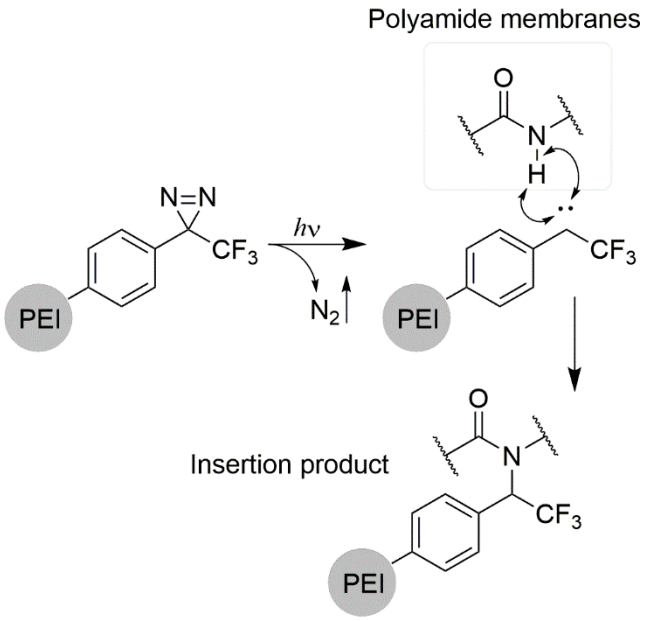


Figure 1.5 Diazirine activation and NH insertion reaction, ChemDrawreaction, ChemDraw18.00

To introduce additional active groups into polymers, various derivatives of diazirine-containing crosslinkers are use[25,26,27,28,1] and have been commercialized. For instance, consider Plastilynx, a product brought to market by XLYNX. These crosslinkers serve as a surface-activating primer, enhancing the adhesion of polyolefin materials. Another offering from the same company is Bodylynx, a line of diazirine molecular crosslinkers. These crosslinkers can usually bond unreactive polyolefins, reinforce polymer textiles, facilitate photo-patternable electronic applications, and contribute to the stability of organic electronics[29].

Singlet carbenes generated from the photochemical or thermal decomposition of diazirines represent an efficient C–H functionalization strategy for polymer cross-linking and biopolymer photoaffinity labeling[24,30].

In this study, it was decided to first test the attachment of PEI-diazirine onto PET surfaces, with the hypothesis that any success with cross-linkers identified in these trials would be broadly applicable to RO surfaces which are polyamide-based, based on the known reactivity of polyamides and carbenes[23]. The aim was to develop covalent modification of RO membranes using diazirine moieties to establish the foundation for further functionalization. Overall, improved

stability, durability, and compatibility make covalent bonding a favorable approach for surface modification of reverse osmosis membranes [31].

## 1.2 Methods

### 1.2.1 Chemicals

All chemicals were utilized in their original form without any further modifications. Polyethylene terephthalate (PET) sheets with a thickness of 0.254 mm were procured from McMaster Carr (8567k92). These PET sheets were cut by laser into circular shapes with a diameter of 15.6 mm. The TriSep ACM3 polyamide RO membrane was obtained from Sterilitech and similarly shaped into circular pieces with a diameter of 12 mm using a punching tool. The PEI-diazirine compounds, with 10 Wt.% and 30 Wt.% concentrations, and Molecule1 (see Fig 1.6), were contributed by XLYNX materials and were used as received.

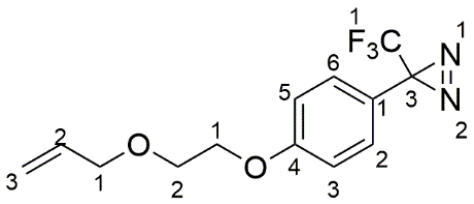


3-(4-(2-(allyloxy)ethoxy)phenyl)-3-(trifluoromethyl)-3*H*-diazirine

Figure 1.6 Molecule1, FTIR samples were mainly treated by this double bond-containing molecule, ChemDraw18.0.

PEI-diazirine synthesis is reported by Nazir et al. [1]. As noted, a commercially available branched polyethyleneimine (PEI) (average Mw 25,000 g/mol) in methanol (completely homogeneous by visual inspection after sonication) is prepared and bubbled with nitrogen or argon for 2 min. Then, the desired amount of 3-(4-(bromomethyl) phenyl)-3-(trifluoromethyl)-3H-diazirine (150 mg for 30 Wt.% and 50 mg for 10 Wt.%) is added dropwise, and the reaction mixture is stirred at room temperature for 72 h in the dark.The solvents are evaporated on a rotary evaporator at room temperature, covered by aluminum foil, and the product is dried under vacuum[1] (See Fig 1.7). The product is recovered as a viscous, colorless gel.

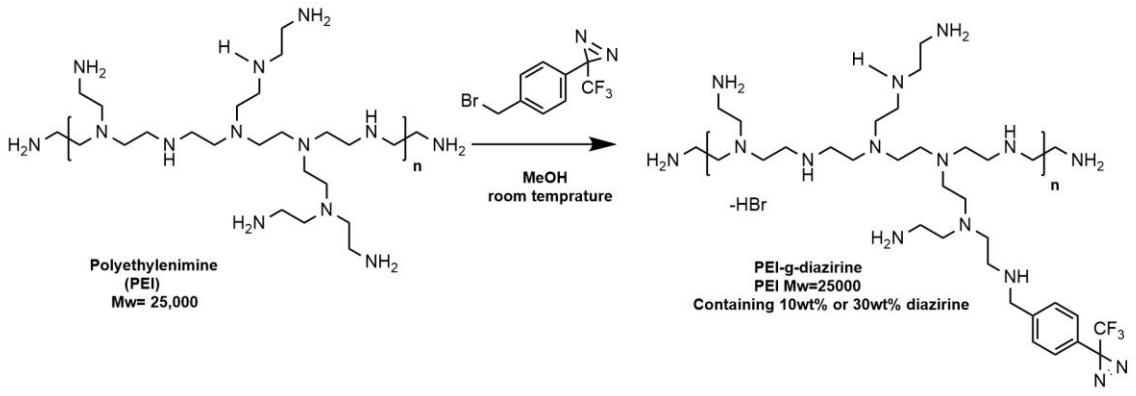


Figure 1.7 Synthesis of diazirine-Amine conjugates1, Re-drawn in Chem Draw 18.0

### 1.2.2 Surface Cleaning for PET and RO Membrane

To ensure the removal of undesired contaminants from the surface of the PET material, samples were subjected to a sonication process using sparkleen1 detergent/ DI water solution (one tablespoon (5 mL) per 3.78 L of DI water as instructed by the producer) and DI water for 20 min. This was followed by a rinsing step and another 20 min sonication using deionized (DI) water. Subsequently, the PET discs were gently wiped with a lint-free Kimwipe and placed in an oven at 130ºC for 20 min to facilitate drying.

Due to the polyamide membrane's porosity and to ensure the foam does not trap in pores, sparkleen/ DI water solution was eliminated from the cleaning procedure for the polyamide membrane. Samples underwent sonication for 20 min using DI water exclusively. After sonication, the samples were left to air-dry for a minimum of 4 h in an open-air environment under a fume hood. Subsequently, the semi-dried samples were stored in a desiccator, ensuring they were kept for no longer than 24 h before their utilization in the experimental procedures

### 1.2.3 sample design and codes

Table 1.1 summarizes sample designs and associated naming. All samples were cleaned as described in section 1.2.2. Details of the PEI-diazirine Treatment, UV curing, and Rinse are outlined in Sections 1.2.4 and 1.2.5.

Table 1.1 Cross-linking experiment sample design

| Sample | Sample description | PEI-diazirine Treatment | UV curing | Rinsing |
|---|---|---|---|---|
| **Blank** | Surface-cleaned membrane without any further processing | No | No | No |
| **NCNR** | The surface-cleaned membrane was modified with PEI-diazirine but not cured or rinsed. | Yes | No | No |
| **NCR** | Surface cleaned membrane, modified with PEI-diazirine, not cured, rinsed | Yes | No | Yes |
| **CNR** | Surface cleaned membrane, modified with PEI-diazirine, cured, not rinsed | Yes | Yes | No |
| **CR** | Surface cleaned membrane, modified with PEI-diazirine, cured, rinsed | Yes | Yes | Yes |

For Blank coupons, PEI-diazirine treatment was skipped, so there was no UV curing step or Rinse.

NCNR is the acronym used for the samples treated with diazirine compound but not UV activated, with no post-treatment rinsing step. CNR describes samples that were diazirine treated and UV activated, again with no post-treatment rinsing step.

NCR is used to code samples treated with diazirine compound without a UV activation step, which includes a post-treatment rinse. Lastly, CR is associated with diazirine-treated samples activated by UV radiation, followed by a rinsing step.

Both PET and RO samples used the same sample design and coding. Each experiment and characterization were conducted using triplicates of each sample design.

1.2.4 Light Source and Irradiation Parameters

To activate the diazirine, a UV chamber with the following specifications was used: a foil-lined box in which a 365 nm floodlight (realUV™ LED Flood Light, Waveform Lighting, 20W) was suspended 18 cm from the bottom of the box. Circular samples were arranged side-by-side (in single layers) at the bottom of the box for photocuring.

The photochemical activation rate of diazirine depends on the photon flux of the light source. The measured light intensity at the sample was 121 lx (1.26 W/m2); this modest light intensity mandated the use of crosslinking times over 30 minutes.

The same light activation setup was used for PET and RO membrane discs throughout the study.

### 1.2.5 Surface Modification Procedures

Two different procedures were studied to treat PET and polyamide RO membrane surfaces, described in sections 1.2.5.1 and 1.2.5.2, respectively. Ultimately, the one-side coating procedure was chosen over the soaking procedure for further experiments. The justifications behind this choice are reported in section 1.3.1.

#### 1.2.5.1 Soaking procedure

For each coupon (RO membrane/PET disc), 6 mg PEI-diazirine 30Wt% was dissolved in 1 mL of methanol. A micropipette was used to deposit 60 uL of this solution in each well of a 24-well with having 1 coupon in each well. Subsequently, the 24-well plate was placed in a VWR Analog Vortex mixer (speed 8) for 1 h. Following this step, samples with R (R: rinsing) code were washed by a VWR mini vortexer (see Fig 1.8). The coated coupons were allowed to dry for 2 h in a semi-dark environment within a fume hood. After drying, the samples were transferred to a desiccator to completely dry for 24 hours. The photocuring conditions were set to 30 minutes of exposure to UV radiation at a wavelength of 365 nm.

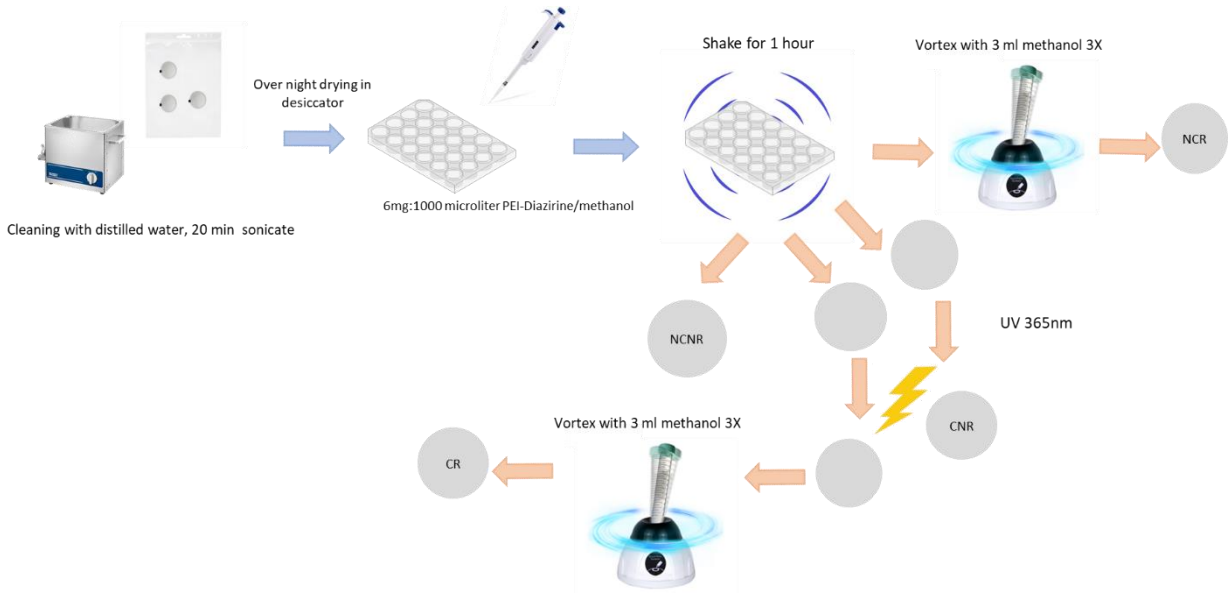


Figure 1.8Sample treating with diazirine compound, soaking approach

### 1.2.5.2 One-side coating surface modification procedure

For each coupon (RO membrane/PET disc), 6 mg PEI-diazirine30Wt% was dissolved in 1 mL of methanol. A micropipette deposited 30 uL of this solution on each coupon surface. Subsequently, methanol evaporated off the coupons for 5 min in a semi-dark environment in a fume hood. After drying, the samples were transferred to a UV box for photocuring. The photocuring conditions found to be sufficient (as measured by Differential Scanning Calorimetry, described below) were 30 min of exposure to UV radiation at a wavelength of 365 nm. Samples with R (R: rinsing) code were washed by a VWR mini vortexer (see Fig 1.9).

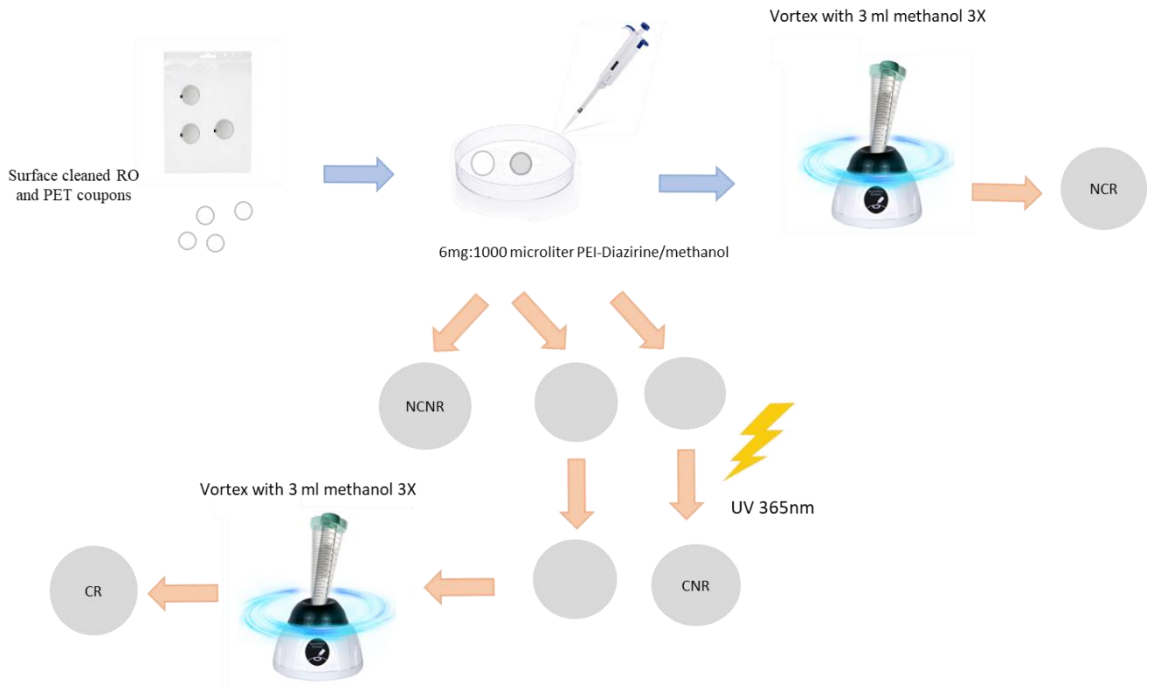


Figure 1.9 Sample treating with diazirine compound, One-side coating approach

1.2.5.3 DSC: a tool to decide on surface treating process

In this study, the efficacy of the soaking procedure was compared to that of one-side coating using DSC. Based on the results presented here, one-side coating was chosen to be applied to coupons further in the experiment. To consider the layered structure of polyamide membrane that can interfere with surface modification efficiency and provide misleading results, the soaking surface modification technique was compared with one-side coating, both tested by DSC.

In 1965, Mogan pioneered the development of composite TFC (Thin Film Composite) membranes using a novel approach called IP (Interfacial Polymerization) surface polymerization[32]. These membranes, characterized by their extremely thin separator layers, have found significant utility in various applications, particularly in water and wastewater treatment processes.

As shown in Figure 1.10, a typical TFC membrane has a multi-layered structure, usually consisting of one top PA selective layer, an intermediate porous polymeric membrane layer, and a base supporting substrate (such as non-woven)[33].

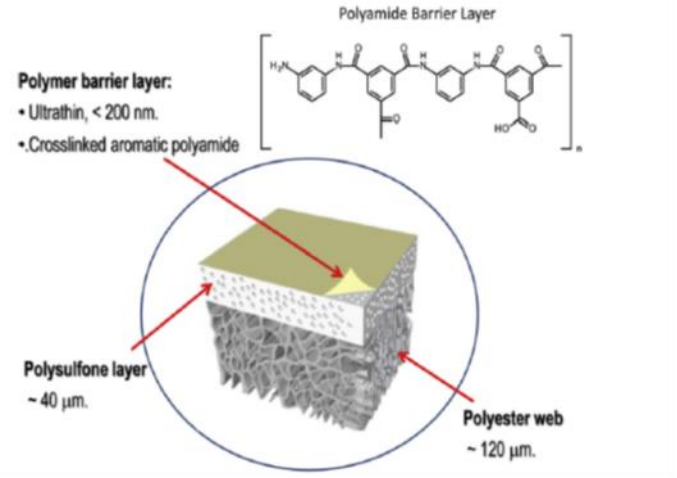


Figure 1.10 Schematic illustration of a TFC membrane, highlighting the different layers of the composite film; (Top) typical chemical structure of the cross-linked aromatic polyamide barrier layer[33]

It is predicted that in the soaking surface modification technique, due to porous supporting layers, surface modification reagents are absorbed in the bulk of the membrane rather than the surface, decreasing the efficiency of surface modification and providing misleading results.

To examine this hypothesis, the soaking procedure was compared to the side coating procedure, which modified the polyamide side of the membrane rather than exposing all layers to PEI-diazirine solution. Samples were chosen to be NCNR for both surface modification procedures and were tested byDSC. Sample preparation was conducted as described earlier in section 2.2 using PEI-diazirine 30Wt%.

In section 1.3.1.1, PEI-diazirine 10 and 30Wt% (in the absence of coupons) were compared in terms of thermal transition by DSC. PEI-diazirine 30Wt% was chosen to proceed with the experiment

1.2.6 Characterization of coupons

Characterization of coupons included a Dye test using Reactive Blue4, Fourier-transform infrared spectroscopy (FTIR), and contact angle test. Coupons were prepared as described in sections 1.2.2-1.2.4 and 1.2.5.2 the DSC was employed to conduct thermal transition analyses of the reverse osmosis membrane and PET samples. Surface analysis was carried out using the Holmarc Contact

Angle Meter and Aliant FTIR-ATR spectroscopy. The Reactive Blue4 (CAS#13324-20-4) dye with a dye content of 35% was procured from Sigma Aldrich.

1.2.6.1 DSC test on PET and RO membrane

Differential scanning calorimetry (DSC) is an analytical method to assess the heat exchange accompanying temperature-induced transformations in a specimen. This technique involves subjecting the sample to a controlled thermal regimen within a regulated atmosphere. In simpler terms, DSC facilitates controlled heating or cooling of a material while monitoring the energy flux resulting from its inherent physical or chemical alterations, manifesting as either energy absorption or release. Any phase transition or reaction that involves heat transfer and causes a change in heat flow, whether of an exothermic or endothermic nature, is detectable using DSC spectra [34]. Diazirine activation is an endothermic process that can be identified by an endothermic peak at about 137ºC [35] (see Fig 1.11).

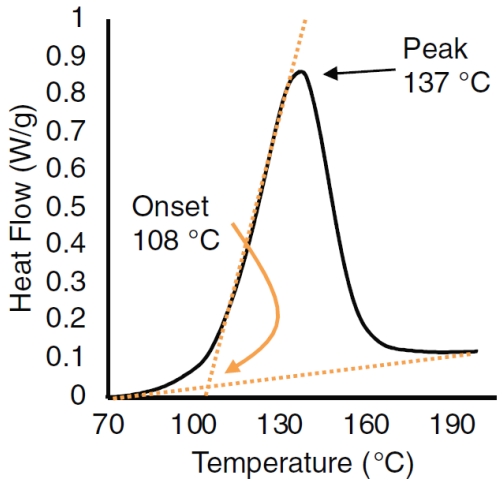


Figure 1.11 DSC indicating the onset and peak reaction temperature of the diazirine[35]

In this study, DSC has been extensively used to confirm the efficacy of the coating process, the satisfactory level of diazirine activation, and activation time. It has also been used to test the PEI-

diazirine concentration level needed for recordable activation. Each of the confirmatory tests mentioned is discussed in 1.3.1.

DSC pans (LOT 216647) and lids (lot 218336) were purchased from TA instruments. PET and polyamide circular samples (all sample codes listed in Table 1.1) were cut using a razor blade to fit the pan (6.2 mm diameter). DSC was also conducted on 10 and 30 Wt% PEI-diazirine itself. Each sample was weighed (at least 5 mg in each pan), the mass was input into the DSC software ( TRIOS35), and the heat flow was normalized to the weight (w/g). Each sample was sealed in a DSC pan using a Tzero DSC Sample Encapsulation Press. A disposable syringe needle was used to puncture the reference and sample pan to avoid seal breakage due to nitrogen gas release in the diazirine reaction (see Fig 1.12).

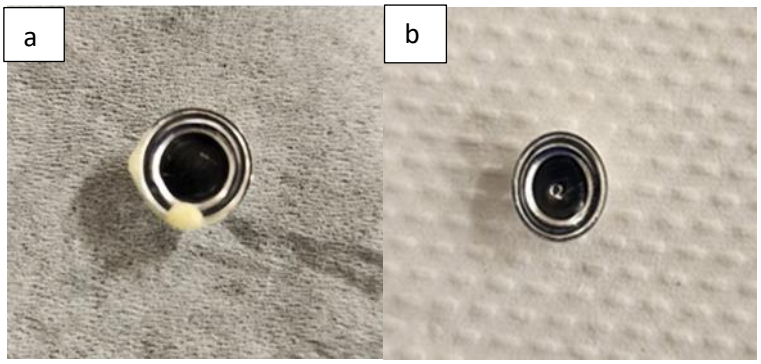


Figure 1.2 a. Diazirine-containing pan after DSC run, with no hole in lid b. Diazirine-containing pan after DSC run, with a hole in the lid

DSC was programmed to do two rounds of heating up to 180ºC and cooling down to 40 º C to make sure all the existing diazirine is activated (diazirine activation temperature ~ 137Cº); the absence of a peak indicates full activation of diazirine. DSC procedure is described in Table 1.2. The procedure remained the same for both PET and polyamide samples. DSC spectra were analyzed using TRIOS software.

Table 1.2 DSC employed procedure

| Steps | Description |
|---|---|
| 1 | Equilibrate 40.00 ºC |
| 2 | Isothermal 3.0 min |

| | |
|---|---|
| 3 | Ramp 10.00 ºC/min to 180.00ºC |
| 4 | Isothermal 3.0 min |
| 5 | Equilibrate 180.00ºC |
| 6 | Ramp 10.00º/min to 40.00ºC |
| 7 | Isothermal 3.0 min |
| 8 | Equilibrate 40.00ºC |
| 9 | Ramp 10.00ºC/min to 180.00ºC |

1.2.6.2 Dye test on PET and RO membrane

To study the attachment of diazirine to the surface, a staining technique was employed using Reactive Blue 4. The dye was expected to successfully stain samples already treated with diazirine and activated. In this case, the expected reaction for Reactive Blue4 was to react with available $NH_2$ groups of PEI and result in a saturated blue shade.

Reactive Blue4 contains two critical functional groups: a reactive group and a chromophore group. The reactive group is a reactive chloride group (-Cl) that can participate in nucleophilic substitution reactions with various nucleophiles [36].Under acidic conditions, the primary and secondary amine groups on the PEI are protonated, forming positively charged ammonium ions ($–NH_3^+$), which result in a positively charged membrane surface. This positively charged surface plays a crucial role in attracting anionic molecules like Reactive Blue 4, a dye that carries negatively charged sulfonate groups ($–SO_3^–$). The sulfonate groups on the dye are strongly attracted to the positively charged ammonium ions on the PEI-modified membrane through electrostatic forces. This electrostatic interaction ensures that the dye is closely held to the membrane surface[36], (See Fig 1.13 )

The absence of blue coloration in the samples indicates the lack of $NH_2$ groups, which suggests that PEI-diazirine was not present on the target surface. Our study anticipated that if PEI-diazirine was adequately activated and covalent bonds with PET and Polyamide discs formed, it would

remain on the surface even after the rinsing procedure. Essentially, the dye test we designed aimed to indirectly assess the presence of covalent bonds between the diazirine compound and the chosen surfaces.

The molecular weight of this dye was 637.43 g/mol 30 mL of methanol was used with 19.12 mg of dye to prepare the 1 mM dye solution. Each sample was immersed in the dye solution (using 24 well plates) for 5 min and then rinsed 3 times with methanol.

A dye test was conducted on the whole sample design set, as described in Table 1.2, for both PET and Polyamide membranes. The Blank control confirmed whether the dye reacts with the polyamide/PET without PEI.

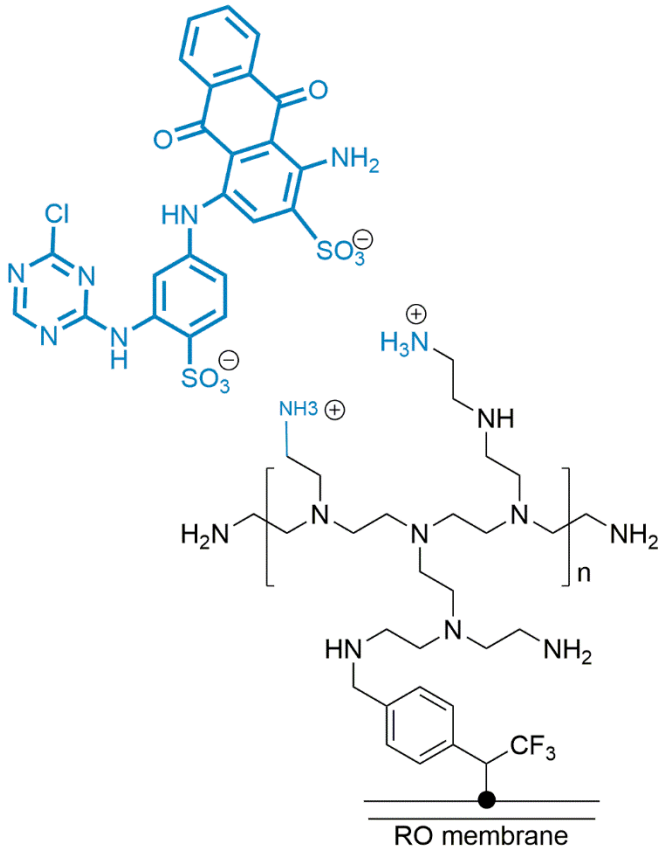


Figure 1.13 Reactive Blue4 molecule (shown in blue) reacted with surface-modified membrane.

The coupon staining procedure commenced with pre-cleaned coupons, as outlined in section 1.2.2. Every sample was coated on a single side using a 20 μL pipette and 30 μL of a 1 mM dye solution. The dye-coated coupons underwent a triple rinse with 3mL of methanol for each rinse, followed by three rounds of vortexing (3ml each time for 1 minute) using the same solvent.

After the rinsing step, PET coupons were dried under an extraction fume hood for 24 h, while RO membranes were moved to a desiccator after 4 hours of exposure to open air and left there for 20 h. The coupon staining procedure was applied to all sample designs for both PET and RO membranes. Qualitative results were recorded as photos from the Samsung S22 camera.

#### 1.2.6.3 Contact angle studies on PET and RO samples

Contact angle measurement has been widely used to characterize the properties of solid surfaces and study liquid–surface interactions[37].

The introduction of PEI-diazirine to both PET and RO surfaces increases surface polarity. As a result, the contact angle test using filtered water as the solvent was chosen to track the surface polarity change due to PEI-diazirine presence. Strip-shaped samples were prepared using a razor blade to have more droplets in one row without overlapping each other. The sample had dimensions of 0.8 cm ×3. 9 cm (see Fig 1.14). After cutting samples to the mentioned size, they were treated as described in sections 1.2.2-1.2.4 and 1.2.5.2 and then fixed on the edge of the glass slides (Fisher Brand). In most static contact angle measurements, the sessile drop is usually formed in an open lab atmosphere by gently dispensing the testing liquid through a micro syringe onto a horizontal solid surface using a motor-controlled dosing unit[39]. The droplet volume was chosen to be 0.002 μL to get a clear image within an acceptable size range for the camera to focus clearly. Unlike other hydrophilic surfaces, droplet shape and contact angle change over time. To make sure all pictures were taken simultaneously after contacting the surface, t=5 s after the water droplet touching the surface was chosen to take photos. There were 3 repeats for each sample design and

3 droplets per each, adding up to 9 spots per sample design. The contact angle instrument was Holmarc (model No: HO-1AD-CAM-01B), with a COS sensor and an imaging resolution of 2592 x 1944 pixels. Holmarc Contact angle measurement software was used to process images.

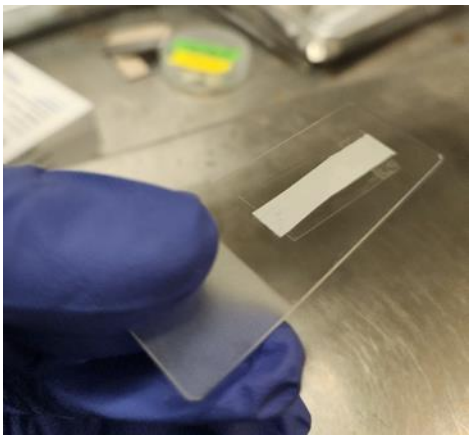

Figure 1.14 Strip-shaped polyamide sample

1.2.6.4 Fourier transform infrared (FTIR)

Fourier transform infrared (FTIR) is a spectroscopic technique commonly used to analyze the surface properties of materials, especially those that are difficult to analyze using traditional transmission methods. In FTIR-ATR, a sample is brought into contact with a high refractive index material (often a crystal) at a specific angle. This interaction between the sample and higher refractive index material allows for detecting evanescent waves that extend into the sample[39].

This study uses ATR-FTIR to assess the chemical composition of RO and PET surfaces due to surface functionalization using PEI-diazirine and Molecule1.

Circular coupons treated with 30Wt% PEI-diazirine and Molecule1 containing C=C bonds were prepared as described in sections 1.2.2-1.2.4 and 1.2.5.2. The procedure for preparing the sample was the same, except for the structure of the diazirine derivative. All sample designs (see section 1.2.3) were tested for PET and RO membranes. The Agilent Cary 630 FTIR setting was set on the transmittance mode with spectra range 650-4000 cm-1, 8 background scans, 12 sample scans, and 4 cm-1 resolution. Each circular coupon was tested in 3 spots. Agilent MicroLab FTIR Software was used for data processing.

To be able to intepertet and compare changes in peak intesities between different samples, peak intensities were normalized to a reference peak (e.g., a non-changing functional group) to account for sample or instrument variations.

## 1.3 Results and Discussion

### 1.3.1 DSC Result

The DSC results, which were used to decide on the surface treatment approach (soaking versus one-side coating) and justify diazirine attachment to PET and RO membrane surfaces, are presented in the 3.1 subsections.

#### 1.3.1.1 Effective PEI-diazirine Wt%

A pre-requirement to do DSC studies is to have a solid thermal transition that is detectable by the instrument and clear enough to make a comparison based on it. To trace the diazirine activation peaks by DSC, PEI-diazirine at Wt% of 10 and 30 were tested, in the absence of PET and RO discs. It was expected to have three-fold more activation heat for 30 Wt% PEI-diazirine than 10Wt% due to more diazirine activation. By comparing the resulting DSC spectra, it was possible to examine how the variation in PEI-diazirine concentration influenced the observed peaks and thermal behavior.

As depicted in Fig 1.15, the normalized enthalpy of activation for 30 Wt% PEI-diazirine is three times greater than that of 10 Wt% PEI-diazirine. This observation positions 30 Wt% PEI-diazirine as a preferable choice to ensure distinct DSC peaks in our subsequent thermal studies.

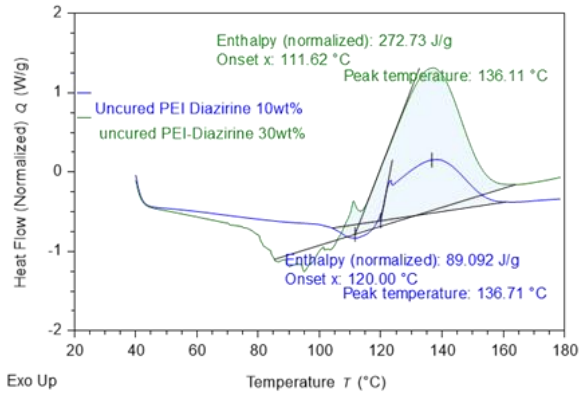


Figure 1.15 Comparison of DSC peaks for 10 and 30Wt% PEI-diazirine, Analyzed in TRIOS 5.1.1

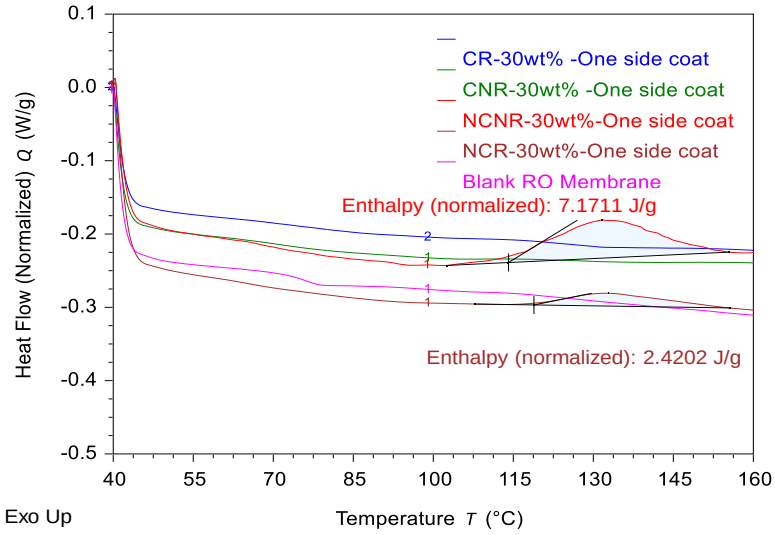


Figure 1.316 DSC spectra for RO samples treated with 30Wt% PEI-diazirine, one side coat, and UV cured for 30 min, Analyzed in TRIOS 5.1.1

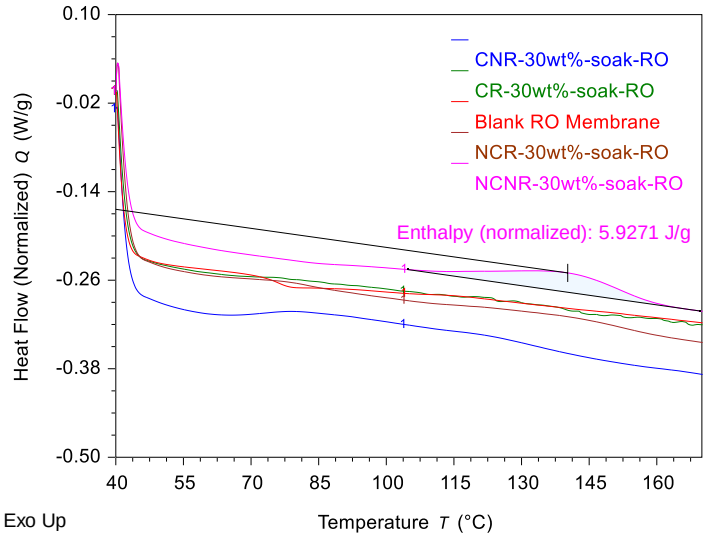


Figure 1.17 DSC spectra for RO samples treated with 30Wt% PEI-diazirine, soaked and UV cured for 30 min, Analyzed in TRIOS 5.1.1

In investigating diazirine activation enthalpy within two different diazirine treating approaches, the impact of one-side coating and soaking on enthalpic variations was studied. Unlike what was expected, there was no substantial difference in diazirine activation enthalpy between one-side coated and soaked samples (See Fig 1.16 and Fig 1.17). This challenges the initial assumption that diazirine compounds would be trapped in the membrane bulk in the soaking method.. DSC analysis indicates that the enthalpic behavior of diazirine activation remains largely unaffected by one-side coating or soaking. These findings provide valuable insights into diazirine-membrane interactions, emphasizing the necessity for further exploration of the underlying mechanisms.

### 1.3.1.2 Sample storage and surface treatment procedure time-length

An additional factor impacting the operational efficiency of surface modification procedures lies in the context of preparation and storage conditions.RO membranes are inherently prone to oxidative degradation. To minimize the degradation, membranes were stored in a desiccator. Diazirine is light sensitive, and for experimental designs where deliberate inhibition of diazirine activation is favored, prolonged exposure to light must be minimized for not cured samples (NC). Table 1.3 presents storage conditions and time for the soaking procedure and one-side coating.

Table 1.3 Sample diazirine treating soaking approach timeline

| Action | | Time | Atmospheric condition |
|---|---|---|---|
| **Absorbing PEI-Diazirine** | Soaking | 1 hour | Dark covered with foil under a fume hood (lid closed) |
| | One-side coating | 20 minutes | Open lid in Petri dish, under fume hood |
| **Drying off methanol** | Soaking | 2 hours | Dark covered with foil under a fume hood (lid open) |
| | One-side coating | At the same time as Absorbing PEI-Diazirine | Open lid in Petri dish, under fume hood |
| **Storage** | Soaking | 24 hours | Semi-dark, in a desiccator |
| | One-side coating | 0 | 0 |
| **DSC sample making** | Soaking | 5 min each sample | Semi dark |
| | One-side coating | 5 min each sample | Semi dark |
| **DSC sample storage** | Soaking | Short before test time (1 hour) | Dark in freezer |
| | One-side coating | 0 | 0 |

The extended duration of the soaking procedure could introduce errors by allowing uncured samples to remain exposed to the risk of activation before undergoing DSC analysis. This prolonged preparation time may lead to the activation of diazirine under ambient conditions, potentially affecting the reliability and accuracy of the DSC results. As presented in Table 1.3, one-side coating is a shorter procedure than soaking.

#### 1.3.1.3 Effective activation time

Polymers that contain O–H or N–H bonds exhibit faster reactivity with carbenes, as observed in polyalcohol or polyamides[24]. On the other hand, C-H insertion is the only available carbene incorporation possible for PET, so slower reactivity is expected. To determine the adequacy of a

30-minute curing time for achieving complete curing of the samples, both the RO and PET samples were subjected to this duration of curing. The DSC results for RO (see Fig 1.18) indicate that a 30-minute curing time was sufficient for the RO samples, as evidenced by the absence of a curing peak for already activated samples (CR, CNR). Similarly, for the same activation time and the same Wt% of PEI-diazirine, no activation peak was observed for PET samples (NCR, NCNR).

DSC failed to detect any thermal transition related to diazirine activation for NCR and NCNR PET samples (see Fig 1.19). The endothermic peak at 120 ºC is the cold crystallization peak of PET. Cold crystallization occurs above Tg when the polymer chain gains sufficient mobility to arrange itself into the ordered structure (i.e., crystalline structure) by chain folding[40].

The absence of diazirine activation peaks can be attributed to insufficient diazirine insertion reactions to PET during the DSC scan, which made the activation peak undetectable by DSC. As a further suggestion for the experiment, the same experiment can be done using higher concentrations of PEI-diazirine to see if DSC can detect the activation peak of diazirine.

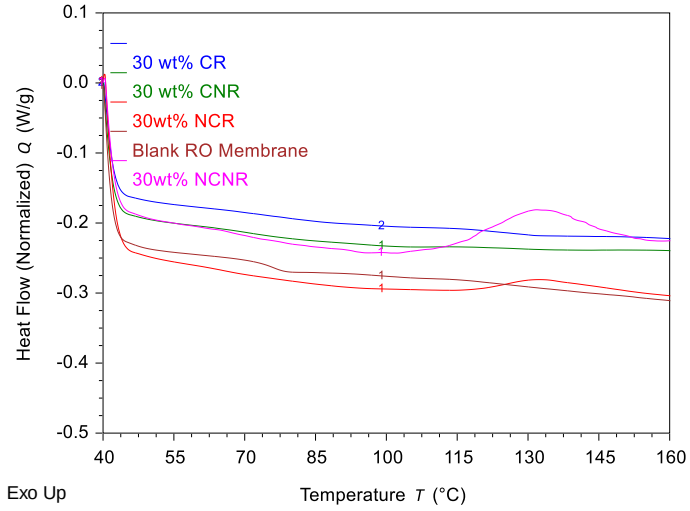


Figure 1.418 DSC result for 30 Wt% PEI-diazirine treated RO membrane, one side coat, already cured samples were UV activated for 30 min, Analyzed in TRIOS 5.1.1

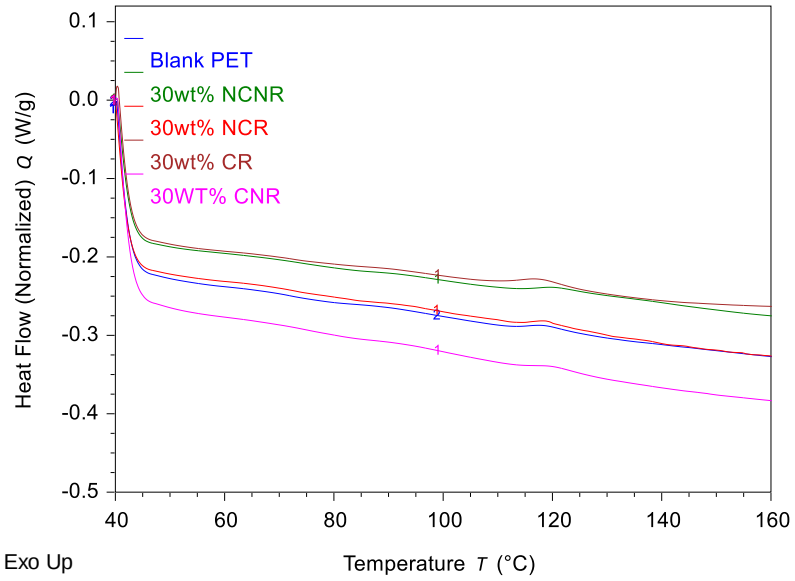


Figure 1.5 30 Wt% treated, one side-coat PET coupons, already cured samples were UV activated for 30 min, Analyzed in TRIOS 5.1.1

Based on studies conducted in section 1.3.1, a one-side coating procedure was chosen to be used throughout the project, using 30Wt% PEI-diazirine and 30 minutes of UV radiation for the diazirine activation process.

### 1.3.2 Dye attachment to coupons

The qualitative assessment of PEI-diazirine stability on PET and RO membrane discs during the rinsing procedure was conducted using a Dye test with Reactive Blue4 dye. The experimental results are presented in Fig 1.20 for PET and Fig 1.21 for RO membranes.

In the case of PET coupon discs, clear colorless samples were obtained for Blank PET, attributed to the absence of $NH_2$ groups. In Fig 1.20, Samples d (CNR) and e (CR) exhibited a similar bluish appearance with reduced transparency. The test did not discern the notable difference in color saturation and transparency between d and e, which indicates the PEI-diazirine group's insertion to the surface rather than bonding to each other. This observation supports a high degree of diazirine insertion into the PET surface, resulting in not losing shade during rinsing.

As shown in Fig 1.20, PET coupons b (NCNR) and d (CNR) were expected to exhibit similar appearances since both had PEI-diazirine groups remaining on the surface (regardless of whether they had been cured or not) as a result of not undergoing the washing process in sample diazirine treatment. However, this expectation was not met.

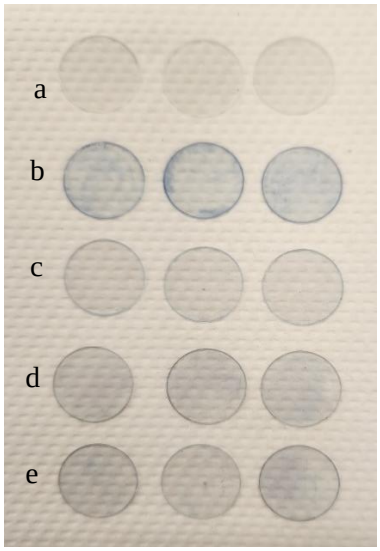


Figure 1.20 Dye test result on PET discs: a) Blank PET, b) NCNR, c) NCR, d) CNR, e) CR

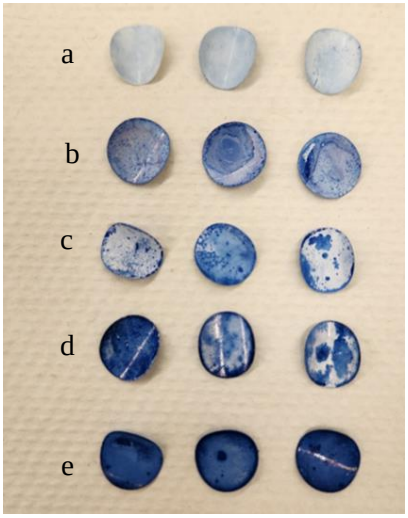


Figure 1.21 Dye test results for RO discs: a) Blank RO, b) NCNR, c) NCR, d) CNR, e) CR

In Fig 1.21, the blank RO membrane exhibited a light blue color. The color saturation increased after introducing PEI-diazirine to the surface in sample b (NCNR). However, in sample c (NCR), the color decreased, indicating that the PEI-diazirine was not cured and rinsed away.

Although sample d (CNR) results are inconsistent, they generally showed high color saturation compared to not-cured samples (b and c), which supports the PEI-diazirine insertion into the RO membrane.

Having the highest color saturation in sample e (CR) and the comparison to sample b (NCNR) indicates the effect of curing on PEI-diazirine insertion and, as a result, having Reactive Blue4 highly bonded to the surface in sample e.

The results of the d series of RO samples were somewhat inconsistent but generally darker than those of the not-cured samples. This suggests that some PEI-diazirine groups left the surface during the washing-off-the-dye step within the dye test process, likely due to some portion of diazirine compounds bonding together rather than to the surface.

Generally, the Dye test results cannot be used solely to conclude PEI-diazirine attachment to PET and polyamide surface and must be accompanied by other characterization methods.

### 1.3.3 Water contact angle result

As described in the methods section, the hydrophilicity of strip-shaped samples of the PET and RO membrane was tested using filtered water. Photos were taken at t=5 s and analyzed with contact angle meter software by Holmarc version 8.0.0.0. Table 1.4 presents the data and the accuracy of measurements. The contact angle measurement was done in triplicate for each sample design, with 3 spots per sample (3×3 water angle measurements).

Table 1.4 Data and Standard deviation (STE.DEV) of contact angle measurements for both PET and RO surfaces

| Coupon | Blank | CNR | CR | NCNR | NCR |
|---|---|---|---|---|---|
| RO | 71.20±1.27 | 45.75±3.70 | 60.37±2.33 | 45.75±1.15 | 59.81±0.65 |
| PET | 64.84±1.63 | 33.07±1.15 | 54.22±1.46 | 32.22±3.25 | 32.39±2.86 |

Contact angles for PET and RO samples were compared. PET, a polyester derived from ethylene glycol and terephthalic acid, is characterized by a nonpolar structure and is generally hydrophobic. In contrast, polyamide, a class of polymers containing amide linkages in their repeating units, can exhibit variable hydrophilicity. Polar amide groups facilitate interactions with water molecules, contributing to increased hydrophilicity in some polyamides [41–43]. As shown in Fig 1.22, introducing PEI-diazirine decreased the contact angle of all samples regardless of the surface type but had a more substantial effect on RO samples. Comparing CR samples with CNR for RO membrane suggests that some of the PEI-diazirine moieties were bonded together rather than the surface and left the surface during the rinsing step, resulting in a higher CR contact angle than CNR. Since the contact angles for CR and NCR are remarkably the same in the case of PET samples, PEI-diazirine insertion into PET was not supported by the water contact angle test.

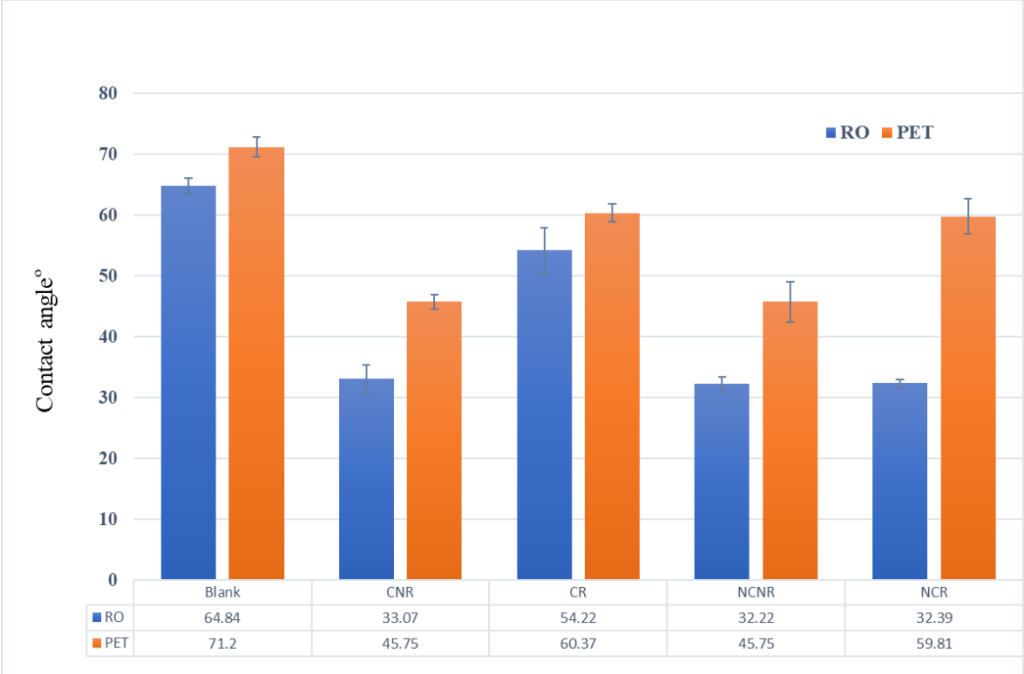


| | Blank | CNR | CR | NCNR | NCR |
|---|---|---|---|---|---|
| RO | 64.84 | 33.07 | 54.22 | 32.22 | 32.39 |
| PET | 71.2 | 45.75 | 60.37 | 45.75 | 59.81 |

Figure 1.22 Contact angle measurements for PET and RO samples

### 1.3.4 FTIR-ATR results

FTIR-ATR analysis was performed on the RO membrane surface treated with 30Wt% PEI-diazirine. Subsequently, this treatment was substituted with Molecule1. Due to substantial spectral

overlaps between the FTIR spectra of polyamide surfaces and Polyethylenimine, the interpretation of the FTIR spectra became intricate. As a result, a decision was made to explore the bonding capacity of the RO membrane and PET to diazirine using Molecule1 as well.

As shown in Fig 1.23, the starred peak at 3335 cm-1[44] is a characteristic peak for all synthetic membranes due to the N-H stretching vibration band, typically found in cross-linked PA layers. A decrease in intensity of this peak was observed for diazirine-treated samples; this can be due to diazirin insertion reactions. The peak at 1650 cm-1[44] depicts the C=O stretching vibrations of amide[45], highlighted in grey. An increase in C=O stretching peak intensity in PEI-diazirine treated samples suggests the formation of covalent amide bonds between amide functional groups of polyamide (-CONH-) and PEI-diazirine leading to the introduction of additional carbonyl groups.

Although PEI does not directily introduce carbonyl groups, but it can go through secondary reactions with oxidative agents leading to formation of carbonyl groups.

The yellow highlighted region in the same FTIR diagram shows the disappearance of a peak shoulder at 1582 $cm^{-1}$ due to treating RO membrane with PEI-diazirine.. The peak itself represents the aromatic C=C stretching within the benzene ring, while the shoulder is attributed to the secondary amide bonds. The disappearance of the shoulder, which is related to the amide bond, can be explained by the insertion of diazirine N-H, indicating the covalent bonding between PEI-diazirine and the polyamide surface.

To overcome this overlap, Molecule1 was chosen for PET and polyamide surface treatment instead of PEI-diazirine, and ATR was repeated.


Figure 1.23 FTIR-ATR result for 30Wt% PEI-Diazirine- treated RO samples, Normalized to max transmittance intensity at 558 cm-1

As a reference, FTIR-ATR was conducted on Molecule1 (See Fig 1.24). The prominent characteristic peaks are 2866 and 2922 cm-1[46], attributed to stretching vibrations of carbon-hydrogen bonds in the allyl and aromatic parts of Molecule1. The peak at 1610 $cm^{-1}$ also corresponds to the stretching vibration of the carbon-carbon double bond in the allyl group. The peak at 1140 $cm^{-1}$[47] is associated with the stretching vibration of the carbon-fluorine bond in the trifluoromethyl group.

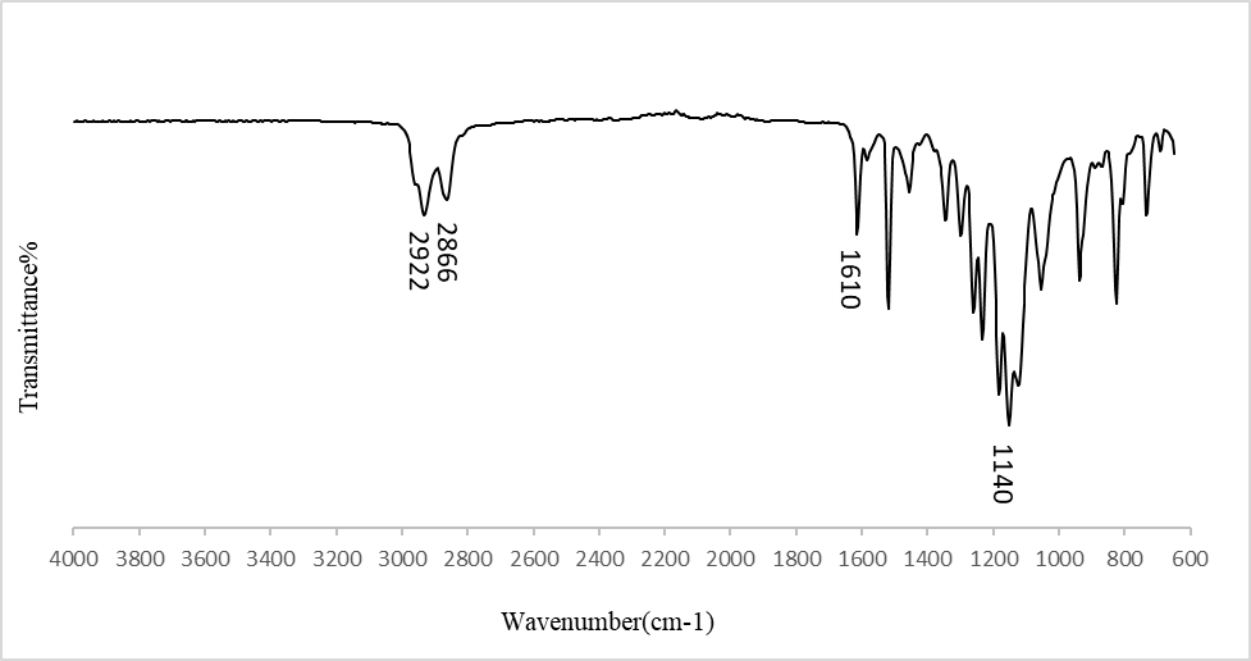


Figure 1. 24 FTIR spectra of Molecule1

Figs 1.25 and 1.26 present the FTIR results of PET and polyamide membranes treated with Molecule1, respectively.

For the PET surface (Fig 1.25), a characteristic peak is present at 2862 cm-1[46], which is distinctive for the sample code of CNR-M1-PET. This peak can be attributed to stretching vibrations of carbon-hydrogen bonds in the allyl and aromatic parts of the Molecule1.

As it is supported by the increased intensity of the 2860 $cm^{-1}$ peak for CNR-M1, it can be interpreted as the presence of M1 on the surface, whether they are inserted into the PET as a result of diazirine activation or diazirine bonding to each other and not leaving the surface since it is an unrinsed sample. Looking at NCNR, the same peak (2860 cm-1) shows an increase in intensity to a lower extent compared with CNR, which can also be attributed to carbon-hydrogen bonds in the allyl and aromatic part of Molecule1. Other than that, the ATR results for PET samples failed to provide substantial proof of the diazirine insertion. In the case of polyamide, diazirine insertion was not strongly confirmed by the resulting peaks, as was the case with the FTIR result for PET.

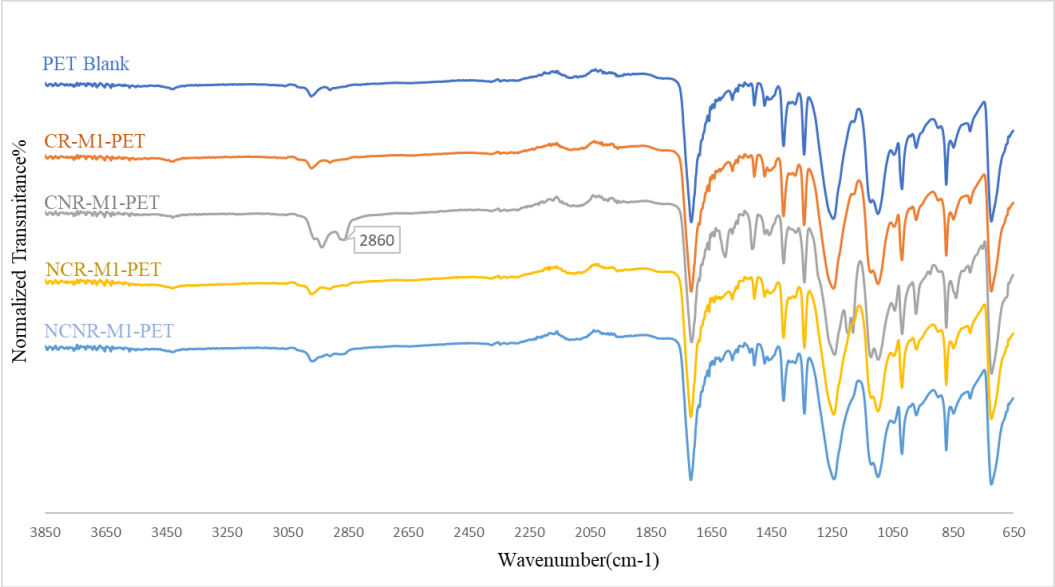


Figure 1.25 FTIR-ATR results for Molecule1-treated PET surface (M1:Molecule1), Normalized to max transmittance intensity, at 1716 cm-1

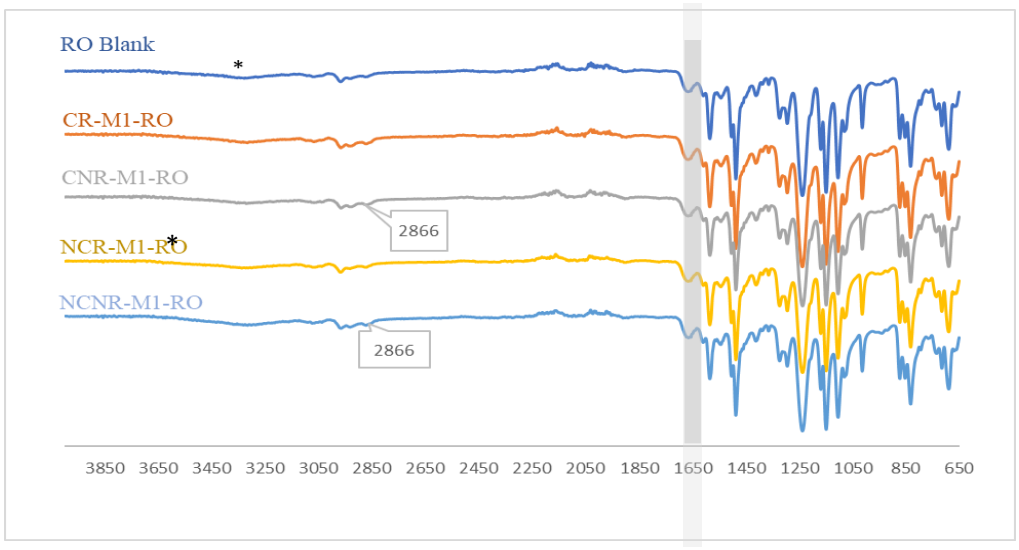


Figure 1.26 FTIR-ATR result for Molecule1 treated RO membrane surface, (M1: Molecule1), Normalized to max transmittance intensity, at 1237 cm-1

As shown in Fig 1.26, the starred peak at 3335 cm-1[44], which is the characteristic peak for all the synthetic membranes due to the N-H stretching vibration band, did not change in intensity among

different sample designs, which can be due to minimal diazirine insertion into the PA surface. The peak at 1650 cm-1[44](highlighted in grey) depicts the C=O stretching vibrations of amide, which also did not experience much change and can be interpreted as covalent amide bonds not forming between polyamide (-CONH-) group, which is highlighted in grey. An increase in 2866 $cm^{-1}$[46] peak is observed for NCNR and CNR samples, which can be attributed to stretching vibrations of carbon-hydrogen bonds in the allyl and aromatic parts of the Molecule1.

Table 1.5 summarizes the characterization methods used, their aim, and the central understanding of each conducted experiment.

Table 1.5 Result Summary

| Method | Aim | Observation | Overall objective support |
|---|---|---|---|
| **Differential scanning calorimetry** | Choose the surface treatment method by comparing the soak vs. one-side coating method. Study and decide on adequate diazirine activation time and PEI-diazirine Wt% for further steps in this study. | One side coating was a more efficient way to do surface treatment. Minimized sample preparation time and limited the treatment to polyamide surface rather than the other supporting membrane layers was observed. PEI-diazirine 30Wt% was shown to provide detectable activation peaks in DSC. 30-minute UV curing was found to be adequate to activate the diazirine compound regardless of the surface vitiation | The DSC results were used to decide the surface treatment methodology, including the surface coating method, diazirine compound weight percentage, and activation time. Based on these results, one-side coating, 30Wt% PEI-diazirine, and 30 min activation were chosen. |
| **Dye attachment test** | Indirect study of the diazirine compound interaction with both PET and RO surface. A qualitative study of | There needed to be more consistency in color shade within sample designs. However, samples with activated diazirine generally | The observation supports the possibility of diazirine moieties bonding together instead of bonding with the surface. This agrees with the change in surface |

| | | | |
|---|---|---|---|
| | potential covalent bonding. The remaining effect of PEI-diazirine on Dye attachment after activation and rinsing will support the existence of covalent bonds between diazirine compound and surfaces and not just to other diazirine-containing molecules. | resulted in a darker blue shade. Activated samples with no rinsing procedure (CNR) showed the darkest shade. | chemistry due to diazirine insertion on polyethylene and polyamide surfaces. And polyamide surfaces while supporting the possibility of diazirine moieties bonding together rather than the surface. This observation agrees with the change in surface chemistry due to diazirine insertion. |
| **Water contact angle** | Study surface characteristics change as a result of diazirine treatment. The remaining effect of PEI-diazirine on surface hydrophilicity after activation and rinsing will support the exitance of covalent bonds between diazirine compounds and surfaces, not just to other diazirine-containing molecules. | The introduction of PEI-diazirine induced a decrease in contact angles across all samples, regardless of surface type, with a particularly pronounced effect observed in RO samples. Upon comparing C/R samples with CNR, it was discerned that specific PEI-diazirine moieties underwent intermolecular bonding rather than surface attachment. Consequently, during the rinsing step, these moieties disassociated from the surface, culminating in an elevated C/R contact angle compared to C/NR. | This observation shows diazirine compound covalent bonding to PET and polyamide surfaces while supporting the possibility of diazirine moieties bonding together rather than the surface. Overall, this observation provides proof of surface chemistry changes due to PEI-diazirine bonding to the surface. |

| | | | |
|---|---|---|---|
| **Fourier Transform Infrared Spectroscopy** | ATR-FTIR is used to assess the chemical composition of RO and PET surface surfaces due to surface functionalization using PEI-diazirine and Molecule1. The remaining effect of the diazirine compound on surface chemistry after activation and rinsing will support the existence of covalent bonds between the diazirine compound and surfaces, not just to other diazirine molecules. | Due to the similarity of the polyamide membrane's primary and secondary amines to PEI peaks, FTIR peaks at lower wavelengths are not helpful to analyze. The FTIR results for PET samples failed to provide further proof of the diazirine insertion. In the case of polyamide, PEI-diazirine insertion was confirmed by the resulting peaks, while FTIR failed to provide evidence for the case of PET. | The FTIR(ATR) result did provide sufficient evidence to support the covalent insertion of diazirine into the PA surface while the evidence was not sufficient for case of PET. |

## 1.4 Conclusion

In conclusion, this study introduced an innovative approach aimed at augmenting the surface properties of reverse osmosis (RO) polyamide-based membranes. The focus of the study was on advancing surface modification procedures through the incorporation of covalently bonded diazirine-containing molecules. The key objective was to establish a foundational understanding, demonstrating the successful covalent attachment of diazirine to polyamide membranes. This groundwork sets the stage for subsequent functionalization processes to impart foul-release properties to the reverse osmosis membrane surface. Although we could not prove the covalent attachment, we did have (indirect) observations that can support the presence of activated diazirine on the surface. The dye and water angle tests disproved the idea that diazirine molecules react exclusively to each other rather than the surface.

DSC was primarily implemented to study diazirine crosslinking in the soak method versus the one-side coating method of sample treatment and optimize the appropriate weight percentage of the used diazirine and activation time. DSC supported 30Wt% diazirine, the 30-minute activation time, and the one-side coat method, which was chosen over other variations.

A Dye test using ReactiveBlue4, Water contact angle, and FTIR-ATR was conducted to study diazirine insertion into PET and polyamide surfaces.

The dye test observation suggests that not all PEI-diazirine groups were inserted, and some left the surface during the rinsing step. Therefore, the dye test cannot be used alone as proof of diazirine insertion and needs to be accompanied by quantitative characterizations.

The addition of PEI-diazirine caused a decrease in the contact angle for all samples, showing that it interacted with the surfaces. This effect was more noticeable in RO samples. The reduced contact angle in CR samples suggests that diazirine is incorporated into the surfaces rather than bonding with nearby diazirine active sites.

Although FTIR demonstrated limited efficacy in corroborating the formation of diazirine chemical bonds on PET and polyamide surfaces, further characterization through advanced analytical techniques such as X-ray photoelectron spectroscopy (XPS) and nuclear magnetic resonance (NMR) is suggested for future studies. These techniques can offer detailed insights into the

chemical modifications occurring at the molecular level. XPS can provide information about the surface's elemental composition, chemical states, and bonding environments, confirming the presence of new elements or shifts in binding energies. XPS can compare diazirine-treated membrane surfaces with control samples and analyze binding energy shifts corresponding to relevant elements (e.g., N, C, O). Looking for new peaks ( Flourine element) or changes in peak intensities ( decreasing impact on O,C and increasing impact on N) indicating chemical modifications and quantifying elemental compositions for treated and untreated samples is a valuable study using XPS. On the other hand, NMR spectroscopy, especially solid-state NMR in the case of polymer interactions, can elucidate changes in the local environment of specific nuclei, revealing alterations in molecular structures and potential interactions between functional groups. Comparing results for treated polyamide membranes with blank control samples provides information on chemical shifts, peak intensities, and new peaks indicating covalent bond formation and evaluating coupling constants and peak patterns for structural details.

These complementary techniques allow validation of the proposed chemical reactions and understanding of the intricate surface modification between the polyamide membrane and diazirine-containing compounds.

## 1.5 References


(1) Nazir, R.; Bi, L.; Musolino, S. F.; Margoto, O. H.; Çelebi, K.; Mobuchon, C.; Takaffoli, M.; Milani, A. S.; Falck, G.; Wulff, J. E. Polyamine–Diazirine Conjugates for Use as Primers in UHMWPE–Epoxy Composite Materials. *ACS Appl. Polym. Mater.* **2022**, *4* (3), 1728–1742. https://doi.org/10.1021/acsapm.1c01577.

(2) Zhao, S.; Liao, Z.; Fane, A.; Li, J.; Tang, C.; Zheng, C.; Lin, J.; Kong, L. Engineering Antifouling Reverse Osmosis Membranes: A Review. *Desalination* **2021**, *499*, 114857. https://doi.org/10.1016/j.desal.2020.114857.

(3) Hock, J. *Water Walk : A Research-Driven Guide to Clean Water in Indigenous Communities*. https://doi.org/10.14288/1.0397283.

(4) *Membranes | Free Full-Text | Biofouling of Water Treatment Membranes: A Review of the Underlying Causes, Monitoring Techniques and Control Measures*. https://www.mdpi.com/2077-0375/2/4/804 (accessed 2023-08-30).

(5) *Reverse Osmosis: Industrial Processes and Applications, 2nd Edition | Wiley*. https://www.wiley.com/en-au/Reverse+Osmosis:+Industrial+Processes+and+Applications,+2nd+Edition-p-9781119145776 (accessed 2023-08-30).

(6) *Irrigation Water Demand Model as a Comparative Tool for Assessing Effects of Land Use Changes for Agricultural Crops in Fraser Valley, Canada*. https://www.scirp.org/journal/paperinformation.aspx?paperid=111504 (accessed 2023-08-30).

(7) *Combination of cupric ion with hydroxylamine and hydrogen peroxide for the control of bacterial biofilms on RO membranes - ScienceDirect*. https://www.sciencedirect.com/science/article/abs/pii/S0043135416309484?casa_token=lxWghpeEx-AAAAAA:tNu2jrmEIu9ytUS_wuPfr2Owenn9FlQSUV1sVxysAHVS_dB6Up4cGWn0nVyDAMJbRn-v6I151i4 (accessed 2023-08-30).

(8) Bastos, P. D. A.; Santos, M. A.; Carvalho, P. J.; Velizarov, S.; Crespo, J. G. Pilot Scale Reverse Osmosis Refinery Wastewater Treatment – a Techno-Economical and Sustainability Assessment. *Environ. Sci.: Water Res. Technol.* **2021**, *7* (3), 549–561. https://doi.org/10.1039/D0EW00936A.

(9) *Membranes | Free Full-Text | Biofouling of Polyamide Membranes: Fouling Mechanisms, Current Mitigation and Cleaning Strategies, and Future Prospects*. https://www.mdpi.com/2077-0375/9/9/111 (accessed 2023-08-30).

(10) *M. Fazel and E. D. Darton, "A Statistical Review of 150 Membrane Autopsies," in Proceedings of the 62nd Annual International Water Conference, Pittsburgh, PA, USA, 2001, pp. 21–25.* ZjaHJvbWUqBggAEEUYOzIGCAAQRRg7MgYIARBFGDzSAQc5NDZqMGo3qAIAsAIA&sourceid=chrome&ie=UTF-8 (accessed 2023-12-11).

(11) *Antifouling, fouling release and antimicrobial materials for surface modification of reverse osmosis and nanofiltration membranes - Journal of Materials Chemistry A (RSC Publishing)*. https://pubs.rsc.org/en/content/articlelanding/2018/ta/c7ta08627j/unauth (accessed 2023-08-30).

(12) Liang, S.; Kang, Y.; Tiraferri, A.; Giannelis, E. P.; Huang, X.; Elimelech, M. Highly Hydrophilic Polyvinylidene Fluoride (PVDF) Ultrafiltration Membranes via Postfabrication Grafting of Surface-Tailored Silica Nanoparticles. *ACS Appl. Mater. Interfaces* **2013**, *5* (14), 6694–6703. https://doi.org/10.1021/am401462e.

(13) Mo, Y.; Zhang, F.; Dong, H.; Zhang, X.; Gao, S.; Zhang, S.; Jin, J. Ultrasmall Cu3(PO4)2 Nanoparticles Reinforced Hydrogel Membrane for Super-Antifouling Oil/Water Emulsion Separation. *ACS Nano* **2022**, *16* (12), 20786–20795. https://doi.org/10.1021/acsnano.2c07977.

(14) Jhang, J.-C.; Cheng, C.-C.; Huang, C.-H.; Chen, Y.-S.; Lin, J.-H.; Lou, C.-W. Application of Polyhexamethylene Guanidine Hydrochloride to Polylactic Acid/Polyphenylene Block Copolymer Antibacterial Composite Membranes: Manufacturing Technique and Property Evaluations. *Journal of Applied Polymer Science* **2022**, *139* (27), e52504. https://doi.org/10.1002/app.52504.

(15) Chen, X.; Huang, G.; An, C.; Feng, R.; Wu, Y.; Huang, C. Plasma-Induced PAA-ZnO Coated PVDF Membrane for Oily Wastewater Treatment: Preparation, Optimization, and Characterization through Taguchi OA Design and Synchrotron-Based X-Ray Analysis. *Journal of Membrane Science* **2019**, *582*, 70–82. https://doi.org/10.1016/j.memsci.2019.03.091.

(16) Tang, H.; Qi, C.; Bai, Y.; Niu, X.; Gu, X.; Fan, Y. Incorporation of Magnesium and Zinc Metallic Particles in PLGA Bi-Layered Membranes with Sequential Ion Release for Guided Bone Regeneration. *ACS Biomater Sci Eng* **2023**, *9* (6), 3239–3252. https://doi.org/10.1021/acsbiomaterials.3c00179.

(17) Li, Q.; Pan, X.; Qu, Z.; Zhao, X.; Jin, Y.; Dai, H.; Yang, B.; Wang, X. Understanding the Dependence of Contact Angles of Commercially RO Membranes on External Conditions and Surface Features. *Desalination* **2013**, *309*, 38–45. https://doi.org/10.1016/j.desal.2012.09.007.

(18) Tang, C. Y.; Kwon, Y.-N.; Leckie, J. O. Effect of Membrane Chemistry and Coating Layer on Physiochemical Properties of Thin Film Composite Polyamide RO and NF Membranes: II. Membrane Physiochemical Properties and Their Dependence on Polyamide and Coating Layers. *Desalination* **2009**, *242* (1), 168–182. https://doi.org/10.1016/j.desal.2008.04.004.

(19) *In Situ Surface Chemical Modification of Thin-Film Composite Forward Osmosis Membranes for Enhanced Organic Fouling Resistance — University of Edinburgh Research Explorer*. https://www.research.ed.ac.uk/en/publications/in-situ-surface-chemical-modification-of-thin-film-composite-forw (accessed 2023-12-11).

(20) Bera, A.; Jewrajka, S. K. Tailoring Polyamide Thin Film Composite Nanofiltration Membranes by Polyethyleneimine and Its Conjugates for the Enhancement of Selectivity and Antifouling Property. *RSC Adv.* **2016**, *6* (6), 4521–4530. https://doi.org/10.1039/C5RA21941H.

(21) *Enhancement in membrane performances of a commercial polyamide reverse osmosis membrane via surface coating of polydopamine followed by the grafting of polyethylenimine - RSC Advances (RSC Publishing)*. https://pubs.rsc.org/en/content/articlelanding/2015/ra/c5ra20891b (accessed 2023-12-11).

(22) *Performance enhancement of TFC FO membranes with polyethyleneimine modification and post-treatment - ScienceDirect*. https://www.sciencedirect.com/science/article/pii/S0376738817302612?casa_token=6bcL6gYw-WIAAAAA:xwZuewS39_XePreoINMlz4a1Jd5gOZkkmKco8oGU1_5ytsDnU1hsPRVR675KGf-DdoG2BP8O-w (accessed 2023-12-11).

(23) Brunner, J.; Senn, H.; Richards, F. M. 3-Trifluoromethyl-3-Phenyldiazirine. A New Carbene Generating Group for Photolabeling Reagents. *Journal of Biological Chemistry* **1980**, *255* (8), 3313–3318. https://doi.org/10.1016/S0021-9258(19)85701-0.

(24) *A broadly applicable cross-linker for aliphatic polymers containing C–H bonds | Science*. https://www.science.org/doi/full/10.1126/science.aay6230?casa_token=Y2ZC548Awd4AAAAA%3A8v8zGIfQLI4sIBztrBFj2ukp-s6mFy7lbJGzEjbjh4snshLBFfohWM2fQFLkAmRqxsNmL5by5pn1gbA (accessed 2023-08-30).

(25) Hashimoto, M.; Hatanaka, Y. Recent Progress in Diazirine-Based Photoaffinity Labeling. *European Journal of Organic Chemistry* **2008**, *2008* (15), 2513–2523. https://doi.org/10.1002/ejoc.200701069.

(26) P. Conway, L.; M. Jadhav, A.; A. Homan, R.; Li, W.; Sanchez Rubiano, J.; Hawkins, R.; Michael Lawrence, R.; G. Parker, C. Evaluation of Fully-Functionalized Diazirine Tags for Chemical Proteomic Applications. *Chemical Science* **2021**, *12* (22), 7839–7847. https://doi.org/10.1039/D1SC01360B.

(27) Zhao, X.; Bi, L.; Khatir, B.; Serles, P.; Filleter, T.; Wulff, J. E.; Golovin, K. Crosslinking Inert Liquidlike Polydimethylsiloxane Brushes Using Bis-Diazirine Chemical Insertion for Enhanced Mechanical Durability. *Chemical Engineering Journal* **2022**, *442*, 136017. https://doi.org/10.1016/j.cej.2022.136017.

(28) Dorner, J.; Korn, P.; Gruhle, K.; Ramsbeck, D.; Garamus, V. M.; Lilie, H.; Meister, A.; Schwieger, C.; Ihling, C.; Sinz, A.; Drescher, S. A Diazirine-Modified Membrane Lipid to Study Peptide/Lipid Interactions – Chances and Challenges. *Chemistry – A European Journal* **2021**, *27* (59), 14586–14593. https://doi.org/10.1002/chem.202102048.

(29) Admin. *HOME*. XlynX Materials. https://xlynxmaterials.com/ (accessed 2023-08-31).

(30) Ge, S.-S.; Chen, B.; Wu, Y.-Y.; Long, Q.-S.; Zhao, Y.-L.; Wang, P.-Y.; Yang, S. Current Advances of Carbene-Mediated Photoaffinity Labeling in Medicinal Chemistry. *RSC Advances* **2018**, *8* (51), 29428–29454. https://doi.org/10.1039/C8RA03538E.

(31) *Design of Antibacterial Poly(ether sulfone) Membranes via Covalently Attaching Hydrogel Thin Layers Loaded with Ag Nanoparticles | ACS Applied Materials & Interfaces*. (accessed 2023-08-30).

(32) Maruf, S. H.; Ahn, D. U.; Greenberg, A. R.; Ding, Y. Glass Transition Behaviors of Interfacially Polymerized Polyamide Barrier Layers on Thin Film Composite Membranes via Nano-Thermal Analysis. *Polymer* **2011**, *52* (12), 2643–2649. https://doi.org/10.1016/j.polymer.2011.04.022.

(33) Askarizadeh, M.; Honarvar, B.; Mansousrizadeh, A. The New Method for Making Polyamide Membranes for Water Treatment. *Journal of Middle East Applied Science and Technology* **2014**, *13*, 514–519.

(34) *Practical Uses of Differential Scanning Calorimetry for Plastics | 8 |*. https://www.taylorfrancis.com/chapters/edit/10.1201/9780203911983-8/practical-uses-differential-scanning-calorimetry-plastics-andrew-salomon-kenneth-fielder (accessed 2023-08-30).

(35) *Covalent functionalization of polypropylene filters with diazirine–photosensitizer conjugates producing visible light driven virus inactivating materials | Scientific Reports*. https://www.nature.com/articles/s41598-021-98280-6 (accessed 2023-08-30).

(36) *Characterization of the textile anthraquinone dye Reactive Blue 4 - ScienceDirect*. https://www.sciencedirect.com/science/article/pii/S014372080400261X?casa_token=q7a3jc2W-XsAAAAA:zcE_HuDi-vYbwrsfqB3QC4bDW9UDa4zmjwMz_OZrGfWqgqIFGv1msPoWZcWJ90gWylDThZvr4g (accessed 2023-09-27).

(37) Ismail, M. F.; Islam, M. A.; Khorshidi, B.; Tehrani-Bagha, A.; Sadrzadeh, M. Surface Characterization of Thin-Film Composite Membranes Using Contact Angle Technique: Review of Quantification Strategies and Applications. *Advances in Colloid and Interface Science* **2022**, *299*, 102524. https://doi.org/10.1016/j.cis.2021.102524.

(38) Fracture Mechanics: Fundamentals and Applications Surjya Kumar Maiti: Cambridge University Press, 2015 295 Pages, $71.95 ISBN 9781107096769. *MRS Bulletin* **2016**, *41* (8), 635–636. https://doi.org/10.1557/mrs.2016.179.

(39) Liu, G.-L.; Kazarian, S. G. Recent Advances and Applications to Cultural Heritage Using ATR-FTIR Spectroscopy and ATR-FTIR Spectroscopic Imaging. *Analyst (London)* **2022**, *147* (9), 1777–1797. https://doi.org/10.1039/D2AN00005A.

(40) Thomsen, T. B.; Hunt, C. J.; Meyer, A. S. Standardized Method for Controlled Modification of Poly (Ethylene Terephthalate) (PET) Crystallinity for Assaying PET Degrading Enzymes. *MethodsX* **2022**, *9*, 101815. https://doi.org/10.1016/j.mex.2022.101815.

(41) *Contact Angle, Wettability and Adhesion, Volume 2*; Mittal, K. L., Ed.; CRC Press: London, 2002. https://doi.org/10.1201/b11975.

(42) Vesel, A. Surface Chemistry of Polymers. *Polymers (Basel)* **2020**, *12* (11), 2757. https://doi.org/10.3390/polym12112757.
(43) *Atlas of Polymer Structures | ScienceDirect*. https://www.sciencedirect.com/book/9781569905579/atlas-of-polymer-structures (accessed 2023-11-30).
(44) Oshiro, M.; Takashima, K.; Furukawa, Y. Infrared Stark Spectra for a Nylon 6 Film. *Chemical Physics Letters* **2019**, *728*, 32–36. https://doi.org/10.1016/j.cplett.2019.04.068.
(45) Yew, C.; Lai, G. S.; Lau, W. J.; Yusof, N.; Goh, P.; Emadzadeh, D. Impacts of Hydrophilic Nanofillers on Separation Performance of Thin Film Nanocomposite Reverse Osmosis Membrane. *Jurnal Teknologi* **2016**, *78*. https://doi.org/10.11113/jt.v78.10068.
(46) Durig, J. R.; Klaassen, J. J.; Deodhar, B. S.; Gounev, T. K.; Conrad, A. R.; Tubergen, M. J. Microwave, Infrared, and Raman Spectra, *r*0 Structural Parameters, Conformational Stability, and Vibrational Assignment of Allyl Thiol. *Spectrochimica Acta Part A: Molecular and Biomolecular Spectroscopy* **2012**, *87*, 214–227. https://doi.org/10.1016/j.saa.2011.11.041.
(47) Beg, M.; Clark, H. CHEMISTRY OF THE TRIFLUOROMETHYL GROUP: PART I. COMPLEX FORMATION BY PHOSPHINES CONTAINING THE TRIFLUOROMETHYL GROUP. *Canadian Journal of Chemistry* **2011**, *38*, 119–124. https://doi.org/10.1139/v60-012.

# Chapter 2: Unraveling Alginate's Recycling Potential: A Study on Molecular Changes, Structural Integrity, and Ca Crosslinker Removal for Sustainable Practices


## Abstract

This study explores sustainable methods for recycling alginate-based bioplastics sourced from kelp. The primary objective of this research is to address concerns regarding the environmental impact of petroleum-derived plastics. The study assesses the effectiveness of a proposed recycling protocol in terms of yield and purity. Additionally, it provides insights into $Ca^{2+}$ crosslinker removal through analysis of recycled sodium alginate hydrogels and investigates structural alterations in alginate films resulting from recycling. To study the recycling effect on sodium alginate properties, sodium alginate hydrogel films were made from three sources; two commercial sodium alginates as well as a locally sourced kelp-extract alginate. Hydrogels were then recycled and hydrogel films were made of recycled sodium alginate. To validate the findings, commercial sodium alginates are used to examine the impact of changes in the M/G ratio on recycling outcomes, regarding yield and structural changes. Alginate extraction is conducted in replicates (5 series) and each extraction series was characterized as well as characterizing a mixture of all extractions. The Fourier-transform infrared spectroscopy with attenuated total reflection (FTIR-ATR) method tracks calcium crosslinker while recycling yield is calculated based on initial and recycled alginate amounts. Non-destructive tests such as nuclear magnetic resonance (NMR) and gel permeation chromatography (GPC), assess structural changes. Tensile testing compares material properties before and after recycling. The recycling yield ranged from 52.5% to 62%. The M/G ratio analysis revealed that the recycling procedure caused I-2 and I-2G a considerable increase in M/G ratio, indicating lower guluronic acid content, while the M/G ratio stayed unchanged for the case of kelp-extract alginate. FTIR and EDX analyses confirmed the effectiveness of the recycling process in minimizing residual calcium ions. Studied by tensile test, tensile strength decreased for recycled I-2 and I-2G compared with their base material as a result of increased M/G ratio, while tensile strength was improved for the case of EX which showed no change in M/G ratio in terms of recycling. The study aims to contribute to sustainable materials research by providing insights into alginate extraction and recycling processes for environmentally

conscious bioplastic utilization. As a result, it will advance the development of eco-friendly alternatives in the plastics industry.

Keywords:

- Sodium Alginate
- Kelp-extract sodium alginate
- Bioplastic
- Recycling

## 2.1 Introduction

Petrochemical plastics are widely used around the world in society owing to their low cost and durability. As a result, more than 360 million tons of plastic are produced annually, and 95-99% of all plastic on the market is derived from petrochemicals[1,2]. In 2020, the main sectors of plastics produced included packaging (40%), building (20%), and automotive (8%)[2]. Plastic packaging plays a role in product containment, protection, and food safety[1].

Despite their many advantages, these products have been determined as the most significant source of waste globally, with about 96.6% of packaging going unrecycled each year due to their recyclability challenges[3]. Petroleum-derived plastics are not biodegradable, resulting in increased solid waste accumulation[4]. Overall, it is estimated that more than 7.8 billion tons of plastic waste have accumulated globally, causing concerns for the natural environment, aquatic life, and human health[5]. Oceanic plastic is one of today's most troubling pollution issues, not only because it disrupts marine ecosystems but also because it is extremely challenging to collect and remove[5].

Unlike other materials, plastics don't decompose; they continuously break down into microplastics but never truly disappear. Microscopic-sized microplastics swirling within striated, vast, and deep oceans make collecting oceanic plastic pollution nearly impossible[5]. Recycling plastics in general is aligned with strategies to reduce marine litter and decrease plastic waste.

### 2.1.1 Bio-based Plastics

To transition to a more sustainable economy, bioplastics, sourced from renewable feedstock, have been investigated as an alternative to conventional plastic packaging[6]. Bio-based plastics are not all biodegradable, depending on the polymers' chemical and physical characteristics/composition they can still contribute to plastic pollution. Biodegradable plastics refer to materials rapidly degraded in a bioactive environment by biological microbes (i.e., soil) or through direct hydrolysis without releasing pollutants[7]. Biodegradable plastics offer a reasonable way to reduce the negative impact of increased landfills, plastic pollution, and hazards to humans and the environment. In addition, they are applied in various fields, including food packaging (52% of total production), but also textiles (10%), consumer goods (10%), automotive (7%), agriculture (7%), adhesives

(7%), construction (4%), and other sectors (3%)[8]. Biodegradable bioplastics have started to make inroads into the plastic industry with 2.15 MT reported in 2019.

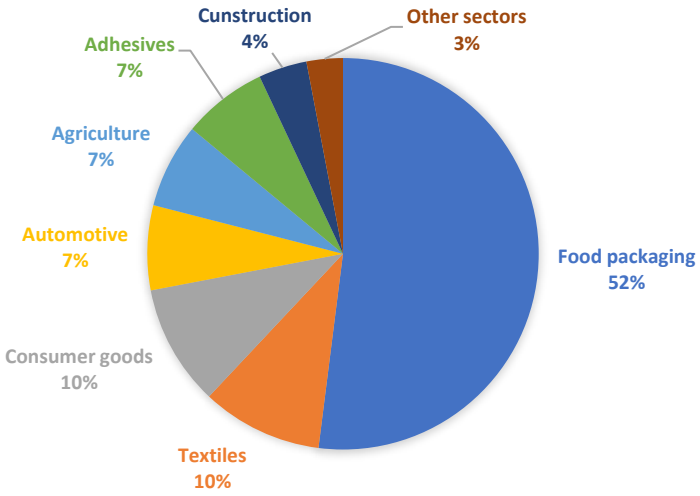


Figure 2.1 Main global bioplastic use, 2019[8]

Despite the many benefits, some bioplastic production requires significant use of freshwater, energy, and land, contributing to global warming, water scarcity, and biodiversity challenges[9]. Further, the advancement of biodegradable plastics is limited by higher processing costs and poor mechanical properties[1].

Crop-based feedstock is an example of a bioresource that requires arable land, nutrients, and freshwater to grow. Moreover, its use as a bioplastic source competes with food production. Agricultural waste is another potential source for bioplastic production which has limited resources and it is insufficient in terms of volume and quality. Bioplastics can be considered more sustainable than traditional plastics when they are derived from renewable resources, have a lower carbon footprint, are biodegradable or compostable, and are produced with minimal environmental impact. However, to achieve full sustainability, challenges such as land use, waste management, and production efficiency need to be addressed.

Unlike the general downsides to bio-based plastic production and their properties, alginate, a natural polymeric extract from kelp, is a promising feedstock for the application of bioplastics due to its biodegradability, low cost, biocompatibility, and, more importantly, from a bioplastic perspective, excellent film-forming capabilities[10]. Unlike other biomass, seaweed can be harvested

from the ocean, requires no fertilizers or freshwater to farm, and can withstand harsh weather conditions[11]. Seaweed polysaccharides can be useful in various food industry applications such as texture modification, colloidal stabilization, fat reduction, and shelf-life extension[12]. It is also possible to produce biodegradable water bottles made from seaweed[13]. Other applications include lenses, coatings for telephones and DVDs, and packaging materials[14].

Brown seaweeds (also known as macroalgae) are abundant on numerous coastlines, and they are a valuable marine resource that is almost unexploited. This biomass constitutes a production system of bioactive compounds such as polysaccharides, proteins, minerals, and lipids including polyunsaturated fatty acids, pigments, vitamins, antioxidants, etc., which are known to have antibacterial, antifungal, antiviral, antioxidative, anti-inflammatory, and antitumor properties[15].

### 2.1.2 Alginate Composition

The composition of alginate varies depending on several factors, including the proportion and sequence of two uronic acid monomers: mannuronic acid (M-blocks) and guluronic acid (G-blocks) (Fig 2.2). The contents of M and G-blocks, as well as molecular weight, depend primarily on species and growth environment[16].

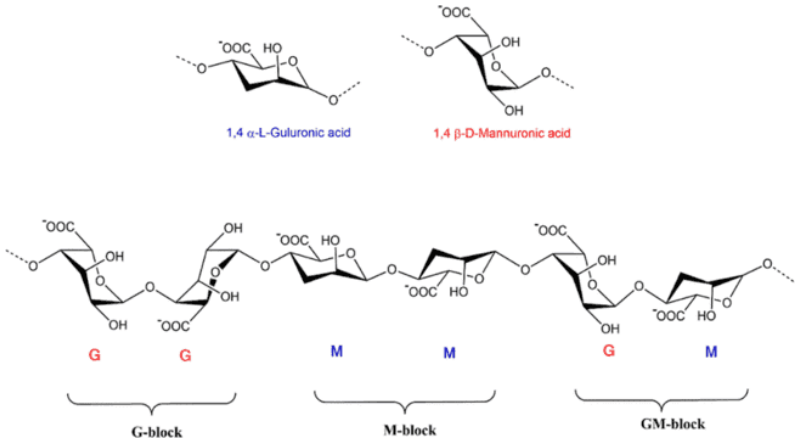


Figure 2.2 Examples of monomers and block distributions in alginate[16]

In addition to the kelp species and origin, the alginate composition and polymer molecular weight also depend on the method of alginate extraction. According to the literature, different extraction protocols can control the properties of alginate to derive alginate of a particular character and application[17–20]. For the isolation of alginates, the typical extraction methods from kelp generally include the following steps (Fig 2.3). The algal material is dried, milled, and treated with

depigmentation agents (e.g., formaldehyde, ethanol, bleach) to eliminate color. The solution is then treated with acid to remove salts and homopolysaccharides associated with kelp, like fucoidan and laminarin. Simultaneously, there is an ion exchange of cations for $H^+$ ions, converting alginate to alginic acid, followed by alkaline treatment. Alkaline extraction is the central step of the process, which converts alginate into a soluble form that passes into the aqueous phase. Once alginate is extracted, precipitation and isolation of alginate are completed to remove residual kelp residue and acquire a pure compound[17–20].

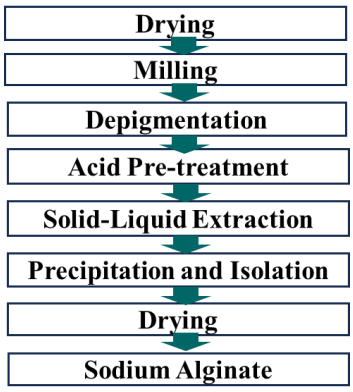


Figure 2.3 Common treatment steps for sodium alginate extraction[17]

The extraction parameters (e.g., temperature, pH, solvent type, concentration, reaction time) impact the alginate molecular characteristics, including molecular weight, mannuronic and guluronic acid contents[17,18]. Controlling the chemical process and operating condition makes it possible to adjust the alginate properties[17–20]. For example, Sterner et al. have reported that selecting solvents in the alkaline extraction step that operate at a higher pH, such as sodium hydroxide and sodium carbonate solutions, produce an alginate extract with a higher mannuronic acid content than using chelating solutions at a pH closer to neutral[18]. Further, higher temperatures and longer reaction times during extraction may lead to the breakdown of uronic acid chains and consequently lower the molecular weight[19].

The extracted alginates can form thin-film hydrogels, which can be used for bioplastics[21,22] . Alginate hydrogels (alginate films) are typically produced through physical crosslinking in the presence of divalent ions (e.g., calcium ions), which facilitate bridging carboxylic acid groups of primarily G-block rich segments to each other and the adjacent polymer chains forming a stable

"egg-box" network[23] (Fig 2.4). The G-block chain configuration is more extended and stiffer than the M-block because of the hindered rotation around the glycosidic bond linkages[24]. The crosslinking properties depend on the G-block content and the arrangement of G and M-blocks along the chain; therefore, the stiffness of the hydrogel increases in the following order: MG blocks < MM blocks < GG blocks[25]. In this regard, the physiochemical properties (e.g., viscosity and mechanical strength) of alginate are dependent on its molecular weight, the concentration of divalent cations, alginate concentration, the ratio of guluronic and mannuronic acid content (M/G ratio), and the distribution and segment length of M or G-blocks along the chain. As mentioned earlier, most of these factors are influenced by kelp source, species, and extraction process. Studies have shown that increased molecular weight and concentration of G-blocks result in a brittle or more robust hydrogel, while higher M-block and MG-block content enhances the elasticity of the alginate film[26]. For the application of alginate for material purposes, ultra-high-molecular weight is beneficial for producing alginate hydrogels with better mechanical properties, improving tensile strength, and percentage elongation[23]. However, extremely high molecular weight in alginate solutions can lead to extreme viscosity, which can cause processing challenges in extrusion or 3D printing of materials, including clogging during the extrusion process and inconsistent deposition, causing defects within the final product[27].

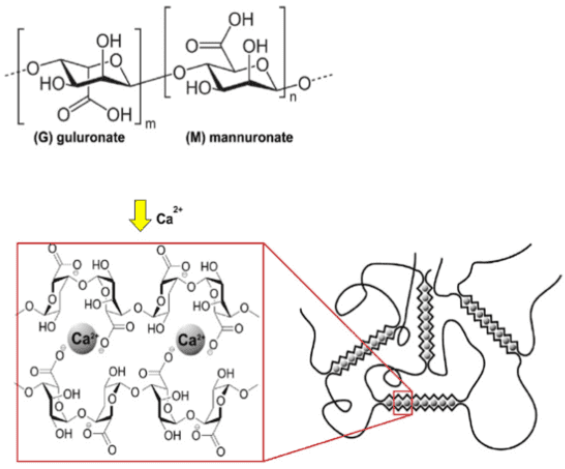


Figure 2.4 Alginate hydrogel mechanism in the presence of calcium ions ($Ca^{2+}$)[28]

From a sustainability perspective, the conventional methods for alginate extraction are not eco-friendly, often involving harsh processing conditions, high volumes of fresh water, and large

quantities of reagents and chemical solvents, which can produce hazardous waste streams and generate a substantial carbon footprint[29]. Enhancing the sustainability and efficiency of processing methods was previously studied in our research group by PhD candidate (at the time of writing this thesis) Hayley Smith, and an optimized extraction procedure was established.

### 2.1.3 End of life options for bioplastics

The most suitable end-of-life option for any waste product depends on the material, its market volume, and the available collection and processing infrastructure. According to the European Directive on Waste Management[30], waste should be managed following a precise hierarchy that indicates a priority order in legislation and policy for waste prevention and management: (i) prevention; (ii) preparing for re-use; (iii) recycling; (iv) other recovery, e.g. energy recovery; and (v) disposal (see Fig 2.5).

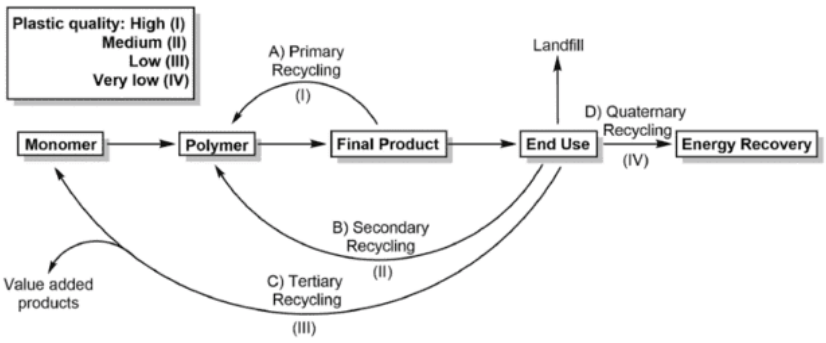


Figure 2.5 Different plastic waste recycling options and associated plastic quality[31]

Since recycling is the second-best option for waste management after preparing for reuse, the lifecycle of every plastic material is truly sustainable only if its disposal options include recycling. While there is a consensus on the convenience of recycling non-biodegradable plastics, whether derived from natural sources or not, biodegradation is often considered the only suitable end-of-life option for biodegradable plastics. However, most commercial biodegradable bioplastics degrade slowly under ambient conditions, even in the presence of microorganisms, as they have been engineered to degrade in specific conditions, such as in composting plants[32]. Although biodegradation can be seen as a recycling option and is sometimes referred to as "organic

recycling"[33], it is usually not aimed at recovering plastic materials or monomers to be reintroduced into the lifecycle of plastic products. On the other hand, this is specifically the objective of other types of recycling options, such as mechanical (primary or secondary) and chemical (tertiary) recycling.

### 2.1.4 literature review on chemical recycling of bio-based plastics

The aim of the chemical recycling methodologies is the maximum preservation of the synthesis effort invested during preceding monomer production. This relates to the maximum integrity of the chemical structure and functionality[34]. Ideally, chemical recycling yields compounds that can be reused as monomers for polymerization, applied directly in other fields (e.g., as solvents), or used as substrates for further chemical conversions[34].

Polyhydroxyalkanoates (PHA) are biopolymers synthesized as internal carbon and energy storage polymers by different bacteria[35]. Being microbial storage polymers, bacteria naturally possess enzymes for the depolymerization of PHA and the metabolization of the resulting monomers. Post-consumer PHA is thus amenable to enzymatic degradation. However, the enzymatic machinery for the hydrolysis of the polymer is intracellular in most bacteria. For easy access, extracellular PHA-depolymerases are needed and have already been identified, for example, in the bacterial predator Bdellovibrio bacteriovorus[35,36]. Also, for short-chained PHA (polyhydroxybutyrate) degradation, exoenzymes are known. The product of enzymatic PHA degradation is the original monomer, 3-hydroxyalkanoic acid, with the respective chain length[37].

PLA is among the most extensively studied bioplastics in terms of recyclability. It can biodegrade under specific conditions, such as in the presence of oxygen and moisture[38]. While PLA's biodegradability significantly reduces its environmental impact, understanding changes in its properties through multiple processing cycles and recycling efforts remains crucial. Industrial processes inevitably generate waste, necessitating online grinding of offcuts and blending with neat polymer[39]. Moreover, reusing post-production PLA waste can extend its service life before disposal in composting facilities[40,41]. Therefore, achieving the recycling of industrial wastes is essential to maintain PLA's low environmental impact[39]. Two main processes are employed for the chemical recycling of PLA. The first method involves hydrolysis at elevated temperatures to

yield lactic acid[42–45]. The second method is thermal degradation, converting PLA into L, L-lactide, a cyclic dimer used in the production of new PLA[46–48.] Hydrolysis, which necessitates water and high temperatures, breaks down PLA into highly pure lactic acid. This lactic acid can then be polymerized to create virgin PLA, completing the recycling loop in a cradle-to-cradle process[37,44] . Research by Faisal et al.[44] indicates that recycling efficiency is heavily influenced by operational factors such as temperature, reaction time, and the water-to-sample ratio.

Thermoplastic starch (TPS) is one of the most abundant polysaccharides available in nature and is widely used for the production of biodegradable polymers for functional applications. most commonly used biopolymer and consists of restructured starch[49]. Pure starch-based bioplastic is usually brittle. To counteract this and facilitate thermoplastic processing, plasticizers such as glycerol, glycol, and sorbitol are added[50]. Not all plasticizers added to TPS are biocompatible and can thus affect biodegradability[51]. Enzymes for the depolymerization of starch are abundant in nature, with amylases being a prime example. Glucose is the main product of enzymatic degradation of TPS; however, due to the random cleavage of glycosidic bonds, other malto-oligosaccharides are also observed[52].

Cellulose esters derived from cellulose esterification are valuable biodegradable materials sourced from renewable biomass. Among them, thermoplastic cellulose acetate is highly favored in industry[53]. Much of the manufacturing and post-consumer waste of cellulose acetate still ends up in landfills, highlighting the need for improved recycling processes[54]. Recent advancements include patent disclosures on hydrolyzing cellulose acetate waste with a hydrolyzing agent to obtain water-soluble products like monosaccharides and acetic acid, aiming to enhance biodegradability and product functionality[54] .

The existing literature emphasizes the importance of recycling various bio-based polymers such as starch and cellulose, highlighting their significant impact on the environment and natural resource preservation. However, kelp-extract sodium alginate (SA), a natural polysaccharide renowned for properties like biosafety, biocompatibility, and renewability, has been largely neglected in these discussions.

### 2.1.5 Study Objectives

This study aims to advance sustainable practices by exploring the recycling potential of kelp-extract alginate. Recycling alginate offers numerous benefits that have driven our focus toward this investigation. Firstly, recycling alginate preserves valuable resources by reintegrating previously used materials into the production cycle, reducing the demand for fresh raw materials. Moreover, by recycling alginate-based products, we can diminish the volume of waste destined for landfills, aligning with waste reduction goals and minimizing environmental impact. Implementing closed-loop systems facilitates collecting and recycling alginate-based items by fostering a circular approach where materials are continually repurposed sustainably. Furthermore, recycling alginate helps lower the environmental footprint associated with the extraction, processing, and transportation of virgin resources, thereby supporting eco-friendly practices. Participating in alginate recycling also supports the principles of a circular economy by extending the life cycle of materials, reducing waste generation. Incorporating recycled alginate into production processes promotes sustainable manufacturing practices, aligning with global efforts to minimize environmental impact. Additionally, recycling alginate may offer economic advantages by reducing the costs associated with raw material acquisition and waste management, ultimately making processes more cost-effective in the long run.

Bioform Solutions Inc., a Vancouver, BC-based startup start-up, has developed a patented 3D extrusion printing technology customized to manufacture 100% homecompostable packaging derived from alginate and wood pulp. Their technology has produced various tubes and films of similar mechanical strength, functionality, and cost to petroleum-based products. Bioform has established that the molecular weight and composition of alginate and the cellulose fiber ratio play a critical role in producing bioplastic products that are competitive with conventional plastics. Bioform is committed to using local kelp as the primary feedstock; however, alginate sourced from the Canadian coastline is largely unexplored, with limited information on alginate composition in literature.

To advance the transition to higher-grade bioplastics, we have partnered with Bioform to investigate the properties of alginate, sourced from kelp native to Canadian coastlines. As a part of an ongoing collaboration with Bioform, Hayley Smith (PhD candidate in the Green Safe Water Lab) has tested various sodium alginate extraction methodologies and optimized the most efficient methods. This study builds on our learnings about sustainable extraction protocols and goes a step further to explore the recycling potential of the films formed by the best protocol determined in the previous work. This research proposes and assesses the utility of one possible recycling protocol, and will indicate whether it is an appropriate method for consistent recycling. Data and methods drawn from this research will further allow Bioform to gain control of the recycled material and the affecting parameters.

In this study, our focus lies on establishing and assessing the effectiveness of the recycling protocol in terms of yield and purity, providing insights into Ca crosslinker removal through analysis, and investigating structural alterations in alginate films resulting from the recycling process.

## 2.2 Methods

### 2.2.1 Chemicals

All chemicals were utilized in their original form without any further modifications. Commercial sodium alginates I-2 and I-2G were purchased from Kimica. Bioform provided dry Macrocystis pyrifera seaweed. Sodium citrate dihydrate (LOT 223578A) and sodium hydroxide (LOT185531) were used for sodium alginate extraction and were purchased from Fisher Chemicals. Sodium carbonate anhydrous (CAS#497-19-8) was from Bio Basic Canada Inc. Hydrochloric acid (LOT226081) 36.5-38% was from Fisher Chemicals. Ethyl alcohol (95%) and anhydrous ethyl alcohol (commercial grade) were from Greenfield Global. Glucino delta lactone, a tofu coagulant purchased from Elo's Premium, is used in hydrogel film formation. Calcium carbonate (LOT 192879A) and calcium chloride (LOT 224469) were from Fisher Chemicals and used for hydrogel film formation.

### 2.2.2 Extraction Procedure

Sodium alginate extraction methods from kelp were previously studied by Hayley Smith, a PhD candidate in the Green Safe Water Lab at the time of writing this thesis. An optimized extraction procedure (adapted from Albers et al.,2021[57]; Sterner et al.,2017[21]) was provided for this study.

Kelp was ground into ~ 0.5 $cm^2$ pieces using Magic Bullet (MBR-1701) and stored in a desiccator at 4°C. sodium citrate solution (0.124M) was prepared and adjusted to pH 9.3±0.1 using NaOH to conduct the chelation step. 720 g of the prepared sodium citrate chelating solution (0.124 M) was added to a 1 L centrifuge bottle and stirred using a stir bar for 1 min and 150 rpm. The centrifuge bottle was shaken well before being placed in an incubator shaker (New Brunswick126) (150 rpm, 1h, 49.5 °C).

After the chelation treatment, the sample was centrifuged for 30 min at 15,000 x g at 21 °C. The supernatant was collected in a separate centrifuge bottle.

Hydrochloric acid (6 M) was used to set the supernatant's pH to 1.0 ± 0.2 to precipitate alginic acid. It was mixed using a stir bar for 30 s and 200 rpm.

The centrifuge (thermoscientific sorvall LYNX4000) was used for 20 min at 15,000 x g and separated; the pellet (alginic acid) was collected, and the supernatant was discarded.

The alginic acid pellet was washed in 100 mL of 0.1 M hydrochloric acid (pH ~1.50) and again centrifuged (15,000 x g for 10 min), collecting the pellet. This step was done twice.

100 mL of DI water was added to the pellet. Alginic acid pellets were neutralized with $Na_2CO_3$ (1 M) to pH 7. The solution was placed on a stir plate for 20 min at 200 rpm.

Sodium alginate was precipitated by adding an equal volume of anhydrous ethanol. The solution was gently agitated and manually stirred until only one liquid phase was visible and all sodium alginate had been precipitated. The mixture was centrifuged (15,000 rpm), and the sodium alginate pellet was collected. The supernatant was disposed of in organic waste storage.

The sodium alginate pellet was washed in 200 mL of a 70% (Wt/Wt) aqueous ethanol solution (shaken well for 10 s) and centrifuged for 10 min, collecting the pellet and disposing of the supernatant was in organic waste storage. This step was performed two times for each sample. Samples were oven-dried at 40 ºC for 48 h and weighed afterward to calculate the extraction yield.

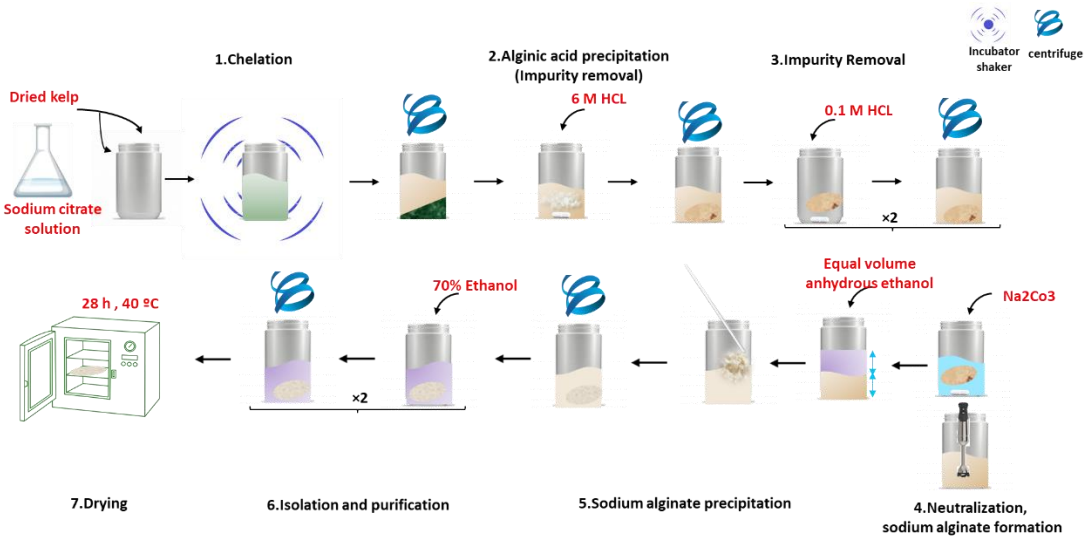


Figure 2.6 Sodium alginate extraction procedure

### 2.2.3 Hydrogel Film Formation Procedure

The Hydrogel film formation procedure used in this study was previously studied and optimized by Nathan Leonard, an undergraduate student in the Green, Safe Water Lab. This procedure is based on the study by Panday et al[55]. on the formation of calcium silicate-reinforced alginate composite hydrogel films.

This procedure used a combination of calcium carbonate and gluconic-delta-lactone (GDL) to pre-gel a film of alginate, which was then crosslinked using a dilute solution (100 mM) of calcium chloride. A concentration ratio of 50 mM GDL to 25 mM calcium carbonate was used for all film sets.

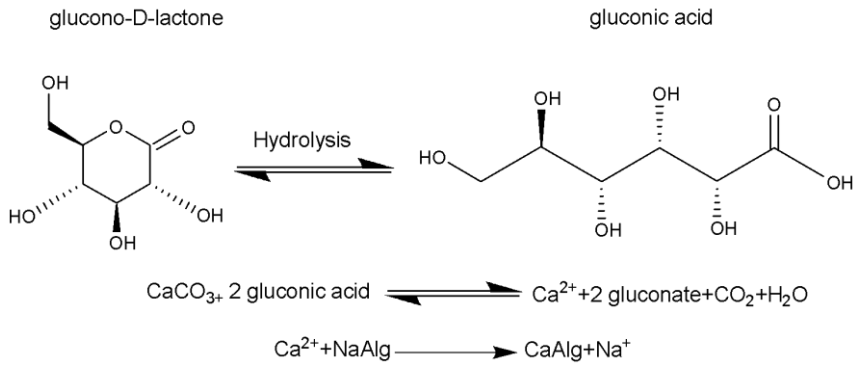


Figure 2.7 Pre-gelation reaction of alginate film, ChemDraw 18.00

A 3% (w/v) suspension of sodium alginate was used. Typically, 250 mL is prepared. 7.5 g of sodium alginate was combined with 250 mL of deionized (MilliQ) water and was blended using a household Magic Bullet blender(3×30s). This suspension was left overnight to remove bubbles.

125 g of sodium alginate suspension was measured using a top-loading balance, to which 1.11 g of GDL was added and mixed thoroughly. Afterward, 0.31 g of calcium carbonate was suspended in ~8 mL of water and combined with the sodium alginate and GDL mixture. The suspension was mixed very thoroughly using a glass rod.

35 g of suspension was added to a petri dish (150×15 mm) using a top-loading balance. The petri dish base was tapped aggressively against a lab bench surface to remove bubbles. It was left to sit for approximately 15 min, and tapping was repeated. The film-forming suspension was allowed to gel for 24 h, covered, at ambient temperature and humidity. After that, 70 mL of 100 mM calcium chloride was added to the pre-gelled film in the glass petri dish. After adding the cross-linker solution, the petri dish was gently swirled to detach the film from the base of the petri dish to allow for even crosslinking. After 30 min, the cross-linker solution (neutral aqueous waste) was poured off, and the film was gently rinsed with water. The mass and diameter are recorded at this time, see Fig 2.8 for the process schematic.

The films were then pinned to pieces of wood and compressed foam lined with plastic wrap, with a space of about 1 cm at the border. After at least 24 h (up to 72 h), the pins were removed after the films were dry. The mass and diameter were recorded at this time.

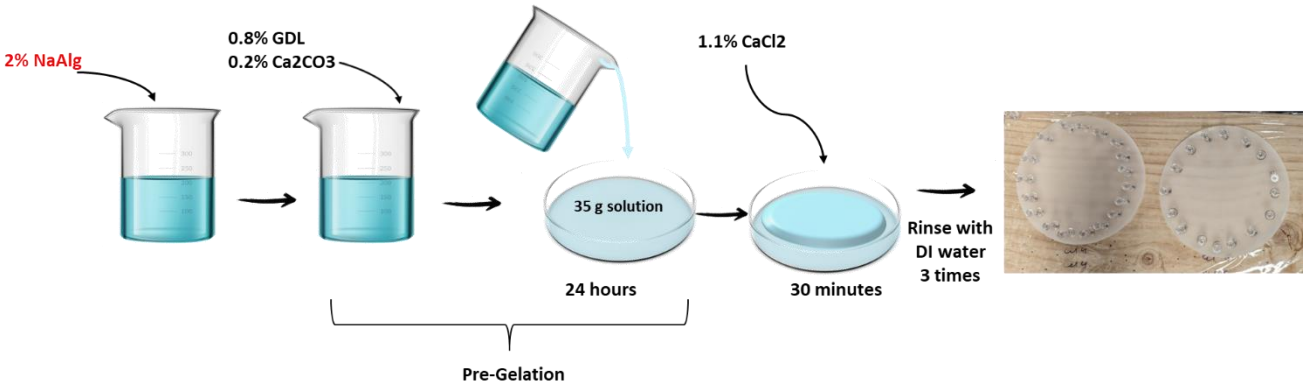


Figure 2.8 Alginate film development schematic

## 2.2.4 Recycling Procedure

The recycling procedure has almost the same steps as extraction from raw kelp, except the chelation step was skipped as it was not necessary because the desired compounds were already in a chelated form from the initial extraction. This process was optimized to increase recycling yield, resulting in up to 62% recycling yield.

Sodium alginate film was ground using a ball mill (find model) with 30 Hz frequency for 30 s. 15 g of ground alginate film was placed in a 1 L centrifuge bottle, and 70 mL DI water was added. In

the next step, the alginate film/water mixture was acidified to pH 1 using 10 M hydrochloric acid to precipitate alginic acid, then centrifuged for 35 min,15 ºC, and 15000×g. The pellet was filled with 150 mL of 0.03 M hydrochloric acid and centrifuged for 20 min, 15000×g, 15 ºC. This step was done two times for each sample. The pellet was neutralized using 1 M sodium carbonate and mixed at 200 RPM for 1 h. 250 mL DI water was added to ease the stirring and reduce the solution viscosity. Anhydrous ethanol was added to the centrifuge bottle in the same volume to precipitate sodium alginate. The sample was centrifuged for 20 min,15000×g, and 15 ºC. The sample was oven-dried at 35 °C for three days, and the alginate was weighed. See Fig 2.9 for the process schematic.

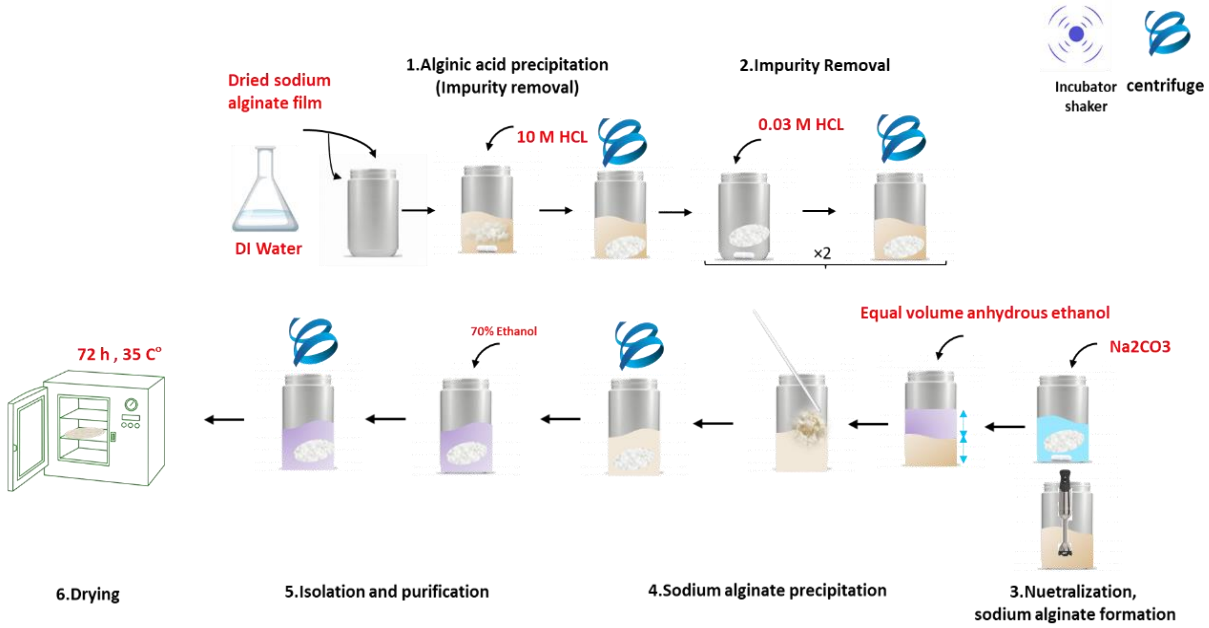


Figure 2.9 Sodium alginate recycling procedure

### 2.2.5 Hydrogel Film Formation Procedure from recycled kelp-extract sodium alginate

The film formation process with recycled extracted alginate (REX-1) encountered challenges due to rapid gelation, high viscosity, and difficulties with leveling. To make the film formation procedure described in section 2.2.3 applicable for the case of recycled kelp-extract sodium alginate following modifications were applied:

For the second recycled extracted alginate (REX-2), the sodium alginate solution was prepared in small quantities, enough for making one sample at a time. This was done to reduce the filmmaking process time and prevent pre-gelation before pouring the hydrogel solution. To adjust the viscosity, 5.7% distilled water was added to the original formula (2g of water per 33g of sodium alginate solution). Due to the adjustment and additional water content, the tensile properties of the dried hydrogel film may not be comparable to the other samples.

Hydrogel film samples used in mechanical properties characterization were tested for moisture content and thickness.2.2.6 Sample Design

Sample codes associated with 3 sodium alginate sources (Commercial I-2, Commercial I-2G, and extracted) at different stages of the film formation (assigned with F), recycling (assigned with R), and recycled sample film (R-F) are presented in Table 2.1. To obtain a sufficient quantity of kelp-extracted alginate, five extraction series (ex1-ex5) were performed. EX represents the combined kelp-extracted sodium alginate, consisting of equal amounts of sodium alginate from each extraction series. To validate the reproducibility of the findings from recycled kelp-extract sodium alginate, recycling was conducted in 2 replicates, labeled as REX-1 and REX-2.

Table 2.1 General sample design

| Sample | Description | Sample film | Description | Recycled sample | Description | Recycled sample film | Description |
|---|---|---|---|---|---|---|---|
| I-2 | Commercial sodium alginate 1 | I-2F | I-2 hydrogel | RI-2 | Recycled I-2 | RI2-F | Recycled I-2 hydrogel |
| I-2G | Commercial sodium alginate 2 | I-2GF | I-2G hydrogel | RI-2G | Recycled I-2G | RI-2GF | Recycled I-2G hydrogel |
| EX | mix of sodium alginate extractions (5 extraction series: ex1,ex2, ex3, ex4, ex5) | EXF | Mix of extractions hydrogel | REX-1 | Recycled Ex, Serie1 | REX-1F | Recycled(serie1) Ex hydrogel |
| | | | | REX-2 | Recycled Ex, Serie2 | REX-2F | Recycled(serie2) Ex hydrogel |

## 2.2.7 Characterization Methodology

### 2.2.7.1 FTIR

Fourier transform infrared (FTIR) is a spectroscopic technique commonly used to analyze the surface properties of materials, specially those that are difficult to analyze using traditional transmission methods. In FTIR-ATR, a sample is brought into contact with a high refractive index material (often a crystal) at a specific angle. This interaction between the sample and higher refractive index material allows for detecting evanescent waves that extend into the sample[56].

All sample designs (see section 2.2.6) were tested in a solid state and were ground by the Retsch MM400 ball mill for 30 s in 30Hz. The Agilent Cary 630 FTIR setting was set on the transmittance mode with spectra range 650-4000 cm-1, 16 background scans, 64 sample scans, and 4 cm-1 resolution. For each sample code, 3 different FTIR runs were conducted. Agilent MicroLab FTIR Software was used for data processing.

2.2.7.2 EDX

Energy-dispersive X-ray spectroscopy (EDS, also abbreviated EDX or XEDS) is an analytical technique that enables the chemical characterization/elemental analysis of materials. A sample excited by an energy source (such as the electron beam of an electron microscope) dissipates some of the absorbed energy by ejecting a core-shell electron. A higher energy outer-shell electron then proceeds to fill its place, releasing the difference in energy as an X-ray that has a characteristic spectrum based on its atom of origin. This allows for the compositional analysis of a given sample volume that has been excited by the energy source. The position of the peaks in the spectrum identifies the element, whereas the intensity of the signal corresponds to the concentration of the element[59]. In this study, EDX was chosen to study the removal of elements like Ca and Cl in the recycling procedure which are added to the sodium alginate as a result of hydrogel formation. EDX is a quantitative method that provides element Wt.% and atom% of the element on the surface.

All sample designs (see section 2.2.6) were tested in a solid state and were ground by the Retsch MM400 ball mill for 30 S in 30Hz. To prepare samples, double-sided tape was attached to each SEM specimen stub, and powdered sample placed on the tape (See Fig 2.10). Cressiongton carbon coater (208 carbon) was used to coat EDX samples. Each sample was coated for 24 s which is about 6nm of the carbon layer. Carbon coating improves the electrical conductivity of the sample, which is especially important for non-conductive or poorly conductive materials. Enhanced conductivity helps to reduce charging effects under the electron beam in the scanning electron microscope (SEM), where EDX is typically conducted. Pointed carbon rods were purchased from TED PELLA, INC. Quantax800 by Brucker was used to quantify and analyze SEM images taken by HF-3300V scanning transmission electron holography microscope (STEHM). SEM images were taken at 3000X magnification, 13Kv HV, and WD of 15mm. Each Sample code was tested at 3 points for O, Na, Mg, Cl, K, Ca, and Fe elements. To calculate normalized weight percentages (Wt.%) accurately, it's essential to account for all elements present in the sample. Focusing solely on element of interest can result in an incomplete picture of the sample's composition, leading to inaccurate normalization. Since normalization adjusts Wt.% values so they sum to 100%, excluding other elements can cause the normalized value of your element of interest to be misleadingly high, giving an incorrect impression of its actual proportion in the sample.

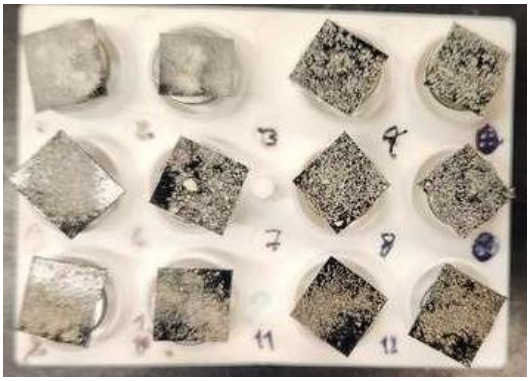

Figure 2.10 EDX samples

2.2.7.3 NMR

1H NMR spectroscopy is a consistent method in literature used to characterize the uronic acid composition of the alginate and block sequences. The relative mannuronic and guluronic acid contents (M/G ratio), block length, and block distribution provide critical information, which directly impacts the polymer stiffness and ionic crosslinking and therefore mechanical properties (e.g., elasticity and rigidity)[17]. The relationship to determine the uronic acid composition and block length of G and M-blocks in alginate can be calculated by the relative integrations of the three resonance peaks [I, II, III] (See Fig 2.11), and the following equations[26,57,58]. I is the anomeric hydrogen of guluronic acid. II is the anomeric hydrogens of mannuronic and the H-5 of alternating blocks (GM-5), and III is the H-5 of guluronic acid residues of the homopolymer G blocks.

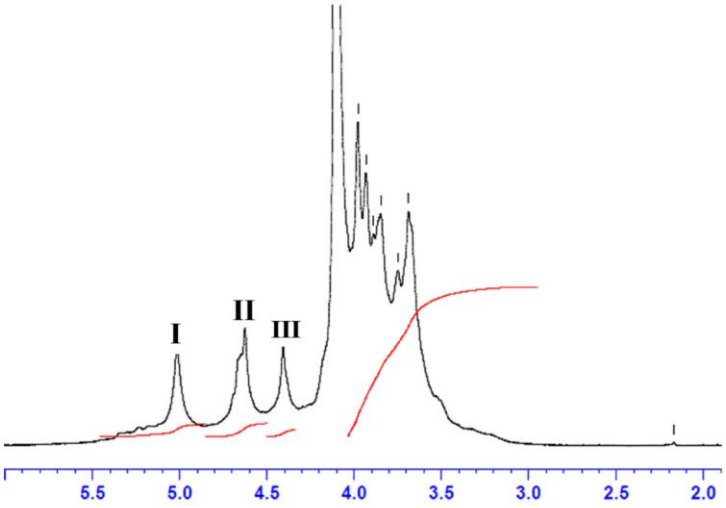


Figure 2.111H NMR analysis of CBA UF extracted from brown seaweed[26]

Eqution1 presents the calculation of the relative mannuronic and guluronic acid contents(M/G), where AI, AII, and AII are the integration of the under peak area for I, II, and III peaks[26,59] .

$M/G = (AII + AIII)\ /(AI - 1\ )$ (Equation 1)

The equation shows block distribution ($\eta$) calculation, where FMG is alternating block content, and FM, and FG are fractions of homopolymer block structures[26,59]

$\eta = F_{MG}\ /(F_M \times F_G)$ (Equation 2)

To calculate the average length of homopolymer blocks (MM, GG), equations 3 and 4 are used.

$N_G = F_G/F_{GM}$ (Equation 3)

$N_M = F_M/F_{MG}$ (Equation 4)

Where:

$F_G$—fraction of individual blocks of G-units

$F_M$—fraction of individual blocks of M-units

$F_{GM}$ or $F_{MG}$—fraction of heterogeneous blocks of alternating M and G units [59]

The M/G ratio, determined through equation 1, will inform us of the M and G-block content; an M/G ratio greater than 1 will have a higher quantity of mannuronic acid content, producing a more elastic hydrogel, while a lower M/G ratio will produce a stiffer hydrogel. The block distribution is

the fraction of homo-polymeric block structures ($F_{MM}$, $F_{GG}$) and alternating blocks ($F_{MG}$, $F_{GM}$), and can be calculated by equation 2[58]. The abundance of homo-polymeric blocks MM and GG generate a $\eta$ value less than 1, while values greater than 1 correspond to greater heterogeneous blocks MG and GM. The block length is the average length of homo-polymeric blocks (MM, GG) and will be calculated via equations 3 and 4[58] . This data will provide insight into the ability to form strong cross-linking junctions, as calcium needs 8-20 adjacent G-blocks to coordinate a stable junction of the "egg-box" formation[60]. The 1H NMR spectra were recorded at 500 MHz on a Bruker DMX-500 spectrometer at 85 Cº and MestReNova software will be used for data procurement.

2.2.7.3.1 NMR Sample Preparation

All sample designs (see section 2.2.6), were tested in triplicate. Due to the risk of degradation, samples were prepared on the same day of NMR testing, with a maximum 2-hour wait time.

To prepare NMR samples of alginate, 25 mg of alginate was dispersed in 125-mL deuterium oxide (99.9 atom% D, Sigma Aldrich (151882-100G)) to make 2wt% solution. A glass pasture pipette was used to take 125 mL of deuterium oxide.

For mixing, a small centrifuge container was used and secured by a rack. A vortexer was used to mix the solution. A syringe and needle were used to mix manually between vortexes, and this process was repeated several times until all particles were well dispersed and did not show obvious precipitation, and stayed stable in dispersion. Alginate was observed to disperse rather than make clumps, and it was acceptable to have bubbles at that point.

The NMR tube was filled using the syringe and needle. The tube was shaken down several times to get the solution down, ensuring there were 3 finger lengths of material in the tube. The tube was capped, and the top and surroundings were sealed using parafilm.

2.2.7.4 GPC

Gel permeation chromatography is widely used for the molecular weight characterization of alginates[17]. Molecular weight impacts the physical and mechanical properties of the alginate hydrogel, such as stiffness, toughness, strength, and viscosity[26]. From GPC, we measured the weight-average molecular weight (Mw) and number average molecular weight (Mn); from the

ratio of Mw/Mn, we measured the polydispersity index (PDI). The polydispersity index is a useful parameter that allows molecular weight distribution estimation and indicates alginate depolymerization during the extraction or purification procedure's steps[22]. The molecular weight distribution of the sodium alginate samples was determined through gel permeation chromatography (GPC) using a Waters 2695 separation module equipped with a DAWN HELEOUS-II multiangle laser light scattering (MALLS) detector and an Optilab T-rEX refractive index detector (Waters, USA). Waters Ultrahydrogel high-performance liquid chromatography (HPLC) columns (including guard, linear, and 120) were employed for analysis. The samples were analyzed in 10 mM phosphate-buffered 0.1 M NaNO3 at pH 7.

Key parameters such as weight-average molecular weight (Mw), number-average molecular weight (Mn), polydispersity index (Mw/Mn), and intrinsic viscosity were determined to characterize the biopolymers.

2.2.7.5 Characterization of Hydrogel Properties

Tensile testing is a destructive test process that provides information about the tensile strength, yield strength, and ductility of the specimen. It measures the force required to break a composite or plastic specimen and the extent to which the specimen stretches or elongates to that breaking point. Tensile testing also provides tensile strength (at yield and break), tensile modulus, tensile strain, elongation, and percent elongation at yield, elongation, and elongation at percent break. The main equations in tensile testing are summarized in Table 2.2:

Table 2.2 Definition of main tensile testing parameters

| Tensile stress | Tensile strain | Young's modulus |
|---|---|---|
| Force per unit area which is associated with stretching and denoted by σ. | Deformation or elongation of a material when it is stretched by a tensile force or stress. | Young's modulus compares tensile or compressive stress to axial strain. |
| The formula is: $\sigma = F/A$<br>Where,<br>● σ is the tensile stress<br>● F is the force acting<br>● A is the area | The formula is: $\varepsilon = \Delta L/L\ 0$<br>Where,<br>● ε is the tensile ΔL strain<br>● ΔL is the elongation<br>● L0 is the initial length of the sample | The formula is: $E = \sigma / \varepsilon$<br>Where,<br>● σ is the tensile stress<br>● ε is the tensile strain |

The tensile testing is carried out by applying longitudinal or axial load at a specific extension rate to a standard tensile specimen with known dimensions (gauge length and cross-sectional area perpendicular to the load direction) till failure[61]. The applied tensile load and extension are recorded during the test for calculating stress and strain. Analyzing the stress-strain curve generated during the test will provide an essential understanding of a polymer's response to applied stress, aiding in material selection, formulation optimization, and the design of polymer-based products. ASTM D3039/D3039M[62] was previously used in the literature to study fabric-reinforced epoxy[63], low-density polyethylene[64], and reinforced polyester composites[65]. Specimens were cut to D3039 regulation for this study.

To cut the dried sodium alginate hydrogel films into strips measuring 10 mm by 7 mm, a laser cutting machine was used. (Aeon Nova 16 Elite) was used with 23% power and 280 mm/s [66].

Samples were conditioned in the tensile testing room at 47% humidity and 23 ºC for 24 h before testing. The mechanical properties were measured with the Instron6800 system (facility at UBC, Pulp, and paper center), providing a stress-strain curve for the various alginate film samples. In the tearing test, one sample leg was fixed to the upper clamp while the other leg was fixed to the bottom with a tensile velocity of 1 mm min until the sample failed (see Fig 2.12).

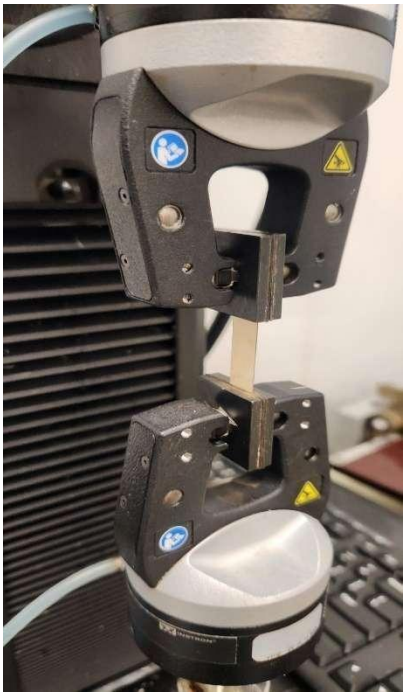

Figure 2.12 Hydrogel film sample placed between two clamps in the instron6800 system, photo by Negar Rahmati, 2024

Moisture content ($M_c$, %) within the films was assessed through a gravimetric approach. The samples were first conditioned under conditions of 23 °C and 47% humidity for 24 h. Subsequently, they were subjected to drying in an oven set at 110°C until a constant weight was achieved. The moisture content values reported in this study represent the averages derived from three separate replicates. To calculate the moisture content, equation5 was employed:

$$Mc\ \% = (W_0 - W_d/W_0) \times 100 \quad \text{equation5}$$

Where $W_0$ represents the initial sample weight before drying (after conditioning), and $W_d$ denotes the sample weight after the drying process.

Hydrogel films' moisture content and thickness (after conditioning) is presented in table 2.3.

Table 2.3 Tensile sample's characteristics

| Sample | Tensile Sample Thickness (mm) | Mc % |
|---|---|---|
| **I-2** | 0.09 | 14.3 |
| **RI-2** | 0.12 | 14.9 |
| **I-2G** | 0.08 | 16.0 |
| **RI-2G** | 0.1 | 22.5 |
| **EX** | 0.08 | 17.7 |
| **REX-2** | 0.1 | 21.3 |

## 2.3 Results and Discussion

### 2.3.1 Yield of Sodium Alginate Hydrogel Recycling, M/G ratio potential impact

Table 2.4 shows the average yield of sodium alginate hydrogel recycling, using commercial I-2, I-2G, and EX. I-2G had the highest average yield (62.0%), followed by EX (56.5,55.7%) and I-2 (52.5%) respectively. The reproducibility of the kelp-extract alginate recycling yield was tested by recycling it in replicates. Recycling kelp-extract alginate was reproducible and comparable to commercial sodium alginate, as shown in Table 2.4.

The M/G ratio was calculated using NMR data (See section 2.3.4). A lower M/G ratio, which indicates a higher proportion of guluronic acid blocks, enhances the gel formation and stability due to the stronger and more effective binding with calcium ions. This interaction results in more robust and cohesive hydrogels[57], which are hypothesized to be less prone to breakdown or degradation during use and recycling. Consequently, it is expected to have more of the hydrogel structure recovered intact, increasing the recycling yield. Alginates with higher G content can have a lower viscosity[67], depending on the molecular weight[68], which can potentially make handling and processing easier and reduce material loss during recycling steps.

Comparing the M/G ratio of I-2 and kelp-extract alginate, kelp-extract alginate has a higher M/G ratio of 1.38, which indicates lower G content, while it presented higher recycling yield compared to I-2. This result suggests that G content is not the only factor impacting recycling yield.

Although all procedure conditions such as temperature, mixing speed, and processing duration were carefully controlled and kept consistent across all recycling attempts, the degree of polymerization or molecular weight of the recycled sodium alginate hydrogel can still impact the recycling process. High molecular weight and a high degree of cross-linking can lead to difficulties in recycling, such as higher viscosity polymer's solution and difficulty in dissolution and processing that can result in lower recycling yields. The molecular weight of the starting material and calcium content% of the sodium alginate films are shown in Table 2.4.

Table 2.4 Recycling yield for 3 sodium alginate sources

| Sample | M/G ratio | Mw (kDa) | Ca Wt% | Recycling Yield% |
|---|---|---|---|---|
| I-2 | 1.01±0.02 | 237 | 13.54 | 52.5% |
| I-2G | 0.25±0.05 | 248 | 4.35 | 62.0% |
| EX-1 | 1.38±0.02 | 104 | 10.99 | 56.5% |
| EX-2 | 1.38±0.02 | 104 | 10.99 | 55.7% |

Although crosslinked samples cannot be analyzed using GPC, the molecular weight of the starting material significantly determines the molecular weight of the resultant hydrogel films. I-2, with an average Mw of 237 kDa and a 13.54% Ca content for the I-2 film, is higher than that of kelp-extract alginate (104 kDa). This higher molecular weight and calcium content make I-2 more challenging to recycle, explaining why its recycling yield is similar to that of kelp-extract alginate, despite having a lower M/G ratio and higher G content.

Both the high G content and the low Ca content (4.35%) of I-2G may justify its high recycling yield of 62%. While this is the highest yield among conducted recycles, it could have potentially been higher with a lower molecular weight material with a similar chemical composition.

### 2.3.2 Recycling Procedure's $Ca^{2+}$ Crosslinker Removal Efficacy

Tracing calcium ions in recycled sodium alginate hydrogel is indispensable due to the pivotal role of $Ca^{2+}$ ions in influencing the structural integrity and performance of the gel. The traceability of calcium ions is essential for understanding their retention levels, which directly impacts the hydrogel's reusability, strength, and stability over multiple cycles. To study the efficiency of $Ca^{2+}$ crosslinker removal in the proposed recycling procedure, FTIR[72] and EDX[73] was employed.

2.3.2.1 FTIR Result

Fourier-transform infrared spectroscopy (FTIR) was utilized to characterize the isolated sodium alginate within the range 650-4000 $cm^{-1}$ as detailed previously by Belattmania et al[57]. In Figure 2.13, the FTIR spectra of kelp-extract alginate are presented alongside a reference to commercially available high-purity sodium alginate, I-2 and I-2G (KIMICA, Japan). Notably, the spectra of the sodium alginates obtained from the investigated protocols closely mirror those of the commercial standards, showcasing similar positions of characteristic bands. This alignment indicates that sodium alginate is the primary polysaccharide constituent in the product.

Several distinctive bands were observed in the FTIR spectra. Broadband with a peak at 1593 $cm^{-1}$ was attributed to the O1-C-O4 asymmetric stretching of the carboxylate group. Additionally, a band with a peak of 1403 $cm^{-1}$ was associated with the C-OH deformation vibration, coupled with the symmetric stretching vibration of O1-C-O. The presence of a band with a peak at 1021 $cm^{-1}$ indicated the presence of the C-O group within the alginate structure. In the anomeric region (950 to 750 $cm^{-1}$), crucial in carbohydrate analysis, distinct bands were observed. Furthermore, bands at 930 to 950 $cm^{-1}$ were linked to the C-O stretching vibration of uronic acid residues.

Peaks at 883 $cm^{-1}$ were specifically associated with the C1-H deformation vibration of β-mannuronic acid residues, while peaks within the range of 815-833 $cm^{-1}$ were attributed to mannuronic acid residues. Notably, a band at 883 $cm^{-1}$ indicative of β-mannuronic acid residues was prominent in samples from I-2. Conversely, the spectra from commercial I-2G and kelp-extract alginate exhibited a weaker band at 883 $cm^{-1}$, reflecting the lower content of β-mannuronic acid residues in these samples.

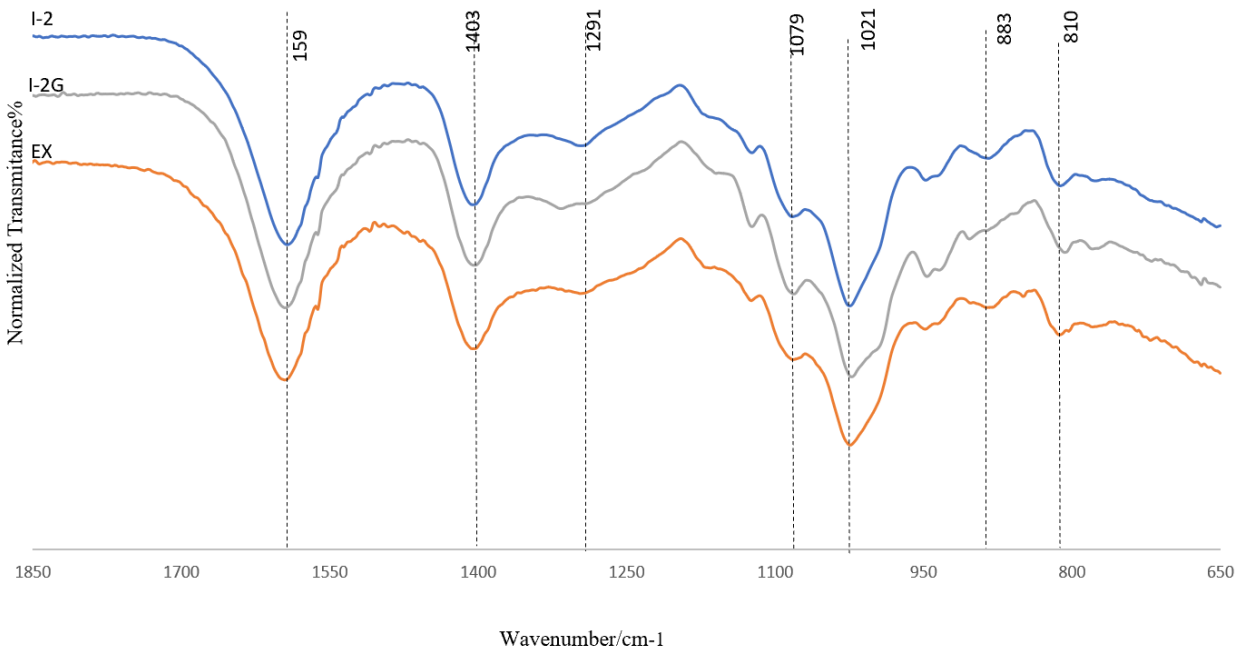


Figure 2.13 FTIR spectra of I-2, I-2G, and EX (kelp-extract sodium alginate), Normalized to max transmittance intensity, at 1021 $cm^{-1}$

The purity of the kelp-extracted alginate was compared to the sodium alginate (I-2 and I-2G). By comparing the position of the characteristic bands, we indicate that sodium alginate is the main polysaccharide found in the extracted sample[57]. The IR spectrum of sodium alginate shows two characteristics peaks at 1596 $cm^{-1}$ and 1404 $cm^{-1}$, which correspond to the asymmetric and symmetric vibrations of the carboxylate (-COO) group, respectively, and are consistent with IR studies of alginate[69].

After cross-linking with $Ca^{2+}$, the peak that shows symmetric vibration of $COO^-$ in alginate shifts to higher wavenumbers, and the peaks that show asymmetric vibration of $COO^-$ and C=O groups shift to lower wavenumbers, that is due to weak interactions between polymeric chains are replaced by robust ionic bonds between $Ca^{2+}$ ions and carboxyl groups of polysaccharides. After recycling sodium alginate, the symmetric and asymmetric vibration peaks return to their original positions, as they were before cross-linking. This shift indicates that the crosslinker and the associated ionic bonds have been successfully removed[70].

For the case of I-2, O-C-O Symmetric stretching showed a peak at 1407 $cm^{-1}$ which was shifted to 1412 $cm^{-1}$ as a result of Ca ion crosslinking in I-2F, followed by a shift to lower wave numbers

(1395 $cm^{-1}$) after recycling. O-C-O Asymmetric stretching presented a peak at 1593 $cm^{-1}$, which was shifted to 1587 $cm^{-1}$ for I-2G and then shifted to a higher wavenumber of 1597 $cm^{-1}$ after recycling. Recorded trends of O-C-O symmetric and asymmetric shifts confirm the successful removal of introduced $Ca^{2+}$ ions as a result of recycling. The observation that O-O=C-O symmetric stretching appeared at a lower wavenumber and O-C-O appeared at a lower wavenumber for RI-2 compared to I-2, indicates the removal of both the initial Ca content in I-2 and the Ca introduced during the hydrogel formation process in recycling (See Table 2.5).

Table 2.5 All sample codes FTIR characteristic peak shifts (cm-1)

| | O-C-O Symmetric stretching ($cm^{-1}$) | O-C-O Asymmetric stretching ($cm^{-1}$) |
|---|---|---|
| I-2 | 1407 | 1593 |
| I-2F | 1412 | 1587 |
| RI-2 | 1395 | 1597 |
| RI-2F | 1416 | 1587 |
| I-2G | 1403 | 1595 |
| I-2GF | 1412 | 1588 |
| RI-2G | 1405 | 1595 |
| RI-2GF | 1411 | 1588 |
| EX | 1404 | 1595 |
| EXF | 1411 | 1589 |
| REX1 | 1404 | 1594 |
| REXF-1 | 1410 | 1590 |
| REX2 | 1404 | 1593 |
| REXF-2 | 1412 | 1589 |

For the case of I-2G, O-C-O symmetric and asymmetric stretching peaks showed at 1403 $cm^{-1}$ and 1595 $cm^{-1}$ respectively. By film formation, the symmetric stretching peak shifted to 1412 $cm^{-1,}$ and the asymmetric stretching peak was recorded at 1588 $cm^{-1}$. After recycling O-C-O symmetric and

asymmetric stretching peaks were recorded at 1405 $cm^{-1}$ and 1595 $cm^{-1}$. While there is evidence of high degree $Ca^{2+}$ removal, O-C-O symmetric stretching peak appearing at a higher wavenumber compared with the starting material can be related to higher $Ca^{2+}$ content compared to I-2G (See Table 2.4).

Kelp-extracted sodium alginate O-C-O stretching peak symmetric, increased from 1404 $cm^{-1}$ to 1411 $cm^{-1}$, while the asymmetric stretching peak shifted from 1595 to 1589 $cm^{-1}$ as a result of film formation. Studied in two replicates, REX-1 and REX-2 presented O-C-O symmetric and asymmetric stretching peaks at 1404,1594 $cm^{-1}$ and 1404,1593 $cm^{-1}$ respectively. While FTIR data support approve a high level of $Ca^{2+}$ content removal from REX, higher peak numbers for asymmetric stretching compared to the same peak for EX, can be related to remaining $Ca^{2+}$ content.

In summary and as presented in Table 2.4 and Fig 2.13-16, the $Ca^{2+}$ removal efficiency of the recycling procedure was confirmed for commercial sodium alginates as well as the kelp-extract alginate. To test the reproducibility of $Ca^{2+}$ ion removal for the case of kelp-extract sodium alginate, FTIR was performed on 2 replicates of its recycling.

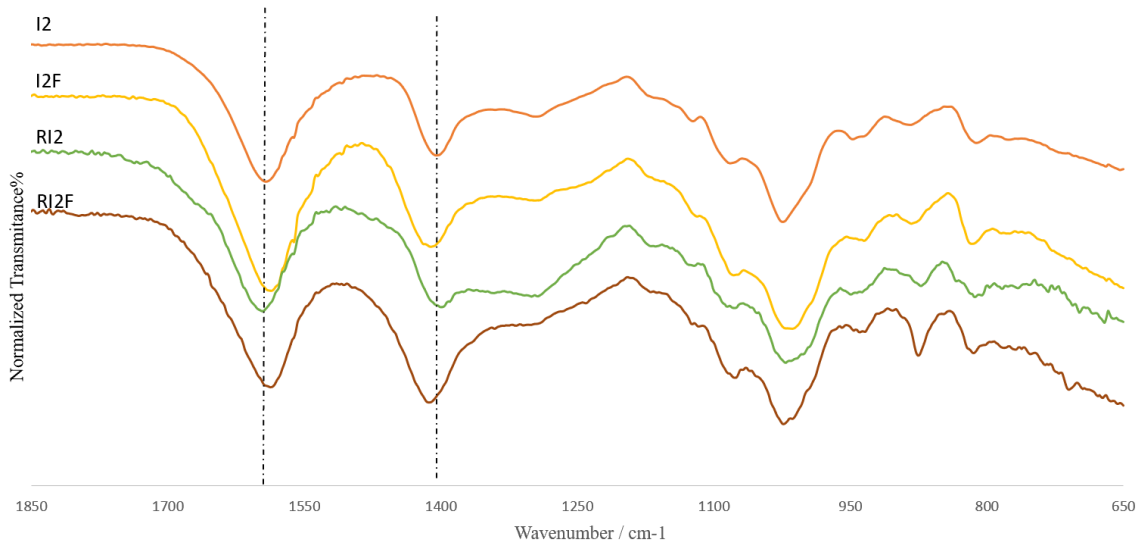


Figure 2.14 FTIR Spectra of I-2, I-2 Film, recycled I-2 and Film of the recycled I-2 status, Normalized to max transmittance intensity, at 1021 $cm^{-1}$

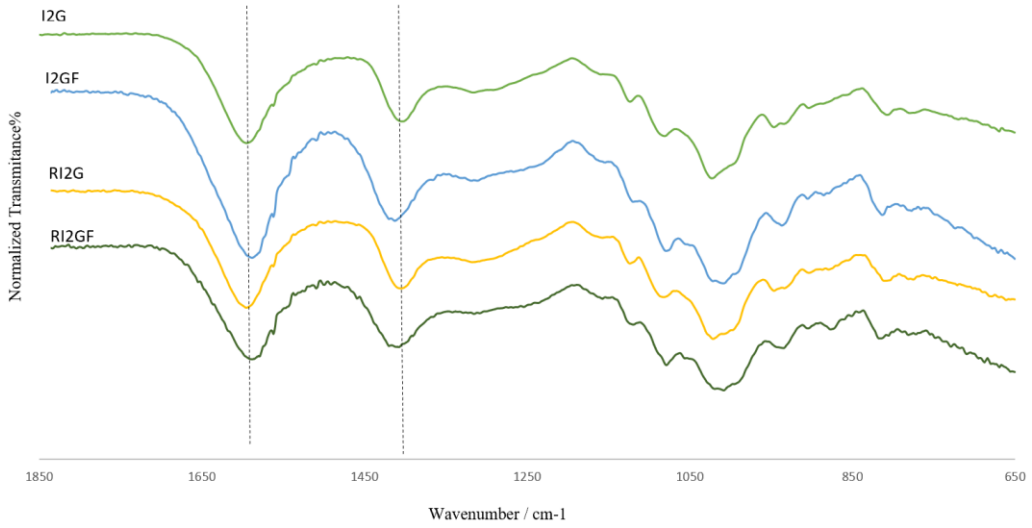


Figure 2.15 FTIR Spectra of I-2G, I-2G film, recycled I-2G, and recycled I-2G film status, Normalized to max transmittance intensity, at 1021 cm-1

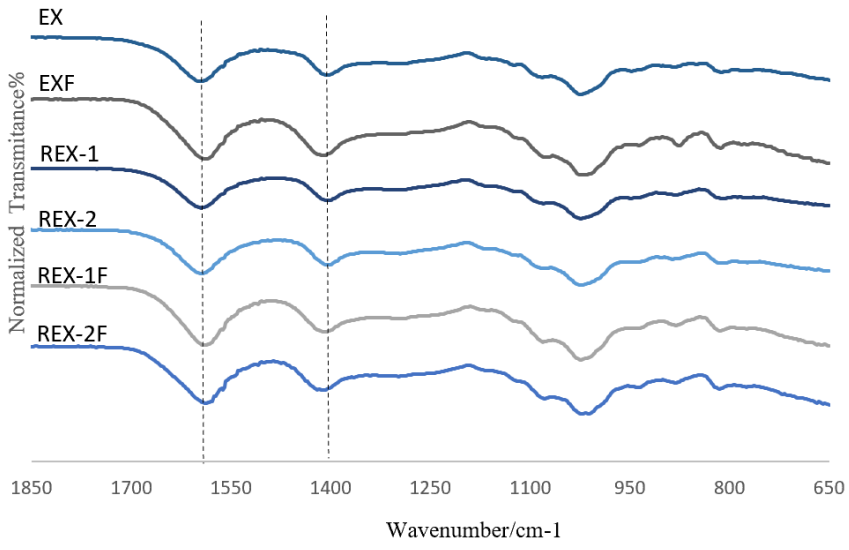


Figure 2.16 FTIR Spectra of KELP-extract alginate, hydrogel, recycled, and recycled hydrogel status, Normalized to max transmittance intensity, at 1021 cm-1

2.3.2.2 EDX Results

Energy dispersive X-ray was utilized to further study the recycling procedure calcium crosslinker removal efficiency[71]. For each of I-2, I-2G, and EX (kelp-extract alginate), normalized wt.% of O, Na, Mg, Cl, K, Ca, and Fe were compared in 4 sodium alginate states: pure Sodium alginate, sodium alginate hydrogel, recycled sodium alginate, and recycled sodium alginate hydrogel.

As mentioned in section 2.2.3 (Hydrogel Film Formation Procedure), a combination of calcium carbonate and gluconic-delta-lactone is used to pre-gel a film of alginate, which is then crosslinked using a dilute solution of calcium chloride. Based on the hydrogel formation, an increase in Ca and Cl element Wt.% was expected as a result of film formation followed by a decrease of Wt.% of these 2 elements after recycling and $Ca^{2+}$ crosslinker removal.

As presented for I-2 in Table 2.5, $Ca^{2+}$ ion, which is vital for crosslinking and formation of egg-box structure, was 0.31 Wt.% in I-2 starting material and increased to 13.54% in I-2 hydrogel. The recycling procedure was effective in reducing Ca Wt.% to 0.06 Wt.%, which is less than the starting material. The traceability of calcium ions is essential for understanding their retention levels, which directly impacts the hydrogel's reusability, strength, and stability over multiple cycles.

Table 2.5 EDX elemental analysis of commercial I-2, I-2G hydrogel film (I2F),recycled I-2 (RI-2) and hydrogel film of recycled I-2 (RI-2F)

| | | I-2 | I2F | RI-2 | RI-2F |
|---|---|---|---|---|---|
| | | Normalized | Normalized | Normalized | Normalized |
| Element | Atomic number | [Wt.%] | [Wt.%] | [Wt.%] | [Wt.%] |
| O | 8.00 | 72.84 | 70.77 | 70.38 | 54.83 |
| Na | 11.00 | 26.05 | 6.28 | 28.71 | 16.83 |
| Mg | 12.00 | 0.34 | 0.11 | 0.11 | 0.22 |
| Cl | 17.00 | 0.25 | 9.26 | 0.73 | 12.67 |
| K | 19.00 | 0.10 | 0.01 | 0.01 | 0.02 |

| | | | | | |
|---|---|---|---|---|---|
| Ca | 20.00 | 0.31 | 13.54 | 0.06 | 15.36 |
| Fe | 26.00 | 0.06 | 0.01 | 0.01 | 0.12 |

Table 2.7 presents elemental analysis for I-2G. The same trend is followed in the Ca element normalized Wt.% in I-2G. This result confirms the calsium crosslinker removal efficiency of recycling procedure for the case of I-2G.

Table 2.6 EDX elemental analysis of commercial I-2G, I-2 hydrogel film (I-2GF), recycled I-2G (RI-2G) and hydrogel film of recycled I-2G (RI-2GF)

| | | I-2G | I-2GF | RI-2G | RI-2GF |
|---|---|---|---|---|---|
| | | Normalized | Normalized | Normalized | Normalized |
| Element | Atomic number | [wt.%] | [wt.%] | [wt.%] | [wt.%] |
| O | 8.00 | 62.88 | 26.62 | 64.65 | 17.61 |
| Na | 11.00 | 35.22 | 34.91 | 32.95 | 27.64 |
| Mg | 12.00 | 0.19 | 0.15 | 0.10 | 0.32 |
| Cl | 17.00 | 1.13 | 33.82 | 0.94 | 38.98 |
| K | 19.00 | 0.44 | 0.14 | 1.08 | 0.06 |
| Ca | 20.00 | 0.13 | 4.35 | 0.27 | 15.34 |
| Fe | 26.00 | 0.02 | 0.00 | 0.01 | 0.07 |

Low Ca content in I-2GF (4.25 Wt%) as compared to I-2F and EXF, which contained 13.54 Wt% and 10.99 Wt% Ca can be related to the difference in G content and the pre-gelation step in hydrogel formation (See section 2.2.3). A potential explanation can be that a high G content contributes to the formation of a dense and rigid gel network (Pre-gelation with the use of $Ca_2CO_3$). While this can enhance the mechanical strength of the gel, it can also make it difficult for crosslinkers to penetrate deeply into the gel matrix, resulting in less efficient crosslinking (with the use of $CaCl_2$).

To study the Ca crosslinker removal of recycling procedure for kelp-extract sodium alginate, EDX was conducted on kelp-extract sodium alginate, the hydrogel form, recycled and the hydrogel of the recycled kelp-extract sodium alginate. As shown in Table 2.8, for the case of REX-1 and REX-2 there is 1.39 and 1.22 Wt.% remaining calcium which is higher than that of I-2 and I-2G. A potential source of this increase in calcium content can be related to the consistency of the recycled sodium alginate pellet during the isolation and purification step of the recycling procedure (See section 2.2). Due to the low molecular weight (See section 3.3.1), the sodium alginate pellets of REX were not as dense as RI-2 and RI-2G. This made it impossible to fully decant and separate

the rinsing solution from the pellets, causing some solution to become trapped within the pellets. As a result, the dried REX-1 and REX-2 samples exhibited a higher content of Ca.

Table 2.7 EDX elemental analysis of kelp-extract sodium alginate (EX), EX hydrogel film (EXF), recycled EX (REX-1, REX-2), and hydrogel film of recycled REX-2 (REX-2F)

| | | EX | EXF | REX-1 | REX-2 | REX-1F | REX-2F |
|---|---|---|---|---|---|---|---|
| | | Normalized | Normalized | Normalized | Normalized | Normalized | Normalized |
| EL | AN | [wt.%] | [wt.%] | [wt.%] | [wt.%] | [wt.%] | [wt.%] |
| O | 8.00 | 74.70 | 48.13 | 74.66 | 75.70 | 75.76 | 65.27 |
| Na | 11.00 | 24.26 | 20.67 | 22.96 | 22.66 | 10.89 | 7.98 |
| Mg | 12.00 | 0.08 | 0.04 | 0.04 | 0.06 | 0.24 | 0.16 |
| Cl | 17.00 | 0.33 | 20.09 | 0.25 | 0.04 | 4.69 | 11.60 |
| K | 19.00 | 0.46 | 0.07 | 0.71 | 0.29 | 0.17 | 0.05 |
| Ca | 20.00 | 0.15 | 10.99 | 1.39 | 1.22 | 8.24 | 14.87 |
| Fe | 26.00 | 0.02 | 0.00 | 0.00 | 0.03 | 0.01 | 0.06 |

Equation 7 is used to calculate Ca element removal efficiency:

$$\text{Calcium Removal\%} = \left( \left| Ca_R - Ca_F \right| / Ca_F \right) \times 100 \quad \text{(Equation7)}$$

Where $Ca_R$ is the normalized Wt.% of Ca recycled sodium alginate and $Ca_F$ is the normalized Wt.% of Ca in sodium alginate film.

In Table 2.9, the Ca removal efficiency of the recycling procedure for three of the starting materials is presented. For commercial I-2 the ca element removal% stayed the highest compared to I-2G and kelp-extract alginate. While for all sodium alginate sources, Ca removal% stayed high, it was less efficient for the case of kelp-extract sodium alginate, with 87.4% and 88.9%. It is expected to see the effect of the remaining Ca element and as a result in remaining crosslinks and polymer entanglement in the further characterizations.

Table 2.8 Recycling procedure Ca element removal efficiency

| Sample | Ca element removal% |
|---|---|
| I-2 | 99.5% |
| I-2G | 93.8% |
| KELP-extract sodium alginate | 87.4%,88.9% |

The calculated Ca removal% from EDX data is in agreement with FTIR findings (See section 2.3.2.1) where C-O-C symmetric and asymmetric peak shifts identified minor remaining Ca content for the case of RI-2G and REX-1, REX-2. While no peak shift from initial I-2 was observed in the case of R-I2, revealing successful Ca removal.

### 2.3.3 Effects of Recycling on Molecular Weight and Polydispersity of Sodium Alginate

#### 2.3.3.1 GPC Result

The molecular weight distribution of the sodium alginate samples was determined by gel permeation chromatography (GPC)[72]. The weight-average molecular weight (Mw), number average molecular weight (Mn), and polydispersity index (PDI) are presented in Figures 2.17, 2.18, and 2.19 and summarized in Table 2.9. Experimental results demonstrate a difference in the weight-average molecular weight before and after recycling for all sodium alginate sources. The lower molecular weight of the recycled I-2 and I-2G compared with the starting material can be due to depolymerization and reduction in molecular weight through hydrolysis of glycosidic linkage[73]. Furthermore, the precipitation of alginate with acid may have degraded the polysaccharide, likely due to acid hydrolysis of the glycosidic bond[74]. The commercial products of I-2 and I-2G demonstrated a decrease in $M_W$ and Mn while the lab-prepared materials were higher after recycling. The depolymerization effect was not confirmed by kelp-extract sodium alginate GPC results. Unlike I-2 and I-2G, Recycled EX resulted in higher molecular weight compared with EX which can be related to removal of low molecular weight polymer chains, which are less probable to be entangled to longer chains, during the purification and isolation steps of the recycling procedure. The presence of higher calcium content in Recycled EX ( See section 2.3.2.2 ) might also helped the polymer chains maintain their integrity during the recycling process, preventing extensive depolymerization and encouraging the formation of longer, more interconnected polymer chains.

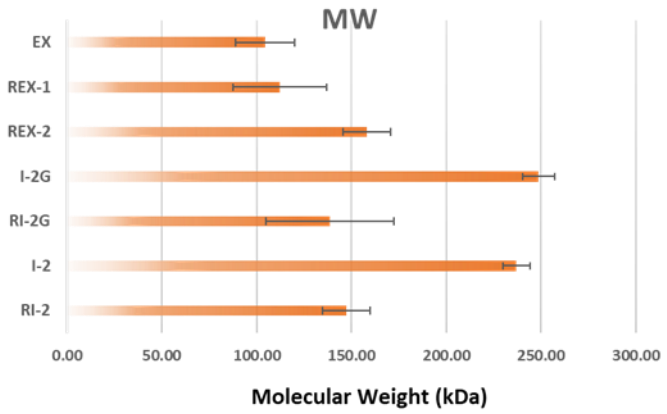


Figure 2.17 Molecular weight comparison among non-film alginate samples

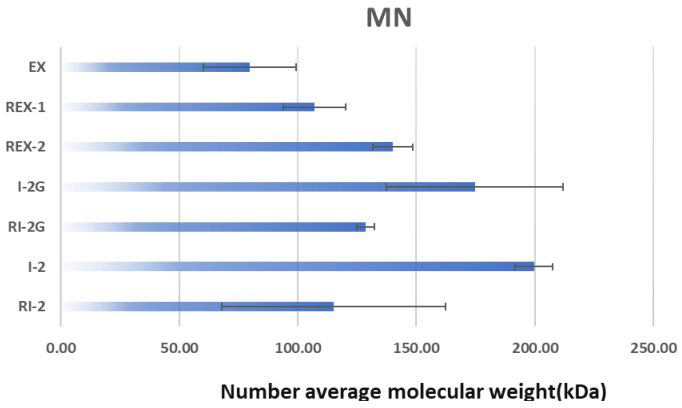


Figure 2.18 Molecular number comparison among non-film alginate samples

The polydispersity index quantifies the heterogeneity of polymer molecular weight distributions by comparing Mw and Mn. A higher PDI indicates a more diverse molecular weight distribution, characterized by a larger difference between Mw and Mn[75,76]. As presented in Table 2.9, recycling did not contribute to an increase in PDI and insignificantly decreased PDI for the case of I-2G and EX sodium alginate sources. A minor increase in PDI was witnessed for commercial I-2.

The significance of the PDI value changes between each pair of starting materials and the recycled version was studied using T-test. The significance level ($\alpha$) is considered to be 0.05, which is 5%

risk error, commonly used in many scientific fields[80]. If the p-value is greater than the significance level (α), the result is not statistically significant.

For the case of I-2 and RI-2, the two-tailed P value equals 0.8285 By conventional criteria, this difference is considered to be statistically insignificant. With I-2G, RI-2G pair, the two-tailed P value equals 0.3435, this difference is considered to be statistically insignificant. EX, REX-1 pair showed a non-significant two-tailed P value of 0.1560. While EX, REX-2 pair two-tailed P value was calculated to be 0.2169, which is considered statistically insignificant.

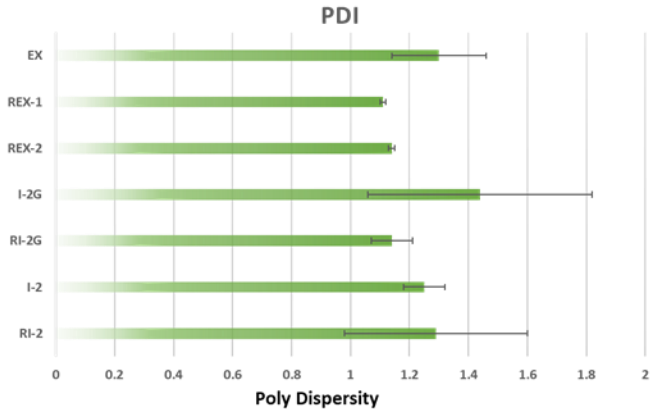


Figure 2.19 Polydispersity index comparison among 3 sodium alginate sources

Alginate with higher molecular weight produces materials that are stronger and lower solubility in water[77]. For instance, Costa et al., (2018) reported that alginate films composed of higher Mw (300 kDa) attained better mechanical properties than films from lower Mw (<200 kDa)[77]. Therefore, the reduced molecular weight of the recycled alginate kelp-extracted alginate will likely produce less tough and lower-strength materials compared with recycled I-2 and recycled I-2G. Optimizing recycling conditions could help optimize the molecular weight and properties of alginates for various applications[73,74].

Table 2.9 Summary of GPC results for non-film sample codes

| Sample | Mw (kDa) | Mn (kDa) | PDI |
|---|---|---|---|
| I-2 | 237±7 | 199±8 | 1.25±0.07 |
| RI-2 | 147±12 | 115±47 | 1.29±0.31 |
| I-2G | 248±8 | 174±37 | 1.44±0.38 |
| RI-2G | 138±33 | 128±4 | 1.14±0.07 |

| | | | |
|---|---|---|---|
| EX | 104±15 | 79±19 | 1.30±0.16 |
| REX-1 | 112±24 | 106±13 | 1.11±0.01 |
| REX-2 | 158±13 | 140±8 | 1.14±0.01 |

### 2.3.4 Effects of Recycling on Uronic Acid Composition of Sodium Alginate

#### 2.3.4.1 NMR Result

The uronic acid composition of both the extracted sodium alginate and commercial samples was analyzed using $^{1}$H NMR spectroscopy, with the results presented in Table 2.10. The relative mannuronic and guluronic acid contents (M/G ratio), block length, and block distribution provide information on the alginate composition and influence its physicochemical properties and potential applications. Specifically, the ratio between mannuronic and guluronic acid blocks (M/G ratio) is recognized for providing information on the ionic crosslinking capabilities with divalent cations, which influence the mechanical properties of alginate-based materials, including elasticity and rigidity[23]. The experimental results indicate that the M/G ratio varied significantly between the commercial and isolated alginates. I-2G, with an average M/G ratio of 0.25, has more G blocks than I-2 (1.02) and the mixture of kelp-extracted sodium alginate (1.38). To study the consistency of the M/G ratio, 1H NMR spectroscopy at 85º C was conducted for each of the 5 series of extraction[78]. The elevated temperature serves two purposes, firstly the decreased sample viscosity results in narrower line-widths and secondly, the water resonance is moved away from the spectral region of interest due to waters temperature dependent chemical shift[78]. As presented in Table 2.10, the M/G ratio for samples ex-1 to ex-4 varied between 1.36 and 1.46, while ex-5 had an M/G ratio of 1.15. Assuming homogeneous mixing, the expected experimental M/G ratio for the EX would be the same as the numerical average of the M/G ratio of ex-1 to ex-5. With a 0.106 difference from the numerical average of 1.35, the experimental M/G ratio of EX was 1.38, indicating a homogeneous EX mixture.

Both RI-2 and RI-2G NMR data showed a 0.11 increase in the M/G ratio from I-2 and I-2G, respectively. During the recycling process, guluronic acid units degrade more readily than mannuronic acid units due to differences in their chemical stability[79]. The G blocks are more prone to degradation due to their stiffer and more extended chain configuration, which is less flexible

than the M blocks. As a result, the G blocks are more susceptible to hydrolysis and other chemical degradation processes[79]. The glycosidic linkages between the sugar monomers of the polysaccharide are prone to cleavage in both acidic and alkaline environments. Under acidic conditions, with pH values below 5, notable molecular weight reduction occurs due to acid hydrolysis of the glycosidic bonds. Conversely, alkaline conditions lead to chain scission at the glycosidic bonds[80]. This selective degradation results in a relative increase in the proportion of mannuronic acid units. Moreover, exposure to oxygen during the recycling process could result in oxidative degradation of the alginate. Since guluronic acid units are more prone to oxidation than mannuronic acid units, this could increase the M/G ratio[79]. Guluronic acid has a structure with the carboxyl group at the C6 position and hydroxyl groups at the C2 and C3 positions[81]. The hydroxyl group at C3 is in the axial position, which makes the molecule more rigid. This rigidity and the spatial arrangement of the functional groups make the G units more accessible to oxidative agents, thereby increasing their reactivity towards oxidation. Due to the axial hydroxyl group at C3, the guluronic acid units have a higher electron density around the oxygen atoms, making them more susceptible to oxidation. Oxidative agents can more easily interact with these oxygen-rich regions, leading to the cleavage of the glycosidic bonds and degradation of the polysaccharide chain. Mannuronic acid also has the carboxylate group at C6 as well as hydroxyl groups at C2 and C3, which are both in the equatorial positions. This configuration makes the M units more flexible and less rigid compared to G units. The equatorial hydroxyl groups in mannuronic acid units distribute the electron density more evenly, making these units less reactive to oxidative agents[81] (See Fig 2.20). The flexibility of M units allows them to avoid some of the oxidative stress that rigid G units cannot escape. This could result in increased the M/G ratio following the recycling procedure.

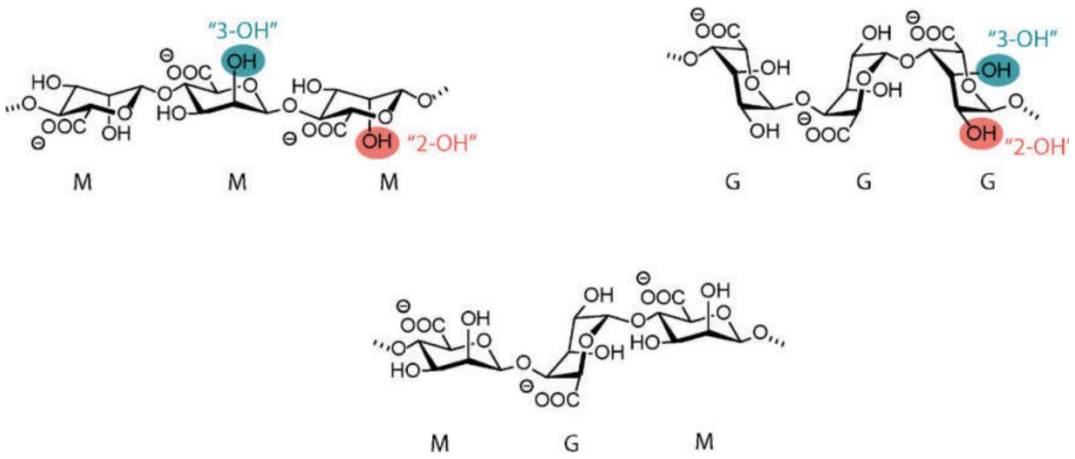


Figure 2.20 Chemical structure of alginate. C2 and C3 hydroxyl groups are highlighted[81]

Mechanical processes involved in recycling steps, such as grinding, and chemical ones such as neutralization, can also cause chain scission. Depending on the conditions, this could preferentially affect guluronic acid-rich regions[79]. Although the same effect was expected for recycled EX (REX-1, REX-2) showed a slightly lower M/G ratio compared with EX (REX: 1.28, EX: 1.37 respectively). This result can be justified by the support of the EDX result, which indicated a notable remaining calcium content in recycled EX (See section 2.3.2.2). Calcium ions have a higher affinity for binding to guluronic acid units compared to mannuronic acid units. In the presence of calcium, these ions preferentially cross-link the G units, forming a more stable and less degradable gel network. This selective stabilization might protect the G units from degradation during the recycling process, resulting in a slightly lower M/G ratio.

The fraction of guluronic acid diads ($F_{GG}$), average block length ($N_G$, $N_M$), and block distribution were calculated using equations in the methodology section 2.2.7.3 (Equations 1-4). The fraction of guluronic acid diads (FGG) improves binding with divalent cations. This enhanced binding improves the crosslinking effect, leading to the formation of stronger and more stable materials[47]. The $F_{GG}$ content in the I-2, RI-2, EX, and REX-2 was~ 0.22, while REX-2 showed an $F_{GG}$ of 0.56 which is close to the calculated FGG values for I-2G and RI-2G.

The average length of G-blocks ($N_G$) impacts the ion-binding and thereby material properties[47]. Recycling caused an increase in $N_G$ of commercial materials as well as the extracted sodium

alginate. RI-2G showed the highest $N_G$, followed by R-EX (1&2) and RI-2 (3.37,2.06,2.24 and 1.84 respectively.

In sodium alginate, "block distribution" refers to the arrangement and sequence of the mannuronic acid (M) and guluronic acid (G) units along the polymer chain[78] (See equation8). The block distribution can be characterized by three main types of sequences:

Homopolymeric M-blocks: Sequences of consecutive mannuronic acid units (M-M-M-M-...).

Homopolymeric G-blocks: Sequences of consecutive guluronic acid units (G-G-G-G-...).

Heteropolymeric MG-blocks: Alternating sequences of mannuronic and guluronic acid units (M-G-M-G-...).

Block distribution=FGM, MG/(FM×FG) (Equation8[78]).

In the context of sodium alginate and based on equation 8, "Lower block distribution" corresponds to smaller numbers and generally refers to a greater degree of homopolymeric block formation within the polymer chain[82]. This means that the sequences of consecutive mannuronic acid (M) or guluronic acid (G) units are longer on average. Lower block distribution can significantly impact the physical and chemical properties of the alginate.

As shown in Table 2.11, the starting materials (before recycling) had the following block distribution numbers: EX had the lowest at 0.85, followed by I-2 at 1.19, and I-2G at 1.79. For the case of I-2 and I-2G, recycling resulted in a decreased block distribution number which indicates an increase in the length of homopolymer blocks. While REX-1 showed the same effect with a lower block distribution number of 0.77 compared with EX, a minor increase was recorded for REX-2.

Understanding block distribution is crucial in tailoring sodium alginate for specific applications, such as in food technology, pharmaceuticals, and biomaterials, where properties like gelation behavior, viscosity, and biocompatibility are influenced by the arrangement of M and G units.

Table 2.10 Processed NMR data using equations: 1-4

| Sample | M/G | FG | FGG | FM | FMM |
|---|---|---|---|---|---|
| I-2 | 1.01±0.02 | 0.51±1.38 | 0.20±0.00 | 0.50±0.01 | 0.20±0.01 |
| RI-2 | 1.12±0.04 | 0.47±0.01 | 0.22±0.01 | 0.53±0.01 | 0.27±0.03 |
| I-2G | 0.25±0.05 | 0.80±0.01 | 0.52±0.01 | 0.20±002 | 0.09±0.02 |
| RI-2G | 0.36±0.08 | 0.74±0.01 | 0.51±0.02 | 0.26±0.04 | 0.09±0.04 |
| ex*-1 | 1.37±0.21 | 0.42±0.04 | 0.20±0.02 | 0.58±0.04 | 0.35±0.09 |
| ex-2 | 1.41±0.01 | 0.42±0.01 | 0.21±0.02 | 0.58±0.1 | 0.38±0.03 |
| ex-3 | 1.46±0.05 | 0.41±0.01 | 0.21±0.01 | 0.59±0.01 | 0.40±0.02 |
| ex-4 | 1.36±0.06 | 0.42±0.01 | 0.21±0.01 | 0.58±0.01 | 0.34±0.04 |
| ex-5 | 1.15±0.04 | 0.46±0.01 | 0.20±0.00 | 0.54±0.01 | 0.27±0.01 |
| EX** | 1.38±0.02 | 0.42±0.00 | 0.29±0.13 | 0.52±0.00 | 0.37±0.01 |
| REX-1 | 1.28±0.14 | 0.44±0.03 | 0.56±0.03 | 0.34±0.08 | 0.36±0.08 |
| REX-2 | 1.37±0.5 | 0.42±0.01 | 0.23±0.00 | 0.58±0.01 | 0.39±0.02 |

* ex is the abbreviation used for each single kelp-extract sodium alginate extraction series
**EX is the abbreviation used for mix of 5 series of kelp-extraction alginate extractions

Table 2.11 Processed NMR data using equations: 1-4

| sample | FGM, MG | Block length, NG | Block length, NM | Block distribution, n |
|---|---|---|---|---|
| I-2 | 0.30±0.01 | 1.67±0.02 | 1.68±0.06 | 1.19±0.03 |
| RI-2 | 0.26±0.02 | 1.84±0.09 | 2.06±0.17 | 1.03±0.06 |
| I-2G | 0.28±0.01 | 2.83±0.08 | 1.86±0.07 | 1.79±0.14 |
| RI-2G | 0.22±0.05 | 3.37±0.58 | 1.24±0.49 | 1.18±0.34 |
| ex*-1 | 0.22±0.06 | 1.96±0.34 | 2.74±0.90 | 0.91±0.22 |
| ex-2 | 0.20±0.02 | 2.07±0.19 | 2.91±0.35 | 0.83±0.09 |
| ex-3 | 0.19±0.02 | 2.11±0.13 | 3.09±0.30 | 0.80±0.06 |
| ex-4 | 0.21±0.02 | 2.02±0.19 | 2.76±0.38 | 0.86±0.09 |
| ex-5 | 0.26±0.01 | 1.76±0.03 | 2.03±0.09 | 1.06±0.03 |
| EX** | 0.21±0.01 | 2.04.08 | 2.81±0.13 | 0.85±0.04 |
| REX-1 | 0.22±0.05 | 2.06±0.32 | 2.67±0.67 | 0.89±0.20 |
| REX-2 | 0.19±0.01 | 2.24±0.10 | 3.06±0.26 | 0.77±0.05 |

### 2.2.3.5 Effect of Recycling on Mechanical Properties of Sodium Alginate Hydrogel Films

To study the impact of the M/G ratio of the starting sodium alginate sources as well as the effect of recycling on the macro properties of the sodium alginate hydrogel, tensile testing was conducted (See section 2.2.7.5). It was expected for hydrogels made of sodium alginate of lower M/G ratio

to show higher mechanical strength due to the increased number of G blocks which contribute to crosslinking and making the egg-box structure[26].

2.2.3.5.1 Tensile Test Results

Mechanical characteristics of both recycled and non-recycled sodium alginate hydrogels are summarized in Table 2.13. For all sample codes, tensile tests were conducted on 4 sodium alginate hydrogel films, using 2 sample strips per disc.

In the case of I-2, recycling caused Young's modulus to decrease by 31.2%, which agrees with the increase in the M/G ratio and degradation of G blocks. See Fig 2.21 for the stress-strain% diagram of I-2 and RI-2.

Although I-2G did not possess higher mechanical characteristics compared to I-2, recycling impacted Young's modulus by 11.4% which indicates I-2G was less impacted by recycling compared to I-2. Although the increase in the M/G ratio was at the same level as in the I-2 case (0.11), the effect on macroscopic mechanical properties was not the same. This suggests the existence of relevant other variables other than the M/G ratio, like inherent differences in sample specifications (See Table 2.4).

The increased moisture% in I-2GF (16.0%) and RI-2GF (22.5 %) compared with I-2F and RI-2F (14.3 and 14.9 respectively), could have contributed to decreased Young's modulus of the I-2G samples. Young's modulus, which is a measure of the stiffness of the hydrogel, decreases with higher water content. This is because the additional water reduces the interactions between polymer chains, making the hydrogel less rigid.

Young's modulus decreased by 15.6% in REX-2F, compared to that of EXF. It needs to be considered that the hydrogel formula of REX-2F was not consistent with other sample codes due to processing difficulties (see section 2.2.3), and making comparisons using REX-2F mechanical properties data might not be valid; as noted previously, REX-1F did not form films.

Unlike RI-2F and RI-2GF, tensile strength was increased in REX-2F in comparison to EXF. Since M/G ratio numbers are in the same range, the remaining Ca element in REX-2F, which was discussed in EDX results (See section 2.3.2.2), can be the justification behind this increasing change. The remaining $Ca^{2+}$ can cause polymer chains to entangle and keep some of the egg-box-

shaped structures in place even after recycling, which could have contributed to an increase in tensile strength.

Table 2.12 Mechanical characteristics of commercial alginate sources, extracted alginate, and recycled material

| | I-2F | RI-2F | I-2GF | RI-2GF | EXF | REX-2F |
|---|---|---|---|---|---|---|
| | Base Material | Recycled | Base Material | Recycled | Base Material | Recycled |
| Young's Modulus (MPa) | 4245±608 | 2893±373 | 4048±527 | 3585±203 | 3587. ±263 | 3024±331 |
| Tensile Strength (MPa) | 109±11 | 71±4 | 85±32 | 78.04±5 | 42±12 | 54±8 |
| M/G ratio | 1.01±0.02 | 1.12±0.04 | 0.25±0.05 | 0.36±0.08 | 1.38±0.02 | 1.37±0.5 |

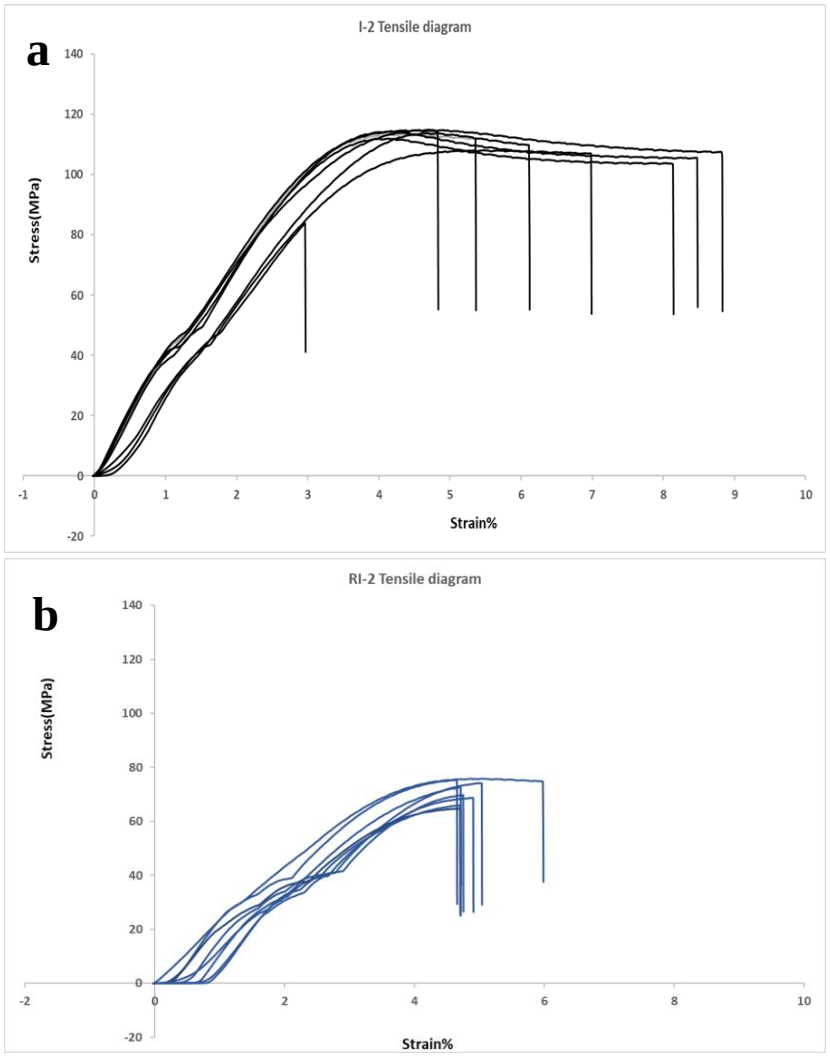


Figure 2.6 a) Stress-strain diagram of commercial I-2 b) Stress-strain diagram of RI-2 , 8 film strips from 4 hydrogel film discs were tested for each condition

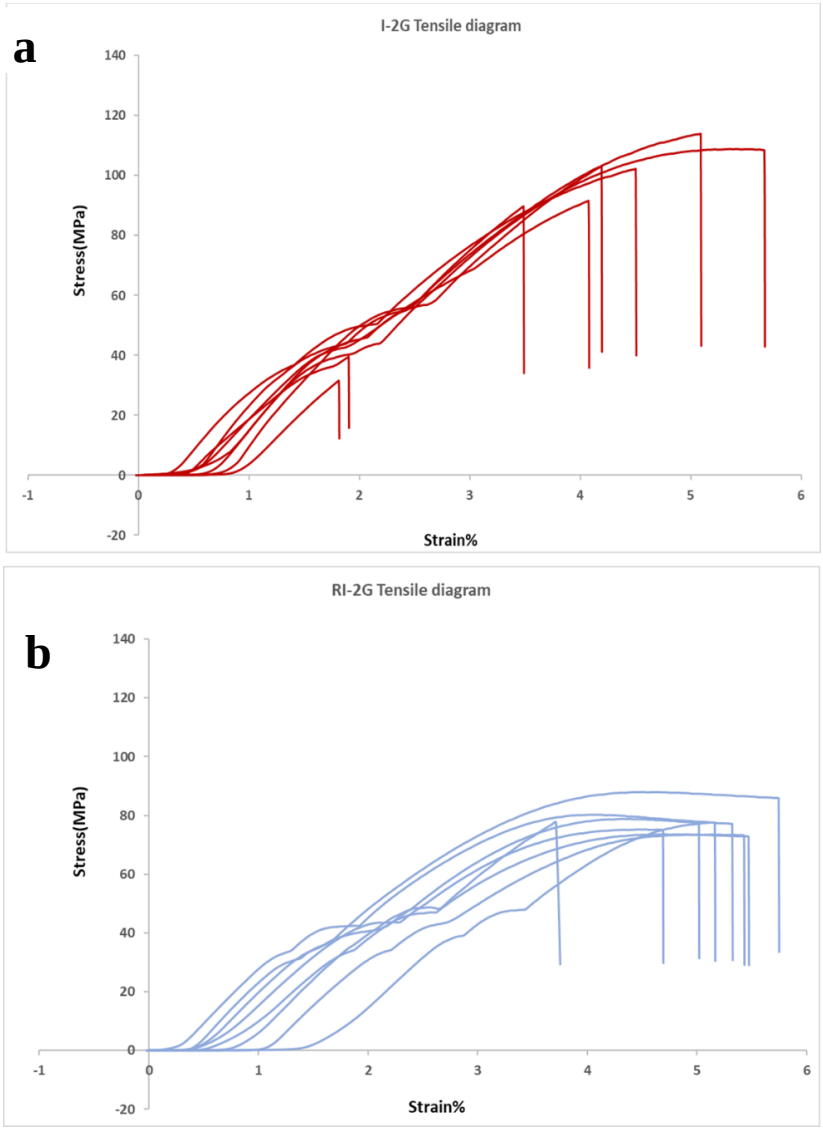


Figure 2.7 a) Stress-strain diagram of commercial I-2G b) Stress-strain diagram of RI2-G, 8 film strips from 4 hydrogel film discs were tested for each condition

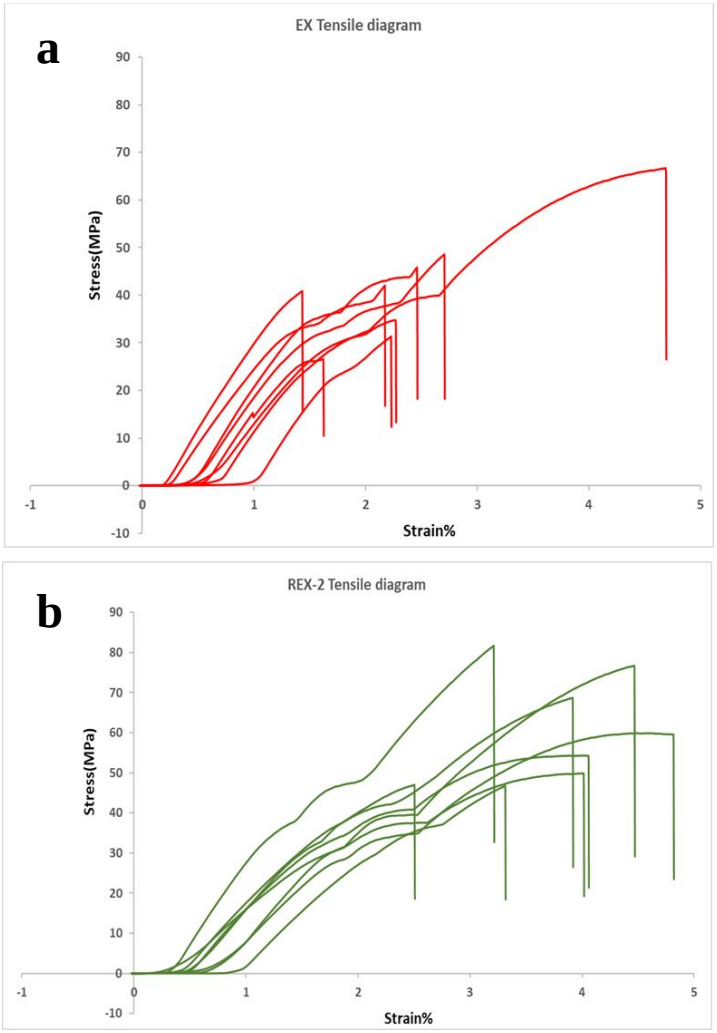


Figure 2.8 a) Stress-strain diagram of kelp-extracted alginate EX b) ress-strain diagram of REX-1, 8 film strips from 4 hydrogel film discs were tested for each condition

### 2.3.6 Summary of Spectroscopic Results: Investigating Structural Alterations in Sodium Alginate

The main goals of this study are to establish and evaluate the recycling protocol's effectiveness in terms of yield and purity, analyze the removal of $Ca^{2+}$ crosslinkers, and investigate the structural changes in sodium alginate caused by the recycling process.

To find out how the M/G ratio, molecular weight, Ca content, and chemical structure of the starting material impact the recycling yield and the structural alteration that the chosen recycling procedure

causes to the selected alginate materials, NMR, GPC, EDX, FTIR result as well as recycling yield and Ca removal data are summarized in Table 2.14.

Table 2.13 Summary of spectroscopic results, and recycling efficiency data

| **Sample** | **$MG_S/MG_R$ ($^1$HNMR)** | **$Mw_S/Mw_R$ (GPC) [KDa]** | **Confirmation of sodium alginate structure (FTIR)** | **Confirmation of Ca removal efficiency (FTIR)** | **Ca content (EDX) [wt.%]** | **Ca element removal % (EDX)** | **Recycling yield%** |
|---|---|---|---|---|---|---|---|
| I2/RI2 | 1.01/1.12 | 237/147 | ✓ | ✓ | 0.31/0.06 | 99.5% | 52.5% |
| I2G/RI2G | 0.25/0.36 | 248/138 | ✓ | minimal remaining Ca effect | 0.13/0.27 | 93.8% | 62% |
| EX/ REX (1&2) | 1.38/1.28,1.37 | 104/112/158 | ✓ | minimal remaining Ca effect | 0.15/1.39,1.22 | 88.2% | 56.5%,55.7% |

To analyze the relationships between key variables and simplify data interpretation, the M/G ratio of the recycled material ($MG_R$) was considered as the dependent variable relative to the M/G ratio of the starting material ($MG_S$). As shown in Table 2.13, a higher M/G ratio in the starting material results in a higher M/G ratio in the recycled material.

In addition, the recycling yield percentage was analyzed as a dependent variable in relation to both $MG_S$ and $MG_R$. Table 2.14 indicates that the highest G content in the starting material (associated with the lowest $MG_S$ and $MG_R$) resulted in the highest recycling yield percentage. However, for samples I2 and EX, where I2/RI2 had a higher G content, the recycling yield was lower than that of EX. It is important to note that factors beyond the M/G ratio, such as operational conditions like mixing intensity during the neutralization step (which can impact pellet integrity and lead to losses due to human error, as discussed in Section 2.2.4), also influence recycling yield.

The molecular weight of the recycled material ($Mw_R$) was considered dependent on the molecular weight of the starting material ($Mw_S$). Since hydrogel film formation of sodium alginate does not involve covalent bonding, no increase in molecular weight was expected. The observed decrease

in $Mw_R$ is likely due to the breakage of polymer chains caused by shear forces during the recycling process.

Lastly, the percentage of calcium removal was examined as a dependent variable in relation to $Mw_S$. Due to the lower molecular weight (see Section 2.3.3.1), the sodium alginate pellets from the REX samples were less dense than those from RI-2 and RI-2G. This made it difficult to fully decant and separate the rinsing solution from the pellets, causing some solution to become trapped within the pellets. Consequently, the dried REX-1 and REX-2 samples exhibited higher calcium content

## 2.4 Conclusion

The recycling of sodium alginate hydrogels presents a promising avenue for sustainable material utilization. In this research recycling from raw materials produced recoveries ranging from 52.5% to 62%. Commercial I-2G exhibited the highest average yield at 62.0%, followed by kelp-extract sodium alginate with an average 56.1% recycling yield.

The M/G ratio analysis revealed that the recycling procedure caused I-2 and I-2G a considerable increase in the M/G ratio, indicating lower guluronic acid content, contributing to weaker gel formation and stability properties of the recycled material. In the case of EX, the M/G ratio remained largely unchanged, which helps maintain the hydrogel structure and thereby maintains the mechanical properties of the hydrogel film. Studied by tensile test, tensile strength decreased for recycled I-2 and I-2G compared with their base material as a result of increased M/G ratio, while tensile strength was improved for the case of EX which showed no change in M/G ratio in terms of recycling. This increasing effect was attributed to high $Ca^{2+}$ content in REX. The remaining $Ca^{2+}$ can cause some of the egg-box-shaped structures in place even after recycling, which could have contributed to an increase in tensile strength.

Efforts to characterize $Ca^{2+}$ crosslinker removal through FTIR and EDX analyses confirmed the effectiveness of the recycling process in minimizing residual calcium ions. This is crucial for maintaining hydrogel integrity. Furthermore, GPC analysis highlighted changes in molecular weight post-recycling, influenced by depolymerization mechanisms and chemical treatments during the recycling process. Notably, while recycled I-2 and I-2G exhibited reduced molecular weights, kelp-extracted alginate showed a slight increase due to the removal of low molecular weight polymer chains during the purification and isolation steps of the recycling procedure.

NMR analysis of the alginate composition demonstrated alterations in the M/G ratio post-recycling, indicating selective degradation of guluronic acid units under recycling conditions. This finding underscores the importance of recycling conditions in preserving the polymer's structural integrity and functional properties.

Overall, the molecular structure specifications of kelp-extract sodium alginate, such as the M/G ratio and molecular weight (Mw), showed improvement after recycling. Additionally, the recycled kelp-extract sodium alginate hydrogel maintained mechanical properties comparable to those of the material prior to recycling. These findings suggest that kelp-extract sodium alginate demonstrated the most efficient recycling performance in terms of preserving material properties. However, it is important to note that the higher calcium content in the recycled kelp-extract sodium alginate likely contributed to this result. While beneficial in the short term, the elevated calcium levels could negatively impact reusability and processing over multiple recycling rounds.

Overall, the study underscores the feasibility of recycling sodium alginate hydrogels as a sustainable strategy. This approach paves the way for their continued application in diverse fields, ranging from biomedical to industrial sectors.

Moving forward, future studies could focus on optimization of Recycling Conditions to investigate further the influence of impacting parameters (e.g., pH, temperature, duration) on the yield and quality of recycled sodium alginate hydrogels. This could include exploring alternative methods or additives to enhance recycling efficiency and minimize degradation

Moreover, exploring different $Ca^{2+}$ crosslinker removal techniques (e.g., filtration, ion exchange) and their impact on the structural and chemical properties of recycled hydrogels could help optimize purification processes. This would further enhance the material's quality and recyclability.

To determine the level of material recovery in recycling processes that ensures sustainability, future research should incorporate comprehensive assessments using methodologies like Material Flow Analysis (MFA) and Life Cycle Assessment (LCA). MFA can quantify material flows throughout the recycling system, pinpointing inefficiencies and identifying potential areas for improvement. Meanwhile, LCA offers a holistic perspective on the environmental impacts across the entire lifecycle of recycled materials, from collection and processing to their final use.

The lack of statistical analysis in this study arises from the limited number of data points, which was due to constraints in the production capacity of kelp-extract sodium alginate and its recycling process. Additionally, while the study included two commercial alginates for comparison, the dataset remained insufficient for robust statistical calculations. This limitation should be explicitly

acknowledged in the thesis to provide transparency about the scope of the findings and the challenges faced during the research.

For future work, it is recommended to expand the production capacity of kelp-extracted sodium alginate as well as the recycling capacity while increasing number of commercial alginate types to generate a larger dataset. This would enable comprehensive statistical analyses, providing greater confidence in the observed trends and allowing for more precise conclusions regarding the molecular weight changes and recycling outcomes. Incorporating statistical validation in future studies will strengthen the scientific rigor and reliability of the results.

The other research gap to focus on could be conducting application-specific studies to evaluate the performance of recycled sodium alginate hydrogels in various fields, such as biomedical applications (e.g., drug delivery, wound healing) or environmental applications (e.g., water treatment, soil stabilization). This would validate their suitability and effectiveness compared to virgin materials. These suggestions aim to advance the understanding and application of recycled sodium alginate hydrogels, addressing key research gaps identified in these studies.

## 2.5 References


(1) Mangaraj, S.; Yadav, A.; Bal, L. M.; Dash, S. K.; Mahanti, N. K. Application of Biodegradable Polymers in Food Packaging Industry: A Comprehensive Review. *J Package Technol Res* **2019**, *3* (1), 77–96. https://doi.org/10.1007/s41783-018-0049-y.

(2) Manger, C. *Bioplastics facts & figures*. European Bioplastics e.V. https://www.european-bioplastics.org/bioplastics-facts-figures/ (accessed 2024-04-18).

(3) Geyer, R.; Jambeck, J. R.; Law, K. L. Production, Use, and Fate of All Plastics Ever Made. *Sci Adv* **2017**, *3* (7), e1700782. https://doi.org/10.1126/sciadv.1700782.

(4) Messerli, P.; Kim, E. M.; Lutz, W.; Moatti, J.-P.; Richardson, K.; Saidam, M.; Smith, D.; Eloundou-Enyegue, P.; Foli, E.; Glassman, A.; Licona, G. H.; Murniningtyas, E.; Staniškis, J. K.; van Ypersele, J.-P.; Furman, E. Expansion of Sustainability Science Needed for the SDGs. *Nat Sustain* **2019**, *2* (10), 892–894. https://doi.org/10.1038/s41893-019-0394-z.

(5) Gross, M. Our Planet Wrapped in Plastic. *Current Biology* **2017**, *27* (16), R785–R788. https://doi.org/10.1016/j.cub.2017.08.007.

(6) Zhu, Y.; Romain, C.; Williams, C. K. Sustainable Polymers from Renewable Resources. *Nature* **2016**, *540* (7633), 354–362. https://doi.org/10.1038/nature21001.

(7) Chandra, R.; Rustgi, R. Biodegradable Polymers. *Progress in Polymer Science* **1998**, *23* (7), 1273–1335. https://doi.org/10.1016/S0079-6700(97)00039-7.

(8) *The Unintended Side Effects of Bioplastics: Carbon, Land, and Water Footprints - ScienceDirect*. https://www.sciencedirect.com/science/article/pii/S2590332220303055 (accessed 2024-06-06).

(9) Atiwesh, G.; Mikhael, A.; Parrish, C. C.; Banoub, J.; Le, T.-A. T. Environmental Impact of Bioplastic Use: A Review. *Heliyon* **2021**, *7* (9), e07918. https://doi.org/10.1016/j.heliyon.2021.e07918.

(10) Vu, C. H. T.; Won, K. Novel Water-Resistant UV-Activated Oxygen Indicator for Intelligent Food Packaging. *Food Chem* **2013**, *140* (1–2), 52–56. https://doi.org/10.1016/j.foodchem.2013.02.056.

(11) *[PDF] Can Seaweed Farming Play a Role in Climate Change Mitigation and Adaptation? | Semantic Scholar*. https://www.semanticscholar.org/paper/Can-Seaweed-Farming-Play-a-Role-in-Climate-Change-Duarte-Wu/048038d651056a55181ba0426bc36c2253b24544 (accessed 2024-04-18).

(12) Venugopal, V. *Marine Polysaccharides: Food Applications*; CRC Press, 2016.

(13) *Rajendran: Seaweeds can be a new source for bioplastics - Google Scholar*. https://scholar.google.com/scholar_lookup?title=Seaweeds%20can%20be%20a%20new%20source%20for%20bioplastics&author=N.%20Rajendran&publication_year=2012&pages=1476-1479 (accessed 2024-05-01).

(14) Nussinovitch, A. Agar. In *Hydrocolloid Applications: Gum technology in the food and other industries*; Nussinovitch, A., Ed.; Springer US: Boston, MA, 1997; pp 1–18. https://doi.org/10.1007/978-1-4615-6385-3_1.

(15) *Algae as production systems of bioactive compounds*. https://analyticalsciencejournals.onlinelibrary.wiley.com/doi/epdf/10.1002/elsc.201400191 (accessed 2024-05-01).

(16) Abasalizadeh, F.; Moghaddam, S. V.; Alizadeh, E.; Akbari, E.; Kashani, E.; Fazljou, S. M. B.; Torbati, M.; Akbarzadeh, A. Alginate-Based Hydrogels as Drug Delivery Vehicles in Cancer Treatment and Their Applications in Wound Dressing and 3D Bioprinting. *J Biol Eng* **2020**, *14*, 8. https://doi.org/10.1186/s13036-020-0227-7.

(17) Magdalena, B. Ł.; Izabela, M.; Jerzy, D. Methods of Extraction, Physicochemical Properties of Alginates and Their Applications in Biomedical Field – a Review. *Open Chemistry* **2019**, *17* (1), 738–762. https://doi.org/10.1515/chem-2019-0077.

(18) Sterner, M.; Edlund, U. Multicomponent Fractionation of Saccharina Latissima Brown Algae Using Chelating Salt Solutions. *J Appl Phycol* **2016**, *28*, 2561–2574. https://doi.org/10.1007/s10811-015-0785-0.

(19) Hernández-carmona, G.; McHugh, D. J.; Arvizu-Higuera, D. L.; Rodríguez-montesinos, Y. E. Pilot Plant Scale Extraction of Alginate from Macrocystis Pyrifera. 1. Effect of Pre-Extraction Treatments on Yield and Quality of Alginate. *Journal of Applied Phycology* **1998**, *10* (6), 507–513. https://doi.org/10.1023/A:1008004311876.

(20) Fawzy, M. A.; Gomaa, M.; Hifney, A. F.; Abdel-Gawad, K. M. Optimization of Alginate Alkaline Extraction Technology from *Sargassum Latifolium* and Its Potential Antioxidant

and Emulsifying Properties. *Carbohydrate Polymers* **2017**, *157*, 1903–1912. https://doi.org/10.1016/j.carbpol.2016.11.077.

(21) Abdul Khalil, H. P. S.; Lai, T. K.; Tye, Y. Y.; Rizal, S.; Chong, E. W. N.; Yap, S. W.; Hamzah, A. A.; Nurul Fazita, M. R.; Paridah, M. T. A Review of Extractions of Seaweed Hydrocolloids: Properties and Applications. *Express Polym. Lett.* **2018**, *12* (4), 296–317. https://doi.org/10.3144/expresspolymlett.2018.27.

(22) MacKenzie, J.; Siren, E.; Daneshi, M.; Melnick, R.; Treskatis, T.; Wachs, A.; Kizhakkedathu, J. N.; Martinez, D. M. Fibre-Reinforced Biocompatible Hydrogel to Replace Single-Use Plastic Tubing in the Clinical Setting. *Chemical Engineering Journal* **2022**, *428*, 131786. https://doi.org/10.1016/j.cej.2021.131786.

(23) Draget, K. I.; Taylor, C. Chemical, Physical and Biological Properties of Alginates and Their Biomedical Implications. *Food Hydrocolloids* **2011**, *25* (2), 251–256. https://doi.org/10.1016/j.foodhyd.2009.10.007.

(24) Gacesa, P. Enzymic Degradation of Alginates. *Int J Biochem* **1992**, *24* (4), 545–552. https://doi.org/10.1016/0020-711x(92)90325-u.

(25) Draget, K. I.; Skjåk-Bræk, G.; Stokke, B. T. Similarities and Differences between Alginic Acid Gels and Ionically Crosslinked Alginate Gels. *Food Hydrocolloids* **2006**, *20* (2), 170–175. https://doi.org/10.1016/j.foodhyd.2004.03.009.

(26) Trica, B.; Delattre, C.; Gros, F.; Ursu, A. V.; Dobre, T.; Djelveh, G.; Michaud, P.; Oancea, F. Extraction and Characterization of Alginate from an Edible Brown Seaweed (Cystoseira Barbata) Harvested in the Romanian Black Sea. *Marine Drugs* **2019**, *17* (7), 405. https://doi.org/10.3390/md17070405.

(27) *(PDF) Rheological Study on 3D Printability of Alginate Hydrogel and Effect of Graphene Oxide*. https://www.researchgate.net/publication/315531460_Rheological_Study_on_3D_Printability_of_Alginate_Hydrogel_and_Effect_of_Graphene_Oxide (accessed 2024-05-01).

(28) Bruchet, M.; Melman, A. Fabrication of Patterned Calcium Cross-Linked Alginate Hydrogel Films and Coatings through Reductive Cation Exchange. *Carbohydr Polym* **2015**, *131*, 57–64. https://doi.org/10.1016/j.carbpol.2015.05.021.

(29) Garcia-Vaquero, M.; Rajauria, G. Chapter 1 - Overview of the Application of Innovative and Emerging Technologies in the Bio-Marine Food Sector. In *Innovative and Emerging*

*Technologies in the Bio-marine Food Sector*; Garcia-Vaquero, M., Rajauria, G., Eds.; Academic Press, 2022; pp 1–12. https://doi.org/10.1016/B978-0-12-820096-4.00021-3.

(30) *Directive 2008/98/EC of the European Parliament and of the C...* https://eur-lex.europa.eu/EN/legal-content/summary/eu-waste-management-law.html (accessed 2024-06-06).

(31) Fredi, G.; Dorigato, A. Recycling of Bioplastic Waste: A Review. *Advanced Industrial and Engineering Polymer Research* **2021**, *4*. https://doi.org/10.1016/j.aiepr.2021.06.006.

(32) Niaounakis, M. Recycling of Biopolymers – The Patent Perspective. *European Polymer Journal* **2019**, *114*, 464–475. https://doi.org/10.1016/j.eurpolymj.2019.02.027.

(33) *Bio-Based Plastics: Materials and Applications | Wiley*. https://www.wiley.com/en-us/Bio-Based+Plastics%3A+Materials+and+Applications-p-9781119994008 (accessed 2024-06-06).

(34) Merchan, A. L.; Fischöder, T.; Hee, J.; Lehnertz, M. S.; Osterthun, O.; Pielsticker, S.; Schleier, J.; Tiso, T.; Blank, L. M.; Klankermayer, J.; Kneer, R.; Quicker, P.; Walther, G.; Palkovits, R. Chemical Recycling of Bioplastics: Technical Opportunities to Preserve Chemical Functionality as Path towards a Circular Economy. *Green Chem.* **2022**, *24* (24), 9428–9449. https://doi.org/10.1039/D2GC02244C.

(35) *Microbial Degradation of Polyhydroxyalkanoates* | Annual Reviews*. https://www.annualreviews.org/content/journals/10.1146/annurev.micro.56.012302.160838 (accessed 2024-07-12).

(36) Lee, S. Y.; Choi, J.; Wong, H. H. Recent Advances in Polyhydroxyalkanoate Production by Bacterial Fermentation: Mini-Review. *Int J Biol Macromol* **1999**, *25* (1–3), 31–36. https://doi.org/10.1016/s0141-8130(99)00012-4.

(37) Chowdhury, A. A. [POLY-BETA-HYDROXYBUTYRIC ACID-SPLITTING BACTERIA AND AN EXOENZYME]. *Arch Mikrobiol* **1963**, *47*, 167–200.

(38) Helfenbein, D. Development of Recycling of PLA Sheet into PLA Pellets without Undergoing Chemical Process. *Atlanta, GA* **2011**.

(39) Pillin, I.; Montrelay, N.; Bourmaud, A.; Grohens, Y. Effect of Thermo-Mechanical Cycles on the Physico-Chemical Properties of Poly(Lactic Acid). *Polymer Degradation and Stability* **2008**, *93* (2), 321–328. https://doi.org/10.1016/j.polymdegradstab.2007.12.005.

(40) Żenkiewicz, M.; Richert, J.; Rytlewski, P.; Moraczewski, K.; Stepczyńska, M.; Karasiewicz, T. Characterisation of Multi-Extruded Poly(Lactic Acid). *Polymer Testing* **2009**, *28* (4), 412–418. https://doi.org/10.1016/j.polymertesting.2009.01.012.

(41) Badia, J. D.; Strömberg, E.; Karlsson, S.; Ribes-Greus, A. Material Valorisation of Amorphous Polylactide. Influence of Thermo-Mechanical Degradation on the Morphology, Segmental Dynamics, Thermal and Mechanical Performance. *Polymer Degradation and Stability* **2012**, *97* (4), 670–678. https://doi.org/10.1016/j.polymdegradstab.2011.12.019.

(42) Mohd-Adnan, A.-F.; Nishida, H.; Shirai, Y. Evaluation of Kinetics Parameters for Poly(l-Lactic Acid) Hydrolysis under High-Pressure Steam. *Polymer Degradation and Stability* **2008**, *93* (6), 1053–1058. https://doi.org/10.1016/j.polymdegradstab.2008.03.022.

(43) Tsuji, H.; Daimon, H.; Fujie, K. A New Strategy for Recycling and Preparation of Poly(L-Lactic Acid): Hydrolysis in the Melt. *Biomacromolecules* **2003**, *4* (3), 835–840. https://doi.org/10.1021/bm034060j.

(44) *[PDF] Recycling Of Poly Lactic Acid Into Lactic AcidWith High Temperature And High Pressure Water | Semantic Scholar*. https://www.semanticscholar.org/paper/Recycling-Of-Poly-Lactic-Acid-Into-Lactic-AcidWith-Faisal-Saeki/bd6d028ea89c39ce88046ea803eae7c8d73ee5e4 (accessed 2024-07-12).

(45) *Comparative study on hydrolytic degradation and monomer recovery of poly(l-lactic acid) in the solid and in the melt - ScienceDirect*. https://www.sciencedirect.com/science/article/pii/S0141391008001948 (accessed 2024-07-12).

(46) Mori, T.; Nishida, H.; Shirai, Y.; Endo, T. Effects of Chain End Structures on Pyrolysis of Poly(l-Lactic Acid) Containing Tin Atoms. *Polymer Degradation and Stability* **2004**, *84* (2), 243–251. https://doi.org/10.1016/j.polymdegradstab.2003.11.008.

(47) Fan, Y.; Nishida, H.; Mori, T.; Shirai, Y.; Endo, T. Thermal Degradation of Poly(l-Lactide): Effect of Alkali Earth Metal Oxides for Selective l,l-Lactide Formation. *Polymer* **2004**, *45* (4), 1197–1205. https://doi.org/10.1016/j.polymer.2003.12.058.

(48) *Control of racemization for feedstock recycling of PLLA - Green Chemistry (RSC Publishing)*. https://pubs.rsc.org/en/content/articlelanding/2003/gc/b304792j (accessed 2024-07-12).

(49) Zhang, Y.; Rempel, C.; Liu, Q. Thermoplastic Starch Processing and Characteristics-a Review. *Crit Rev Food Sci Nutr* **2014**, *54* (10), 1353–1370. https://doi.org/10.1080/10408398.2011.636156.

(50) *Preparation and characterization of starch-based composite films reinfoced by polysaccharide-based crystals - ScienceDirect*. https://www.sciencedirect.com/science/article/pii/S1359836816325811 (accessed 2024-07-12).

(51) Chen, Z.; Ding, D.; Yu, T.; Yang, W.; Li, Q.; Li, Y. Enzymatic Degradation Behaviors and Kinetics of Bio-Degradable Jute/Poly (Lactic Acid) (PLA) Composites. *Composites Communications* **2022**, *33*, 101227. https://doi.org/10.1016/j.coco.2022.101227.

(52) Azevedo, H. S.; Gama, F. M.; Reis, R. L. In Vitro Assessment of the Enzymatic Degradation of Several Starch Based Biomaterials. *Biomacromolecules* **2003**, *4* (6), 1703–1712. https://doi.org/10.1021/bm0300397.

(53) Quintana, R.; Persenaire, O.; Bonnaud, L.; Dubois, P. Recent Advances in (Reactive) Melt Processing of Cellulose Acetate and Related Biodegradable Bio-Compositions. *Polym. Chem.* **2012**, *3* (3), 591–595. https://doi.org/10.1039/C1PY00421B.

(54) Soroudi, A.; Jakubowicz, I. Recycling of Bioplastics, Their Blends and Biocomposites: A Review. *European Polymer Journal* **2013**, *49* (10), 2839–2858. https://doi.org/10.1016/j.eurpolymj.2013.07.025.

(55) Panday, A.; Yadav, H.; Patel, J.; Paliwal, R.; Maiti, S. Calcium Silicate-Reinforced pH-Sensitive Alginate-Gellan Gum Composite Hydrogels for Prolonged Drug Delivery. *Journal of Applied Polymer Science* **2023**, *140* (37), e54392. https://doi.org/10.1002/app.54392.

(56) Liu, G.-L.; Kazarian, S. G. Recent Advances and Applications to Cultural Heritage Using ATR-FTIR Spectroscopy and ATR-FTIR Spectroscopic Imaging. *Analyst (London)* **2022**, *147* (9), 1777–1797. https://doi.org/10.1039/D2AN00005A.

(57) *Molecules | Free Full-Text | Isolation and FTIR-ATR and 1H NMR Characterization of Alginates from the Main Alginophyte Species of the Atlantic Coast of Morocco*. https://www.mdpi.com/1420-3049/25/18/4335 (accessed 2024-01-20).

(58) *A p.m.r. study of the composition and sequence of uronate residues in alginates - ScienceDirect*. https://www.sciencedirect.com/science/article/abs/pii/S0008621500840513 (accessed 2024-01-20).

(59) Grasdalen, H. High-Field, 1H-n.m.r. Spectroscopy of Alginate: Sequential Structure and Linkage Conformations. *Carbohydrate Research* **1983**, *118*, 255–260. https://doi.org/10.1016/0008-6215(83)88053-7.

(60) Malektaj, H.; Drozdov, A. D.; deClaville Christiansen, J. Mechanical Properties of Alginate Hydrogels Cross-Linked with Multivalent Cations. *Polymers (Basel)* **2023**, *15* (14), 3012. https://doi.org/10.3390/polym15143012.

(61) Fazlali, B.; Upadhyay, S.; Ashokbhai Ashodia, S.; Mesquita, F.; Lomov, S. V.; Carvelli, V.; Swolfs, Y. Specimen Designs for Accurate Tensile Testing of Unidirectional Composite Laminates. *Composites Part A: Applied Science and Manufacturing* **2023**, *175*, 107799. https://doi.org/10.1016/j.compositesa.2023.107799.

(62) *ASTM Login*. https://secure.astm.org/login?redirectUrl=aHR0cHM6Ly9jb21wYXNzLmFzdG0ub3Jn&newApproach=true (accessed 2024-05-09).

(63) Paiva, J. M. F. de; Mayer, S.; Rezende, M. C. Comparison of Tensile Strength of Different Carbon Fabric Reinforced Epoxy Composites. *Mat. Res.* **2006**, *9*, 83–90. https://doi.org/10.1590/S1516-14392006000100016.

(64) AlMaadeed, M. A.; Nógellová, Z.; Janigová, I.; Krupa, I. Improved Mechanical Properties of Recycled Linear Low-Density Polyethylene Composites Filled with Date Palm Wood Powder. *Materials & Design* **2014**, *58*, 209–216. https://doi.org/10.1016/j.matdes.2014.01.051.

(65) Gohil, P. P.; Shaikh, A. A. Experimental Evaluation for Mechanical Property of Unidirectional Banana Reinforced Polyester Composites. *Advanced Materials Research* **2010**, *123–125*, 1147–1150. https://doi.org/10.4028/www.scientific.net/AMR.123-125.1147.

(66) He, Y.; Zhao, X. Y.; Rao, P.; Song, H. M.; Yang, Y.; Sun, S. W.; Zhou, J. X.; Chen, Y. M.; Tan, L.; Ma, J. Z. Saline Tolerant Tough-yet-Strong Fiber-Reinforced Gel-Nacre for Soft Actuator. *Chemical Engineering Journal* **2022**, *446*, 137091. https://doi.org/10.1016/j.cej.2022.137091.

(67) Abka-Khajouei, R.; Tounsi, L.; Shahabi, N.; Patel, A. K.; Abdelkafi, S.; Michaud, P. Structures, Properties and Applications of Alginates. *Mar Drugs* **2022**, *20* (6), 364. https://doi.org/10.3390/md20060364.

(68) Zhang, P.; Raza, S.; Cheng, Y.; Claudine, U.; Hayat, A.; Bashir, T.; Ali, T.; Ghasali, E.; Orooji, Y. Fabrication of Maleic Anhydride-Acrylamide Copolymer Based Sodium Alginate Hydrogel for Elimination of Metals Ions and Dyes Contaminants from Polluted Water. *International Journal of Biological Macromolecules* **2024**, *261*, 129146. https://doi.org/10.1016/j.ijbiomac.2023.129146.

(69) Papageorgiou, S. K.; Kouvelos, E. P.; Favvas, E. P.; Sapalidis, A. A.; Romanos, G. E.; Katsaros, F. K. Metal–Carboxylate Interactions in Metal–Alginate Complexes Studied with FTIR Spectroscopy. *Carbohydrate Research* **2010**, *345* (4), 469–473. https://doi.org/10.1016/j.carres.2009.12.010.

(70) *Elucidation of Interactions between Metal Ions and Ca Alginate-Based Ion-Exchange Resin by Spectroscopic Analysis and Modeling Simulation - University of Victoria*. https://search.library.uvic.ca/discovery/fulldisplay?docid=cdi_crossref_primary_10_1021_la026060v&context=PC&vid=01VIC_INST:01UVIC&lang=en&search_scope=MyInst_and_CI&adaptor=Primo%20Central&tab=LIBALL&query=any,contains,Chen,%20J.%20P.;%20Hong,%20L.;%20Wu,%20S.;%20Wang,%20L.%20Langmuir%202002,%2018,%209413%E2%80%939421.&offset=0 (accessed 2024-04-30).

(71) *EDS Analysis | Energy Dispersive Spectroscopy | Thermo Fisher Scientific - CA*. https://www.thermofisher.com/ca/en/home/materials-science/eds-technology.html (accessed 2024-06-06).

(72) Abd El-Mohdy, H. Radiation-Induced Degradation of Sodium Alginate and Its Plant Growth Promotion Effect. *Arabian Journal of Chemistry* **2012**, *78*. https://doi.org/10.1016/j.arabjc.2012.10.003.

(73) Fawzy, M. A.; Gomaa, M. Optimization of Citric Acid Treatment for the Sequential Extraction of Fucoidan and Alginate from Sargassum Latifolium and Their Potential Antioxidant and Fe(III) Chelation Properties. *J Appl Phycol* **2021**, *33* (4), 2523–2535. https://doi.org/10.1007/s10811-021-02453-9.

(74) Gomez, C. G.; Pérez Lambrecht, M. V.; Lozano, J. E.; Rinaudo, M.; Villar, M. A. Influence of the Extraction–Purification Conditions on Final Properties of Alginates Obtained from Brown Algae (*Macrocystis Pyrifera*). *International Journal of Biological Macromolecules* **2009**, *44* (4), 365–371. https://doi.org/10.1016/j.ijbiomac.2009.02.005.

(75) Moradali, M. F.; Donati, I.; Sims, I. M.; Ghods, S.; Rehm, B. H. A. Alginate Polymerization and Modification Are Linked in Pseudomonas Aeruginosa. *mBio* **2015**, *6* (3), e00453-00415. https://doi.org/10.1128/mBio.00453-15.

(76) Extraction and characterization of sodium alginate from Moroccan Laminaria digitata brown seaweed-ScienceDirect. https://www.sciencedirect.com/science/article/pii/S1878535214000793 (accessed 2024-01 20).

(77) Costa, M. J.; Marques, A. M.; Pastrana, L. M.; Teixeira, J. A.; Sillankorva, S. M.; Cerqueira, M. A. Physicochemical Properties of Alginate-Based Films: Effect of Ionic Crosslinking and Mannuronic and Guluronic Acid Ratio. *Food Hydrocolloids* **2018**, *81*, 442–448. https://doi.org/10.1016/j.foodhyd.2018.03.014.

(78) Jensen, H. M.; Larsen, F. H.; Engelsen, S. B. Characterization of Alginates by Nuclear Magnetic Resonance (NMR) and Vibrational Spectroscopy (IR, NIR, Raman) in Combination with Chemometrics. In *Natural Products From Marine Algae: Methods and Protocols*; Stengel, D. B., Connan, S., Eds.; Springer: New York, NY, 2015; pp 347–363. https://doi.org/10.1007/978-1-4939-2684-8_22.

(79) Feng, L.; Cao, Y.; Xu, D.; Wang, S.; Zhang, J. Molecular Weight Distribution, Rheological Property and Structural Changes of Sodium Alginate Induced by Ultrasound. *Ultrasonics Sonochemistry* **2017**, *34*, 609–615. https://doi.org/10.1016/j.ultsonch.2016.06.038.

(80) *Alginates: Biology and Applications | SpringerLink*. https://link.springer.com/book/10.1007/978-3-540-92679-5 (accessed 2024-08-07).

(81) Szabó, L.; Gerber-Lemaire, S.; Wandrey, C. Strategies to Functionalize the Anionic Biopolymer Na-Alginate without Restricting Its Polyelectrolyte Properties. *Polymers (Basel)* **2020**, *12* (4), 919. https://doi.org/10.3390/polym12040919.

(82) Aarstad, O.; Strand, B. L.; Klepp-Andersen, L. M.; Skjåk-Bræk, G. Analysis of G-Block Distributions and Their Impact on Gel Properties of in Vitro Epimerized Mannuronan. *Biomacromolecules* **2013**, *14* (10), 3409–3416. https://doi.org/10.1021/bm400658k.

# Chapter 3: Thesis Overall Conclusion

This thesis addresses key challenges in water purification and material sustainability through two focused projects: enhancing reverse osmosis (RO) membrane technology and advancing the recycling of alginate-based bioplastics. These projects, while distinct in their materials and methodologies, collectively contribute to more sustainable and efficient practices.

In Chapter 1, the research introduced a novel approach to improving RO membrane performance by modifying polyamide membranes with diazirine-containing molecules. Although the study did not definitively prove the covalent attachment of diazirine, it provided valuable insights into the surface modification process. Indirect evidence from dye tests, contact angle measurements, and differential scanning calorimetry (DSC) suggested potential improvements in membrane durability. Future research using advanced techniques such as X-ray photoelectron spectroscopy (XPS) and nuclear magnetic resonance (NMR) is recommended to validate these modifications and further enhance membrane performance. The goal of this work is to reduce maintenance needs and environmental impact, ultimately contributing to more sustainable water treatment technologies.

Chapter 2 explored the recycling potential of sodium alginate hydrogels, focusing on materials derived from kelp. The study demonstrated significant yields and highlighted differences in recycling efficiency among various alginate sources. Key findings included changes in the M/G ratio and molecular weight of recycled alginate, which affect the material's stability and functionality. Effective removal of calcium crosslinkers was confirmed, and the study proposed further optimization of recycling conditions, exploration of alternative removal techniques, and evaluation of the recycled hydrogels' performance in various applications. This research supports sustainable practices by promoting the reuse of materials and advancing the principles of a circular economy.

Overall, this thesis integrates advancements in material science to address pressing issues in water purification and bioplastic recycling. By enhancing RO membrane technology and optimizing alginate recycling processes, the research contributes practical solutions to reduce environmental impact and improve resource efficiency. The findings highlight the potential for material science innovations to drive progress toward a more sustainable future, demonstrating that targeted

research can lead to significant improvements in both industrial applications and environmental stewardship.

In conclusion, this thesis bridges the gap between technological innovation and sustainability, offering insights and solutions that advance resource conservation and reduce ecological footprints. The research underscores the importance of continuous development in material science to address global challenges and support a more sustainable approach to resource use.

# Appendix A: List of Tables and Figures with Raw Data Links

These files are all found in the folder titled "Negar" on the Green Safe Water Lab One Drive, and that links are current as of 28 November 2024. Raw Data will be available upon request.

**Figures**

1. **Figure 1.11**: Comparison of DSC peaks for 10 and 30Wt% PEI-diazirine, Analyzed in TRIOS 5.1.1
   *Page:* 25
   *Raw Data Link*
2. **Figure 1.16**: DSC spectra for RO samples treated with 30Wt% PEI-diazirine, one-side coat, and UV cured for 30 min, Analyzed in TRIOS 5.1.1
   *Page:* 25
   *Raw Data Link*
3. **Figure 1.17**: DSC spectra for RO samples treated with 30Wt% PEI-diazirine, soaked and UV cured for 30 min, Analyzed in TRIOS 5.1.1
   *Page:* 26
   *Raw Data Link*
4. **Figure 1.19**: 30 Wt% treated, one-side-coat PET coupons, already cured samples were UV activated for 30 min, Analyzed in TRIOS 5.1.1
   *Page:* 29
   *Raw Data Link*
5. **Figure 1.22**: Contact angle measurements for PET and RO samples
   *Page:* 32
   *Raw Data Link*
6. **Figure 1.23**: FTIR-ATR result for 30Wt% PEI-diazirine-treated RO samples, normalized to max transmittance intensity at 558 $cm^{-1}$
   *Page:* 34
   *Raw Data Link*
7. **Figure 1.24**: FTIR spectra of Molecule1
   *Page:* 35
   *Raw Data Link*
8. **Figure 1.25**: FTIR-ATR results for Molecule1-treated PET surface (M1: Molecule1), normalized to max transmittance intensity at 1716 $cm^{-1}$
   *Page:* 36
   *Raw Data Link*
9. **Figure 1.26**: FTIR-ATR result for Molecule1-treated RO membrane surface (M1: Molecule1), normalized to max transmittance intensity at 1237 $cm^{-1}$

*Page:* 36
*Raw Data Link*

**Chapter 2**

**Figures**

11. **Figure 2.13**: FTIR spectra of I-2, I-2G, and EX (kelp-extract sodium alginate), normalized to max transmittance
    *Page:* 75
    *Raw Data Link*
12. **Figure 2.14**: FTIR Spectra of I-2, I-2 film, recycled I-2, and recycled I-2 film status, normalized to max transmittance
    *Page:* 77
    *Raw Data Link*
13. **Figure 2.15**: FTIR Spectra of I-2G, I-2G film, recycled I-2G, and recycled I-2G film status, normalized to max intensity
    *Page:* 78
    *Raw Data Link*
14. **Figure 2.16**: FTIR Spectra of kelp-extract alginate, hydrogel, recycled, and recycled hydrogel status, normalized to max intensity
    *Page:* 78
    *Raw Data Link*
15. **Figure 2.17**: Molecular weight comparison among non-film alginate samples
    *Page:* 83
    *Raw Data Link*
16. **Figure 2.18**: Molecular number comparison among non-film alginate samples
    *Page:* 83
    *Raw Data Link*
17. **Figure 2.19**: Polydispersity index comparison among three sodium alginate sources
    *Page:* 84
    *Raw Data Link*
18. **Figure 2.25**:
    a) Stress-strain diagram of commercial I-2
    b) Stress-strain diagram of RI-2
    *Page:* 91
    *Raw Data Link*
19. **Figure 2.26**:
    a) Stress-strain diagram of commercial I-2G

b) Stress-strain diagram of RI-2G
*Page:* 92
*Raw Data Link*

20. **Figure 2.27**:
a) Stress-strain diagram of kelp-extracted alginate EX
b) Stress-strain diagram of REX-1
*Page:* 93
*Raw Data Link*

**Chapter 1**

**Tables**

1. **Table 1.4**: Data and standard deviation (STE.DEV) of contact angle measurements for both PET and RO surfaces
*Page:* 31
*Raw Data Link*

**Chapter 2**

**Tables**

1. **Table 2.5**: All sample codes FTIR characteristic peak shifts (cm-1)

*Page:* 78
*Raw Data Link*

2. **Table 2.6**: EDX elemental analysis of commercial I-2, I-2G hydrogel film (I2F),recycled I-2 (RI-2) and hydrogel film of recycled I-2 (RI-2F)
*Page:* 81
*Raw Data Link*

3. **Table 2.7**: EDX elemental analysis of commercial I-2G, I-2 hydrogel film (I-2GF), recycled I-2G (RI-2G) and hydrogel film of recycled I-2G (RI-2GF)

*Page:* 82
*Raw Data Link*

4. **Table 2.8**: EDX elemental analysis of kelp-extract sodium alginate (EX), EX hydrogel film (EXF), recycled EX (REX-1, REX-2), and hydrogel film of recycled REX-2 (REX-2F)

*Page:* 83
*Raw Data Link*

5. **Table 2.9**: Summary of GPC results for non-film sample codes

   *Page:* 86
   *Raw Data Link*

6. **Table 2.11,2.12**: Processed NMR data using equations: 1-4

   *Page:* 91
   *Raw Data Link*

7. **Table 2.13**: Mechanical characteristics of commercial alginate sources, extracted alginate, and recycled material

   *Page:* 93

   *Raw Data Link*